

POLITECNICO DI TORINO

Facoltà di Ingegneria  
Corso di Laurea in Ingegneria per l'Ambiente ed il Territorio



Groundwater Flow Modeling in a Site Affected by Dense  
Non Aqueous Phase Liquids

Academic Year 2018/2019

Advisor:  
Tiziana Anna Elisabetta Tosco  
Co-Advisor:  
Fernando Barrio Parra  
Alessandro Casasso

Student:  
Francesco Recchia 241602

## Table of Contents

Abstract .....	2
1 Introduction and Objectives .....	3
2 Materials and Methods .....	8
2.1 Description of the site .....	8
2.1.1 Geographical framework .....	8
2.1.2 Geological framework.....	10
2.1.3 Hydrogeological framework.....	14
2.1.4 The Contamination .....	20
2.2 Groundwater Modeling .....	25
2.2.1 Conceptual model of the site.....	25
2.2.2 Description of the field tests carried out.....	27
2.2.3 Groundwater Modeling Tools.....	33
2.2.4 Flow and Transport Modeling with FEFLOW .....	42
2.2.5 Flow and Transport Model Calibration with PEST.....	60
3 Results and Discussion.....	63
3.1 Quantum GIS.....	63
3.1.1 Boundary of the model .....	63
3.1.2 Wells and Piezometers.....	64
3.1.3 Points to apply elevation .....	65
3.2 PEST.....	66
3.3 FEFLOW .....	71
3.3.1 Tracer Test (4 <sup>th</sup> - 9 <sup>th</sup> of June 2018): Results .....	71
3.3.2 Tracer Test (4 <sup>th</sup> - 9 <sup>th</sup> of June 2018): Discussion.....	74
3.3.3 SEAR Pilot Test (9 <sup>th</sup> - 13 <sup>th</sup> of July 2018): Results.....	75
3.3.4 SEAR Pilot Test (9 <sup>th</sup> - 13 <sup>th</sup> of July 2018): Discussion .....	80
3.3.5 General discussion on both episodes.....	82
4 Conclusions .....	83
5 Appendices.....	85
5.1 Appendix A: Ground Control Points used in the georeferentiation.....	85
5.2 Appendix B: Points used to Iterpolate the Initial Piezometry .....	86
5.3 Appendix C: Chemical Properties of Lindane.....	88
Acknowledgements.....	89
References .....	90

## Abstract

Although scientific progress has shown the harmfulness and toxicity to man and the environment of certain pesticides, prohibiting their use, the residues of old productions can still give rise to environmental problems with very significant impacts.

Among these, Dense Non-Aqueous Phase Liquids (DNAPL) are certainly of interest, since, due to their high specific weight, they can migrate deep into the soil, reaching the bottom of the aquifer and accumulating at high depth, giving rise to contaminations difficult to be addressed.

Due to their low solubility, DNAPLs are slowly dissolved in groundwater and hence they can represent a long-term contamination source.

It is therefore necessary to perform a reliable characterization of such contaminated sites and to develop accurate models to be used as a support in the design of the remediation.

For this purpose, over the last years the importance of mathematical models of groundwater flow and contaminant transport has dramatically increased; models are used to better understand the contamination process, to simulate long-term to support the design of the reclamation interventions, comparing alternatives from the point of view of effectiveness, long-term expected impacts, and monetary costs.

This thesis presents a numerical modeling study performed at the Technical University of Madrid on a complex contaminated site in Spain using FEFLOW, a finite-element groundwater flow and transport modelling tool.

A conceptual model of the site is developed and translated into a numerical model to study the interactions between the aquifer polluted by pesticides and connected to a water reservoir used for agricultural, energy and drinking water purposes. The connection between the aquifer and the reservoir is studied based on the seasonal level variations of the reservoir and how they are transmitted to the aquifer, as observed in monitoring wells.

Moreover, transport simulations are used to compare alternative scenarios for the site remediation, considering the injection of soluble reactants and surfactants, for a preliminary evaluation of possible remediation alternative technologies.

# 1 Introduction and Objectives

The present work addresses the contamination of groundwater from pesticides and their by-products in a former production site in Aragon, Spain.

The Food and Agriculture Organization (FAO) defined pesticide as:

*“any substance or mixture of substances intended for preventing, destroying, or controlling any pest, including vectors of human or animal disease, unwanted species of plants or animals, causing harm during or otherwise interfering with the production, processing, storage, transport, or marketing of food, agricultural commodities, wood and wood products or animal feedstuffs, or substances that may be administered to animals for the control of insects, arachnids, or other pests in or on their bodies. The term includes substances intended for use as a plant growth regulator, defoliant, desiccant, or agent for thinning fruit or preventing the premature fall of fruit. Also used as substances applied to crops either before or after harvest to protect the commodity from deterioration during storage and transport.”* (Food and Agriculture Organization of the United Nations. 2002). Pesticides can be classified by target organism in herbicides, insecticides, nematocides, molluscicides, piscicides, avicides, rodenticides, bactericides, insect repellents, animal repellents, antimicrobials, fungicides, and disinfectant (Randall C, et al., National Association of State Departments of Agriculture Research Foundation; 2014).

The most common pesticides are herbicides which account for approximately 80% of all pesticide use (Food Print, GRACE Communications Foundation; 2018).

Despite their main aim is to control harmful organisms, their chemical characteristics, combined with their massive use, made them an environmental and public health problem.

Studies on non-Hodgkin lymphoma and leukemia, neurological problems, birth defects, fetal death and neurodevelopment disorder, showed positive associations with pesticides exposure (Bassil KL, Vakil C, Sanborn M, Cole DC, Kaur JS, Kerr KJ; 2007) (Jurewicz J, Hanke W; 2008).

For what concerns environmental problems, pesticides can affect all the environmental matrices addressed by this study, including water and groundwater:

- Air: pesticides suspended in the air as gas phase or absorbed on soil particles can be carried by wind to other areas, potentially contaminating them. In fact if applied into farming they can volatilize and may be blown by winds depending on weather conditions (high wind velocity implicates high spray

drift and exposure) at the time of application as well as temperature (daily and seasonal) and relative humidity, which can change the spread of the pesticide in the air and their evaporation (Damalas CA, Eleftherohorinos IG; 2011).

- Soil: even if few residues of some pesticides can be degraded by microorganisms, their extensive use in crops can damage microorganisms living in the soil, particularly when these chemicals are overused or misused, depending on persistence, concentration, and toxicity of the applied pesticide and generally resulting in a decrease of biodiversity in the soil (Abdel-Mallek AY, Moharram AM, Abdel-Kader MI, Omar SA; 1994).  
The persistence of pesticides in soil is influenced by degradation and sorption: sorption is dependent on the amount of organic matter in soil, on which pesticides are preferentially sorbed, resulting also in a lower amount of water retention in soils (Kellogg RL, Nehring R, Grube A, Goss DW, Plotkin S; United States Department of Agriculture Natural Resources Conservation Service; 2000). Moreover, as longer a pesticide stay in soil, the more it becomes resistant to degradation, because of the reduced activity of the microorganisms which cannot complete the process.
- Water: pesticides can reach the water in different ways, in fact they may drift outside of the target area if sprayed, they may percolate through the soil and they can be transported by water as runoff or they can also be transported into water by eroding soil. Pesticide's possibility to contaminate water depends on its water solubility, on the distance from the application point to a receptor body, on precipitations, soil type and on methods used to apply the compound (Pedersen TL; 1997).

The main pesticides contamination pathways are shown in Figure 1.

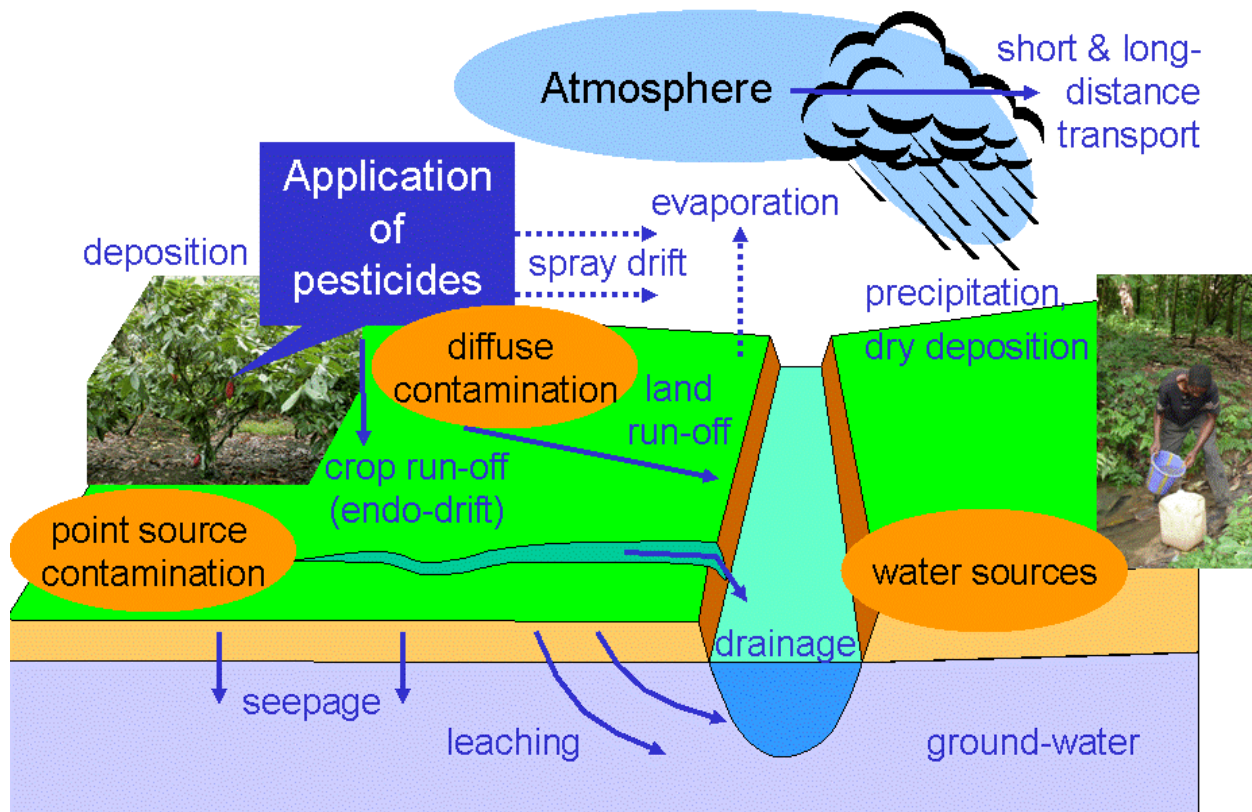


Figure 1: pesticides pathways in air, soil and water (from Wikipedia)

Due to their characteristics, most of the pesticides are considered as persistent organic pollutants.

Persistent Organic Pollutants (POP) are chemical substances relatively high persistence in the environment, due to their high resistance to degradation, they are bio cumulative, settling in the tissues of living beings and increasing the concentration through the food chain, they are highly toxic and cause serious effects on human health and the environment and they have the potential to be transported over long distances, arriving to regions where they have never been produced or used.

Since 2001, an international treaty is adopted, namely "The Stockholm Convention on Persistent Organic Pollutants". It was intended to reduce and to eliminate the production, use, discharge and storage of these type of substances. The mentioned Convention aims to reduce and eventually eliminate the release of 12 particularly toxic persistent organic pollutants, of which 9 were pesticides. Among them there is the hexachlorocyclohexane (HCH).

Non-aqueous phase liquid or NAPLs are liquid solution contaminants that do not dissolve in or easily mix with water (hydrophobic), thus resulting in a physical interface between a mixture of the two liquids (Huling & Weaver, US EPA, 1992). Nonaqueous phase liquids are divided into two general categories, dense (DNAPL)

and light (LNAPL), depending on whether they have a higher or a lower density compared to water.

The compounds found in the NAPL are not prevented from solubilizing into the groundwater, but their solubility is generally much lower than the quantities present in the environment. In fact, what typically happens when a DNAPL moves and accumulates at the bottom of the aquifer, is the continuous dissolution, according to the chemical property of the compound, of the pollutants present in the NAPL, which act as a secondary source of contamination (Yong, Fukue, & Mulligan, 2006).

Generally, DNAPLs in aquifers, are halogenated/non-halogenated semi-volatiles and halogenated volatiles, which are typically found in wastes and waste-producing processes from solvents, wood preserving products, coal tars, and pesticides. The most frequently found contaminants are chlorinated solvents.

Among those hydrocarbons, Hexachlorocyclohexane (HCH) is a compound developed in the twentieth century and used agriculture (Fernández J, Arjol MA, Cach C; 2013). This substance is formed by a six-carbon ring with a chlorine and a hydrogen bond to each ring carbon and it belongs to the chemical family of chlorinated hydrocarbons and to organochlorine pesticides. Among the isomers of this compound appears "Lindane", the gamma-isomer.

In Aragon, the biggest producer of lindane was INQUINOSA (Industrias Químicas del Noroeste Sociedad Anónima), which in 1975 started the manufacturing and commercialization of lindane.

As a product of its activity, INQUINOSA generated different types of waste that had to be disposed: between 1975 and 1983 this was done in Sardas landfill, and from 1984 to 1992, in Bailin landfill, specifically set up to host them. The two landfill sites, together with the former production site, are recognized source of environmental pollution (J.Fernandez, M.A. Arjol, C. Cacho; 2013).

One of the most important characteristics of this site is the Sabiñánigo reservoir, installed for irrigational and energetical uses of the water, which determine oscillations in water level in addition to the natural seasonal and daily variations. Those oscillations influence the groundwater flow and, consequently, the mass transport significantly.

Those implications can be studied and evaluated using a numerical modeling, which is widely used in groundwater decontamination and monitoring, due to the importance of understanding subsurface flow problem in order to apply any kind of reclamation technique, particularly when variations of the water level determine changing in hydraulic gradient and flow direction.

Groundwater Modeling has been developed mostly in terms of Finite Differences, i.e. discretizing the numerical solution of flow and transport equation on a regular grid.

Despite its simpler formulation, finite differences do not allow to evaluate the flow on a non-regular domain, e.g. allowing local refinements to improve the computational (Anderson, Woessner, & Hunt, 2002).

The flow modelled with a Finite Element software allow a more detailed representation of the real domain, due to the possibility to build a non-regular "grid" composed of different size elements. Those local refinements result in a more detailed simulation of the flow, especially in those part of the domain where the solution of the flow and mass transport equations involves in high variation in a short time, needing spatial and temporal appropriate discretization, e.g. points very close to a mass source (Hans-Jörg G. Diersch, 2014).

By using the Finite Elements approach is intended to evaluate the flow and the mass transport considering the challenge of the oscillation of the reservoir, in order to evaluate the possibility of a surfactant enhanced aquifer remediation technique.

To goal those objectives, the finite element groundwater modeling is used in two temporal periods in order to create a valid model useful in different situations, that could be implemented in future in order to evaluate variable density flow problems (NAPLs) and possible reclamation techniques.

Not only the modeling is used to achieve those objectives, but it is also used the numerical estimation of parameters that were not measured or that are difficult to evaluate in field.

The remaining part of this work is divided as follow:

- Chapter 2 "Materials and Methods", which describes geographical, geological, hydrogeological framework, the contamination, the conceptual model of the site, the tools and the related setup used for the groundwater modeling;
- Chapter 3 "Results and Discussion", where the results of the simulation of the groundwater modeling are presented, discussed and analysed based on the characteristics of the site and on its current knowledge.
- Chapter 4 "Conclusions", where the work of this thesis and the findings obtained are resumed and evaluated with respect of the purposed objectives

## 2 Materials and Methods

### 2.1 Description of the site

#### 2.1.1 Geographical framework

The contaminated site is located in the northwest area of the Iberian Peninsula that corresponds to the Aragon Pyrenees, in the province of Huesca, between the municipalities of Sabiñánigo and Sardas. Their location is shown in Figure 2.



Figure 2: location, in Spain, of the province of Huesca, with the location of Sabiñánigo in the focus

The site, reported in Figure 3, is limited on the north by a natural marl outcrop and by the Gallego river, which is collected by the reservoir located on the left of the site, defining the west limit. The marl outcrop follows the perimeter of the site from the north, through the

N330 highway, to the south, defining the eastern and southern limits of the study area.

The Sardas landfill, the source of contamination, is located on the E-SE part of the site, occupying an area of around 4 hectares beside the Gallego river. A reservoir with a surface of 27 hectares was created as a dam was built in 1965 on the course of the river, in the municipality of Sabiñánigo for the production of electricity by the Eléctricas Reunidas de Zaragoza and for agricultural irrigation.

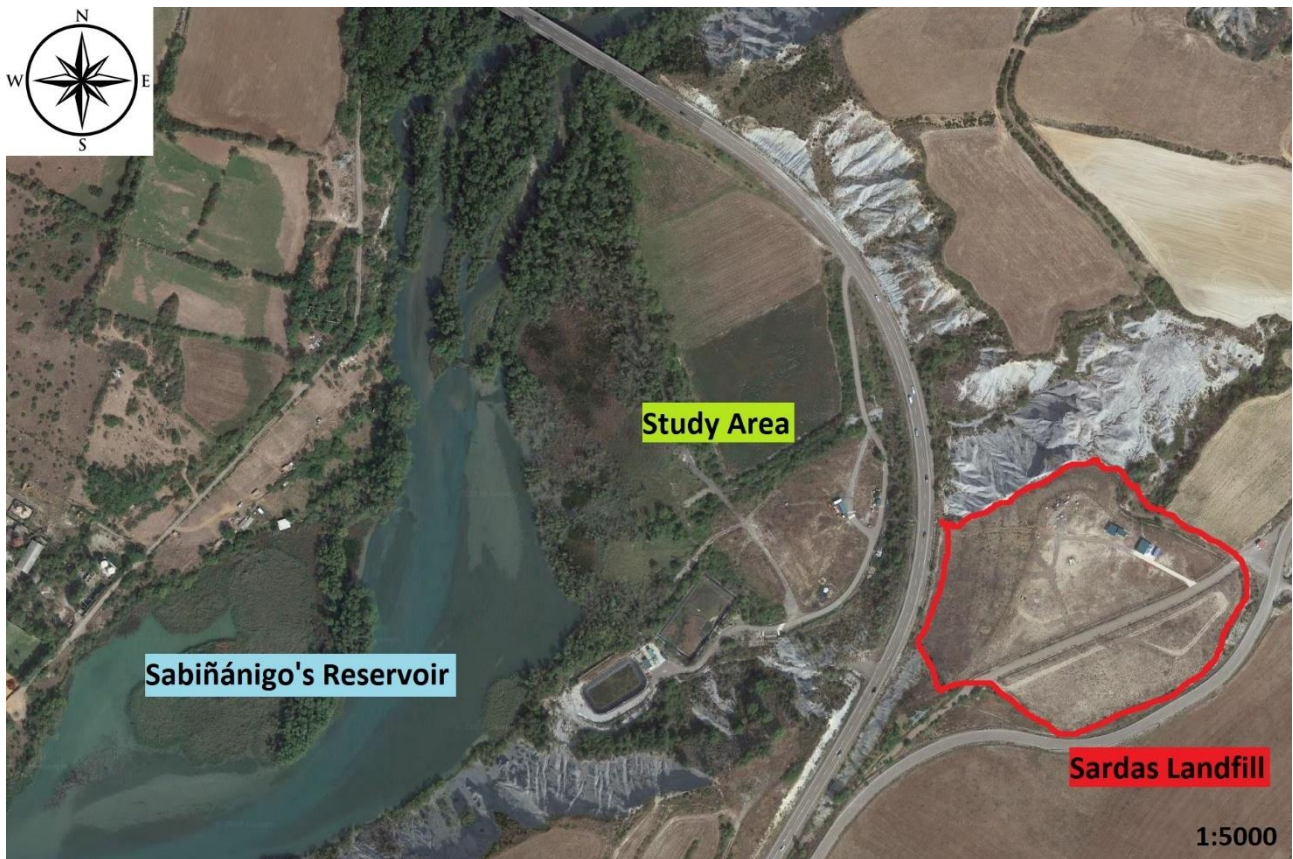


Figure 3: view of the site from satellite (from Google Satellite)

### 2.1.2 Geological framework

The geological framework of the site is in the Southern Pyrenees Area, which is characterized by the vergence in the south direction of the structures, the spatial continuity of the pre-tertiary sediments over all Aragon and finally the tectonic activity that was developed during the Tertiary, which strongly conditioned the sedimentation of materials.

During the Tertiary period, a series of overlapping thrusts led the Basin of the Southern Pyrenees to be a foreland basin. The formation of this basin is a complex process, since it was generated in orogens produced by the continental collision with the Pyrenees.

When this process was carried out, topographical differences were generated between the orogen and the basin, producing two simultaneous processes as the erosion of the orogen and sedimentation within the basin, which generated that the evolution of the basin (Barnolas and Gil-Pena, 2002).

At the end of the Lower Eocene and the beginning of the Middle Eocene, a division of the Southern Pyrenees Basin occur, due to the tectonic activity, which caused the formation of two sub-basins: the Tremp-Graus basin in the east and the Jaca-Pamplona basin in the west.

The study area is located in the Jaca-Pamplona sub-basin, shown in Figure 4, which corresponds to sheet 177-Sabiñánigo of the geological map of the MAGNA series in scale 1:50,000. (IGME, 2012). The table below reports the legend of the geological lithotypes.

The main geomorphological forms found in the area are relate to the processes of erosion and sedimentation around the valley of the Gállego river and the glaciers. This activity formed the depression valleys characteristic of the glaciers, glacis and terraces on both sides of the river, as well as alluvial fans and dejection cones.

In this case study we can distinguish four different geological layers: an anthropic filling located in the most superficial part, silt, gravel due to the fluvial deposit of the Gállego river and gray marls in the deepest zone.

These layers are represented in the cross section shown in Figure 6.

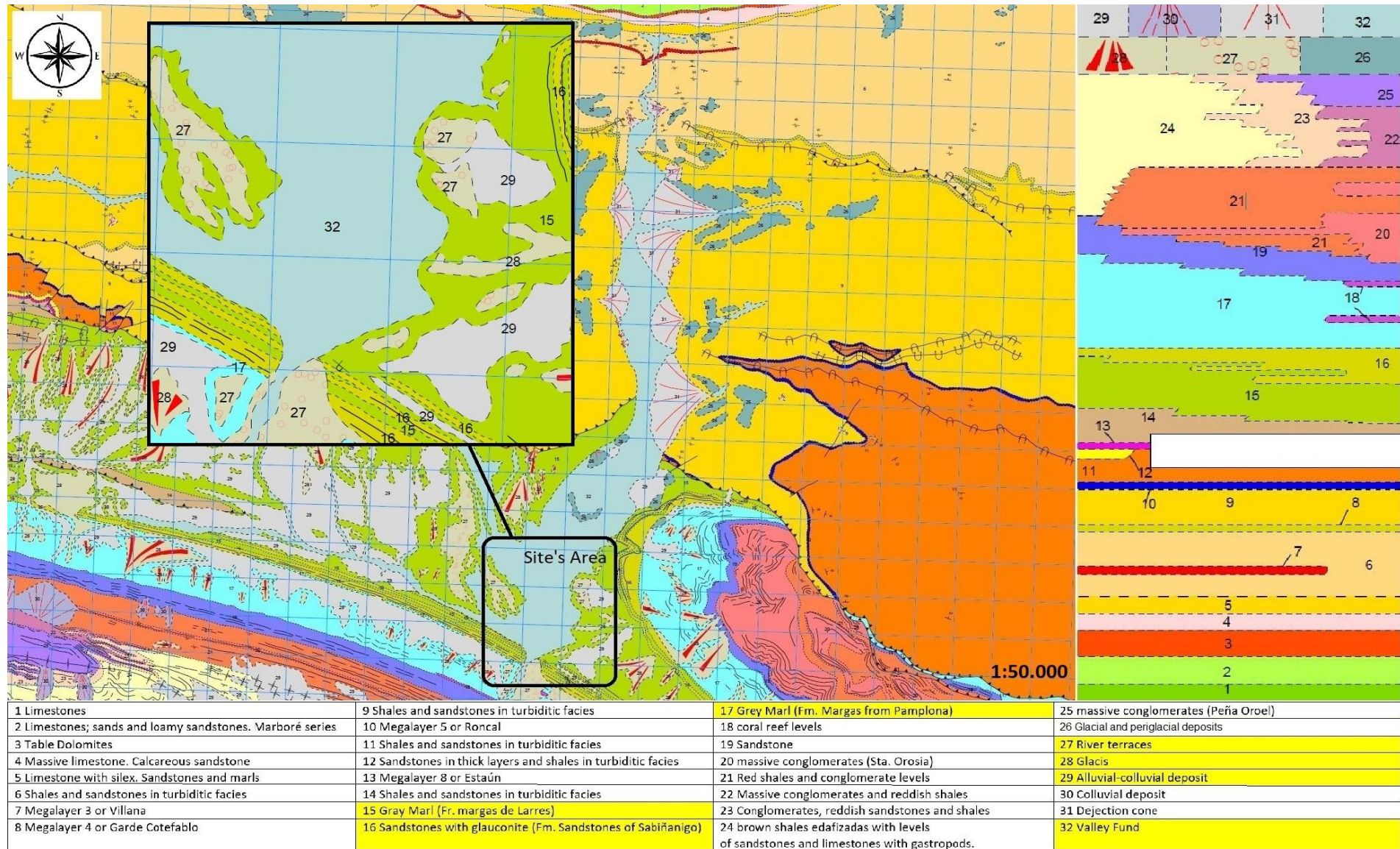


Figure 4: sheet 177 (Sabiñánigo) of the geological map of the MAGNA series in scale 1:50.000 (IGME, 2012), in the table below the legend of the sheet 177 is reported highlighting the lithotypes present in the study site



*Figure 5: linear profile of the cross section of the site*

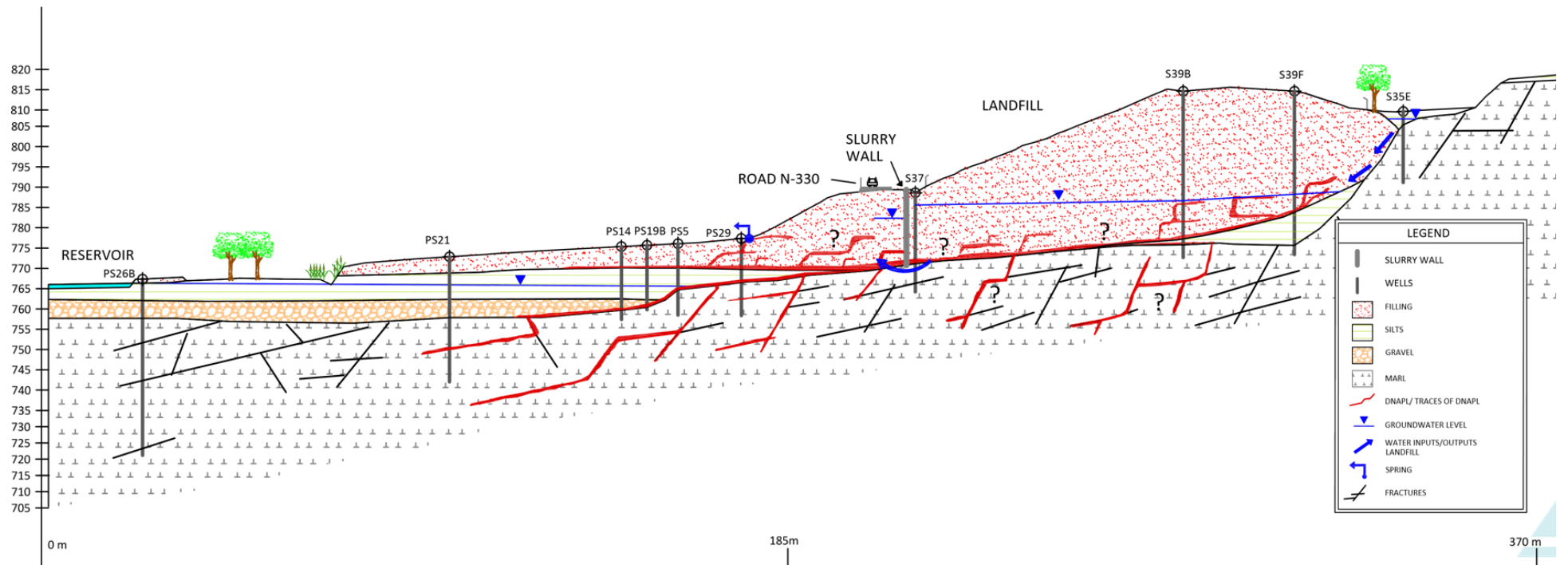


Figure 6: cross section of the study area, from “Strategic Environmental Action Plan against lindane waste contamination in Aragon” (Gobierno de Aragon and EMGRISA, 2016)

Materials that are deposited above the marl layer belong to the Quaternary, are composed of silts and an alluvial formed by sands and gravel with a thickness of approximately 15 meters of power. The presence of these materials is due to the alluvial deposit of the Gállego River. At site, the gravels come in contact with the marls in the area Southwest, since in this area is where the outcrop occurs.

An anthropic filler is deposited on the quaternary materials from the old Sardas landfill and later with the materials from the construction of the N-330 road (bypass of Sabiñánigo), with a thickness of 4 meters. This filling is the most recent material that we found in the area, since the deposit was carried out at the end of the 20th century.

Below this material there is a layer formed by sandy silts that has materials of different sizes. This layer has a depth of about 8 meters, reaching up to 12 meters deep. In this same layer the phreatic level is located of the aquifer to about 9 meters deep.

Between 12 and 16 meters are the sands and gravels that make up the layer alluvial and is where the aquifer is located. It consists of materials from great variety of sizes coming from the deposit of the Gállego river.

Finally, the deepest layer that corresponds to the marls. This layer is considered impermeable and acts as an aquifer wall to be waterproof, reaching a depth of 24 meters. Despite its very low permeability, this layer presents fractures that make possible the migration of water and possible contaminants through them.

### *2.1.3 Hydrogeological framework*

The site is close to the Sabiñánigo reservoir, which is supplied by the water provided by the river Gállego which belongs to the Ebro river basin. The river runs in a north-south direction from the Tena Valley, located in the north of Sabiñánigo, until its junction with the Ebro River, which then passes through Zaragoza. The river's waters are subject to extensive regulation and derivation during its course, thus when it flows into the Ebro its discharge is just some 10 percent of its natural discharge.

The Sabiñánigo reservoir is characterized by a non-stable water table oscillating between 764 and 766 meters of elevation above sea level, due to the rainfall that occurs in the area and the variations in the water level in the reservoir connected to the uses of the water of the reservoir, irrigation and electrical, and to the natural daily and seasonal water level variations ( LI2GA & MENODES, CARESOIL; 2016).

Figure 7 shows the oscillations of the reservoir in the summer and winter season of the 2018.

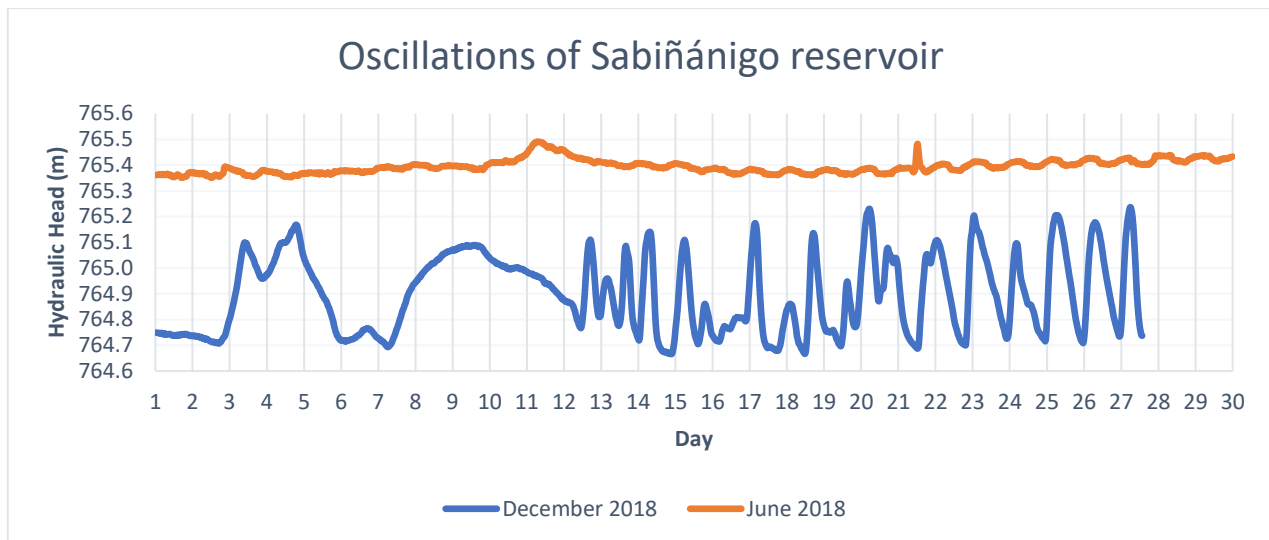


Figure 7: oscillations of the reservoir in the summer and winter season of 2018, the series of December is partially complete (source: EMGRISA's hydrogeological monitoring for the Government of Aragon).

These variations are unusual and, at least in Italy, very uncommon and strongly characterizing the behaviour of the aquifer, which piezometric level is at about 766m above sea level. That correspond to a depth to water table of approximately 5m under the area of the filling material near the reservoir, growing up until about 9-10m under the area relative to the same layer, but in correspondence of the piezometers located near the road N330, on the left (Figure 6). Between the N330 and the end of the slope relative to the road, the piezometric level is unknown.

The direction of flow of the site has a Northwest component, although it is affected by the extractive activity of the numerous piezometers that are in the area and that are used to carry out pumping tests. A representation of the flow is shown in the piezometry shown in Figure 8.

Due to the geology and the lithologies that the area presents, we find an aquifer of confined type. This is due to the presence of a low permeability layer formed by silt in the upper part of the aquifer that prevents the filtration of rainwater from the outside to the gravel layers, and a impervious layer in the deepest zone, which coincides with the fractured marls, which prevents the water from continuing to migrate to deeper layers and acting as an aquifer wall.

The problem with these marls is that they do not act as an insulating layer, but because they have fractures, the pollutant and the water present in the aquifer can migrate to other areas further away from the contaminated area.

The unconfined aquifer is it characterized by an anisotropy concerning its hydraulic properties, as confirmed by a pumping test done in April 2018, which results are reported in Figure 11. The location of all the piezometers used in the monitoring of the site are shown in Figure 9.

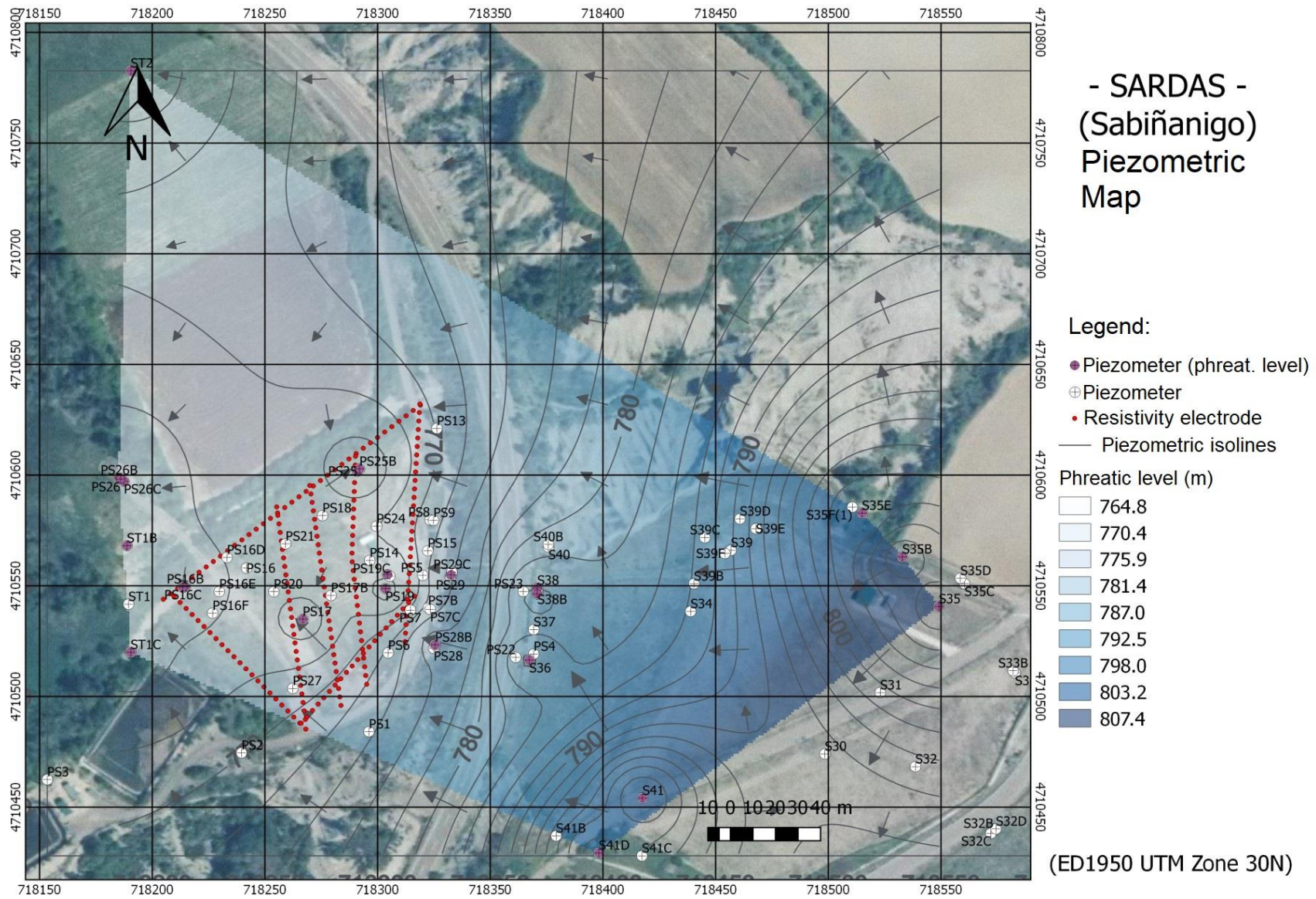


Figure 8: piezometry of the site, with the courtesy of LI2GA Y MENODES and CARESOIL (2016)

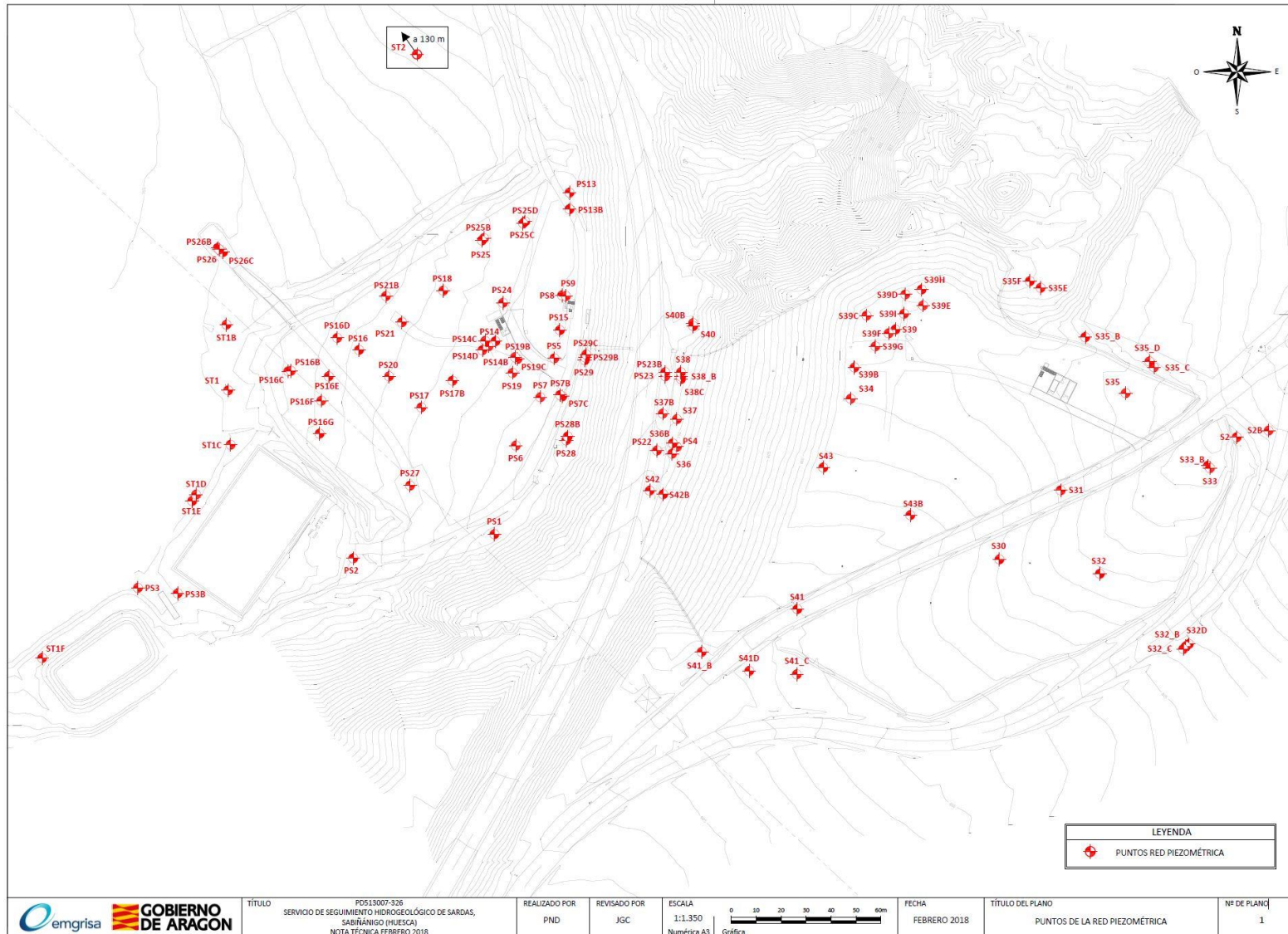


Figure 9: location of piezometers in the site and in the landfill, with the courtesy of EMGRISA

A focus concerning the piezometers used in the pumping test is shown in Figure 10.

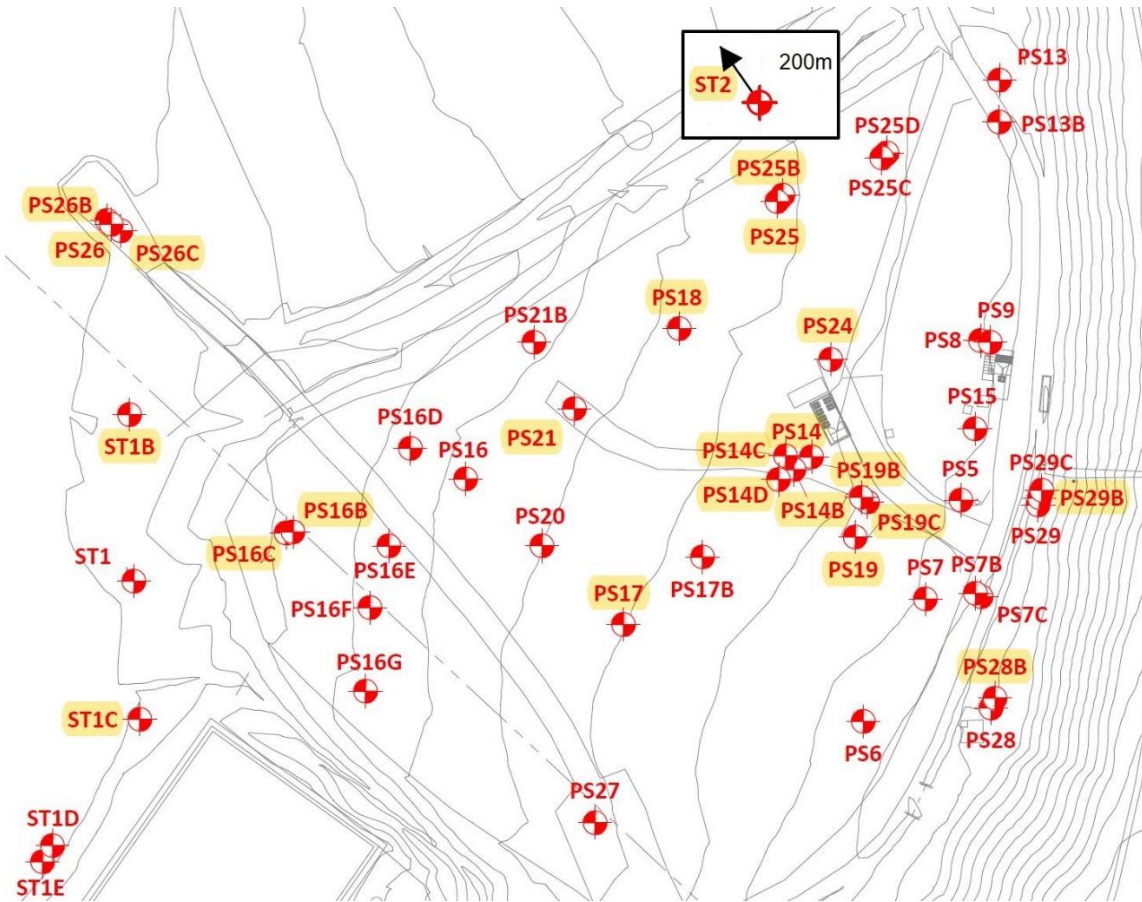


Figure 10: piezometers used in the pumping test done in April 2018, highlighted in yellow

For what concern the pumping test, it was conducted by Gobierno de Aragona, EMGRISA, INPROQUIMA (UCM), MENODES (UPM), LI2GA (UPM) in the context of the monitoring plan of the site, on the 26<sup>th</sup> of April 2018.

The test lasted 12h (720 min) by pumping a constant flow rate of 86.88 m<sup>3</sup>/d in the well PS-14B. This well is characterised by a diameter of 4'' and a screening level which cover the entire sandy gravel layer. The casing of the well is composed of bentonite and of gravel for the screened part. The porosity of the drain material around the screening, gravel, is about 0.25

While performing the test, the water level drop in the monitoring piezometers has been registered in continuous in order to obtain the parameters of interest for an unconfined aquifer.

The results of the pumping test are shown in Figure 11.

**SARDAS: ensayo de bombeo (26/04/2018)**

Duración: 720 minutos

Caudal de extracción: 86,88 m<sup>3</sup>/día

Sondeo	Acuífero		r (m)	T (m <sup>2</sup> /día)	S	k (m/día)	Observaciones
	Profundidad (m)	Potencia (m)					
PS14B	12,5 - 15,5	3,00	0,00	530,0		1,8E+02	Pozo de bombeo
PS14	12,8 - 15,7	2,90	3,50	691,4	2,0E-03	2,4E+02	
PS14C	12,3 - 15,4	3,10	2,50	691,4	2,2E-04	2,2E+02	
PS14D	12,7 - 16,1	3,40	3,00	727,8	1,7E-03	2,1E+02	
PS16B	7,12 - 12	4,88	80,00	622,2	2,8E-03	1,3E+02	
PS16C	7 - 11,8	4,80	81,10	1.728,4	2,0E-03	3,6E+02	
PS17	12,4 - 15,7	3,30	36,30	843,1	2,0E-04	2,6E+02	
PS18	10,7 - 14,6	3,90	29,27	829,6	9,0E-04	2,1E+02	
PS19	13,7 - 15,5	1,80	13,85	691,4	2,9E-04	3,8E+02	
PS19B	13,9 - 15,3	1,40	11,06	576,1	7,5E-04	4,1E+02	
PS19C	-	0,00	12,23				Limos. No afectado
PS21	10,5 - 15	4,50	36,41	777,8	5,4E-04	1,7E+02	
PS24	12,7 - 15,1	2,40	18,69	829,6	4,1E-04	3,5E+02	
PS25	11 - 14,5	3,50	42,92	518,5	7,0E-04	1,5E+02	
PS25B	11,2 - 13	1,80	43,87	777,8	5,1E-04	4,3E+02	No llega a las margas
PS26	4,9 - 9,1	4,20	115,10	622,2	4,9E-04	1,5E+02	
PS26B	4,9 - 9,1	4,20	115,88	307,3	2,4E-03	7,3E+01	
PS26C	5 - 9,1	4,10	113,28	414,8	2,2E-03	1,0E+02	
PS28B	-	0,00	47,56				Limos. No afectado
PS29B	-	0,00	38,70				Relleno. No afectado
ST1B	5,8 - 8,8	3,00	105,67	518,5	9,0E-04	1,7E+02	
ST1C	4,9 - 8	3,10	110,74	691,4	7,0E-04	2,2E+02	
ST2	6 - 10,6	4,60	246,65	518,5	4,7E-04	1,1E+02	

Figure 11: resuming table of the pumping test, the table, in Spanish, shows from left to right respectively: piezometers of interest, height of the 3<sup>rd</sup> layer in that point, influence radius, transmissivity, specific yield, hydraulic conductivity and general observations on the piezometer.

These values obtained show the range of variability of the characteristics of the aquifer, detecting an anisotropy in terms of hydraulic conductivity, which vary in a range of 73 m<sup>3</sup>/d to 430 m<sup>3</sup>/d, and consequently in transmissivity. There are also variations of specific yield over an order of magnitude, from 2e-4 to 2.8e-3.

For what concern the hydraulic characteristics of the top layer (filling material) and the 2<sup>nd</sup> layer (silts) a summary is reported in Table 1.

Those values have been provided by a previous finite differences groundwater model carried out by EMGRISA and AZENTUA (another society which has cooperated within the monitoring of the site). This model can provide the order of magnitude of the properties of those layers giving an idea of the characteristics of the site.

In this work, this model has been used in order to reproduce the layers elevation, using the height values relative to the cell-centres of the finite difference grid of the model as will be further discussed. Moreover, the model parameters have been used as starting values for the parameter estimation (PEST), that will be also further discussed, for those properties that were not measured in field.

Table 1: resuming table of the soil's unknown parameters assigned in the model, basing on the model carried out by EMGRISA/AZENTUA

<b>K<sub>x-y</sub> (m/d)</b>	
<b>Layer 1: anthropic filler</b>	0.01
<b>Layer 1: hydraulic connection</b>	0.1
<b>Layer 2: reservoir</b>	0.01
<b>Layer 2: hydraulic connection</b>	0.1
<b>Layer 2: silt</b>	1
<b>K<sub>z</sub> (m/d)</b>	
<b>Layer 1: anthropic filler</b>	0.001
<b>Layer 1: hydraulic connection</b>	0.01
<b>Layer 2: reservoir</b>	0.001
<b>Layer 2: hydraulic connection</b>	0.01
<b>Layer 2: silt</b>	0.1
<b>Specific Storage (1/m)</b>	
<b>Layer 1</b>	0.006
<b>Layer 2: footprint of layer 1 on layer 2</b>	1.8e-4
<b>Layer 2: reservoir</b>	0.002
<b>Layer 2: silt</b>	0.003

The differentiation inside each layer is discussed in section 2.2.1, concerning the conceptual model of the site.

#### 2.1.4 The Contamination

Sabiñánigo is a small industrial city that developed the most activity during the 20th century, because many chemical companies decided to settle there, because of the amount of energy that could be obtained from the waterfalls found in the zone helping the production of hydroelectric energy. In the Gállego River, there are a total of 6 hydroelectric plants and 29 dams and weirs, with the Biescas plant controlling the Sabiñánigo reservoir and supplying the local industry.

One of those industries, the biggest producer of lindane in Aragon, was INQUINOSA (Industrias Químicas del Noroeste Sociedad Anónima). In 1975 the factory started the manufacturing and commercialization of lindane generating different types of waste that had to be disposed: between 1975 and 1983 this was done in Sardas landfill, and from 1984 to 1992, in Bailin landfill, specifically set up to host them. Between 1988 and 1992 INQUINOSA started to import lindane and to elaborate commercial formulations. In 1994 the factory closed and remained abandoned.

It is thought that 7.000 tonnes of solid waste per year and about 300-600 tonnes per year of liquid were produced (European Community, Ministerio de Hacienda y Administraciones Públicas, Subdirección General de Administración del FEDER) (Gobierno de Aragon & EMGRISA, 2016).

The greatest volume of waste generated was constituted by isomers of HCH, but also water treatment sludges, packaging, lindane production surpluses.

Five HCH isomers can be formed from this structure:  $\alpha$ -HCH,  $\beta$ -HCH and  $\gamma$ -HCH,  $\delta$ -HCH and  $\epsilon$ -HCH, which differ only by the orientation of the chlorine atoms in the molecule. From the Second World War to 1990, the most commonly used isomers in the world were  $\alpha$ -HCH,  $\beta$ -HCH and  $\gamma$ -HCH.

Lindane, the specific compound of interest, is the gamma isomer of hexachlorocyclohexane and it is represented in Figure 12. In Table 18, reported in the Appendix C, a detailed resume of its chemical property is presented.

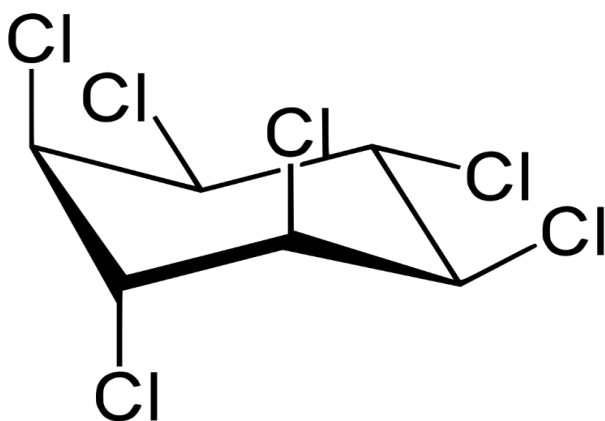


Figure 12: representation of the gamma-isomer of HCH, source Wikipedia

During the 60's, diverse types of residues were dumped close to the Gallego river, including the industrial waste from the lindane manufacturing as well as wastes from other chemical industries: HCH solid and liquid waste, mercury, caustic soda, hypochlorite, dichromate, ditiocarbamates, urban waste, construction and demolition waste.

Once Sardas landfill was filled up, it was abandoned in the 80's, reaching a volume of more than 400.000 m<sup>3</sup> of waste. Between 50.000 to 80.000 m<sup>3</sup> of HCH solid waste and 3.000 m<sup>3</sup> of HCH liquid waste (DNAPL) were dumped there. When the N330 diversion was constructed, at the beginning of the 90's, around 50.000 m<sup>3</sup> of waste, due to the construction, from the landfill was moved to the bottom part of the site.

After the construction of the N330 diversion, the landfill's surface and sides were isolated with the construction of perimeter and front walls of concrete-bentonite and then the landfill was sealed with a high density thermosealed polyethylene layer, covered by a drainage layer of gravel and a layer of topsoil. About 50.000 m<sup>3</sup> of residues deposited in the lower part of the site during the diversion construction were not included in the sealing and remained beside the contiguous reservoir.

The landfill site is recognized as a source of environmental pollution (Gobierno de Aragon & EMGRISA, 2016) (J.Fernandez, M.A. Arjol, C. Cacho; 2013).

DNAPL is the substance that presents the greatest problems for its removal because it migrated from the most superficial layer of anthropic fill, where the waste was deposited, to the alluvial layer, where is the aquifer. Due to its greater density, the liquid continued to advance until it moved to the lower part or wall of the aquifer, where it ran into the marls.

Under normal conditions, the low permeability of this material would have slowed the DNAPL advance, producing an accumulation of the substance at that point and its presence would not have been detected, but the presence of these fractures led to the mobilization of the compound in favour of the hydraulic gradient found in the area (Northwest), causing it to sprout on the shoulder of the road threatening the contamination of the reservoir that is close to the site and that serves as a supply to the city.

In order to detect the polluted area, an electric tomography has been conducted by Gobierno de Aragona, EMGRISA, INPROQUIMA (UCM), MENODES (UPM), LI2GA (UPM). The campaign consisted in the realization of seven geoelectric profiles, distributed throughout the study area, as shown in Figure 13. The device used was a Wenner-Schlumberger type, trying to reach the maximum lateral resolution for the fixed study depth (maximum 15 meters). The study minimum distance between electrodes used was 4 meters, measurements were taken in 10 study levels, reaching a depth slightly higher than 15 meters.



Figure 13: profiles used in the electric tomography test

The resistivity values obtained in the area are generally low, represented in a scale between 1 Ohm·m and 200 Ohm·m, from blue to red respectively. The tomographic sections obtained under the measured profiles are presented in Figure 14. In these sections it can be seen the differentiation of the following geoelectric horizons:

- An anthropic resistive surface horizon: this level has a thickness that reaches 5 m depth, resistivity values vary mainly between 60 Ohm·m and slightly more than 200 Ohm·m. This is found along the entire profile in profiles 1 and 6. Profiles 2, 3 and 4 have lateral variations with decreases in resistivity up to 20 Ohm·m. In profile 2 between 24m to 28m and 60m to 72m, in profile 3 between 48m to 68m, and in profile 4 between 3m to 60m and from 84m to the end of the profile. In the case of profiles 5 and 7 the values of this level vary between 20 and 50 Ohm·m.
- A second very conductive horizon that reaches, from the previous level, a depth between 10m and 13m according to the profile, except in profile 5 that reaches the maximum depth of study. This level has values of resistivity close to 1 Ohm·m and is associated with the presence of pollutants in the water of the formation. By the distribution of the anomalies it is possible to think that there are two differentiated zones of pollutants, one located towards the south of the profiles, with the most conductive values and with a greater extension in depth, and another located in the northern half of the sections, with somewhat less conductive values and a greater lateral extension.
- A third horizon of average resistivity with values of resistivity between 20 and 60 Ohm·m, except in profile 1 in the rest does not find sufficiently defined to the maximum depth of study. As this is the longest profile, it is also where the most depth data have been collected, therefore it is likely that this level corresponds to the resistivity values of the marls.

Due to the results of the tomography tests, which show a non-homogeneity of the distribution of the pollutant in the soil, is it possible to think that the flow finds subzones with different characteristics, bringing it to follow different pathways.

This anisotropy has been confirmed by the pumping test done in April 2018 already presented, which results have been shown in Figure 11.

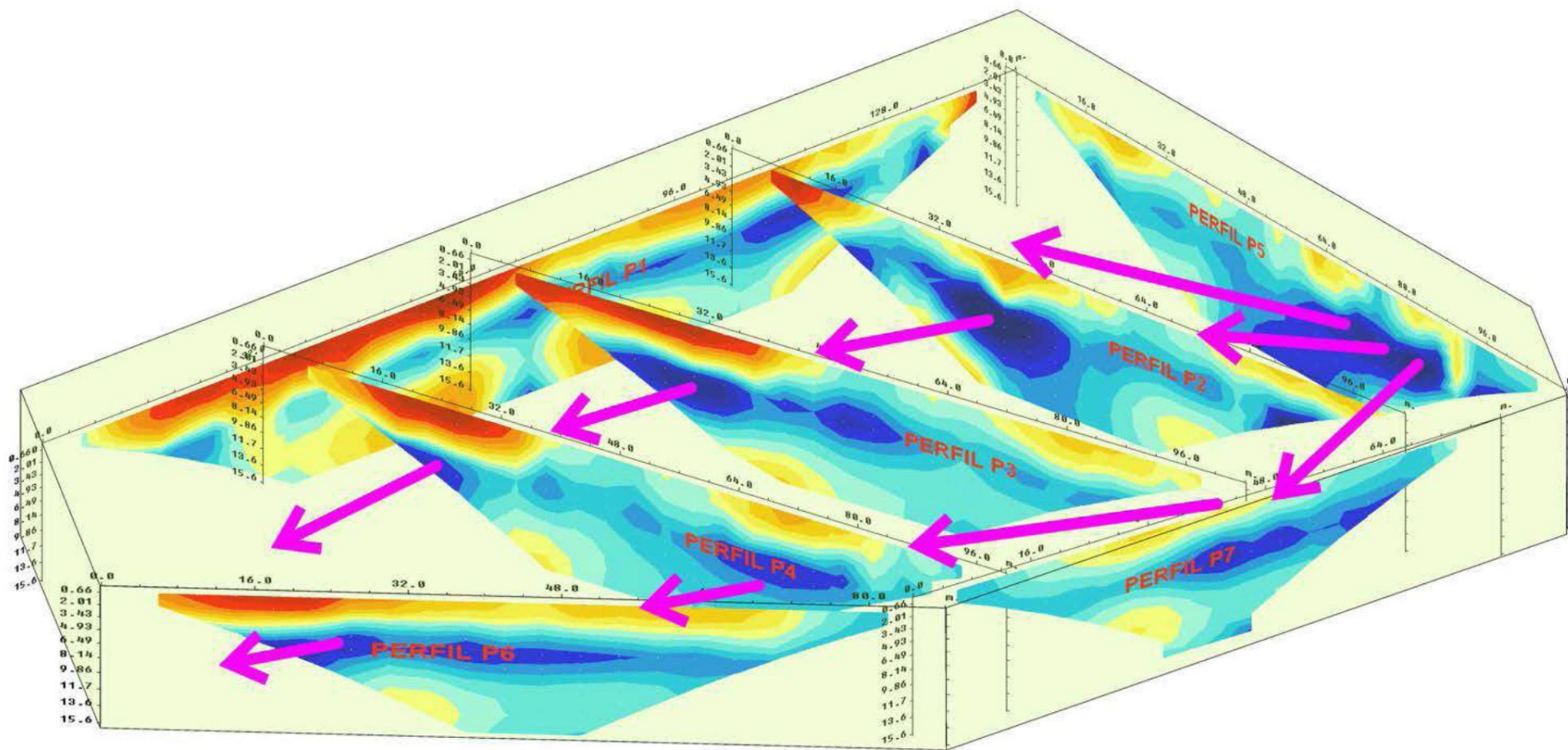


Figure 14: results of the tomography test, in violet the preferential pathway of the flux

## 2.2 Groundwater Modeling

### 2.2.1 Conceptual model of the site

A conceptual model can be defined as a qualitative representation of a groundwater system that obeys to hydrogeological principles and is based on all the information inherent to the behaviour of soil, flux and mass transport. Design of a conceptual model should typically consider those data sources: geomorphology, geology, geophysics, climate, vegetation, soils, hydrology, hydrochemistry/geochemistry, and anthropogenic aspects (Kolm K, Van Der Heijde P, 1996).

A conceptual model should include the characterization of both the hydrogeological and hydrologic systems. A conceptual model for most groundwater flow, at a minimum, should include information on boundaries; hydrostratigraphy and hydrogeologic properties; flow directions and sources and sinks; and a field-based estimate of components of the groundwater budget (Anderson, Woessner, & Hunt, 2002).

According to the above-mentioned principles, the conceptual model of the Sardas site was developed and is hereby described

The contamination problem starts from Sardas landfill, where the leachate is naturally generated due to the weight of the wastes deposited and due to the rainfall infiltration. The leachate starts flowing to the reservoir passing through the anthropic filling layer. Between the landfill and the N330, there is no evidence of the presence of the sandy silt layer and of the sandy gravel layer, because of this part of the site was created during the construction of the landfill, and then of the N330. The filling soil deposited on the natural marl outcrop let that the leachate flows above the marl layer, for its very low permeability and for its gully shape, following the gradient directed to the reservoir.

Below the N330, a slurry wall was installed to increase the stability of the soil on which the road is build. The slurry wall bounds the flow all over the filling and the marl layer. The high difference in hydraulic head generated by the wall triggers the preferential flow through fractures in the marl layer, thus by passing the slurry wall.

The 3D stratigraphic and hydrogeological model was developed based on these assumptions.

Under the road N330 the flow meets a hydraulic connection with a higher conductivity, which brings into contact the filling soil, principally of clay and therefore not conductive, to the silty, and to that formed by gravel and sand, more conductive. The nature of the hydraulic connection is not well known, it can be represented from an outcrop of more conductive material due to fractures occurred in the past geological activity of the site or from a fracture itself.

The bottom layer, the gravel layer, is underneath the silty layer and, given its high conductivity, is strongly influenced by the oscillations of the reservoir. This layer it is also characterized from an unregular anisotropy, which determine differences in terms of hydraulic conductivity, porosity and storage inside this layer, which lead to different manifestations of the hydraulic head's oscillation observable in the monitoring piezometers. The reservoir is located above the silty layer, thus differentiating it into two zones with different characteristics, due to the transport of solids from the Gallego river, which typically obstruct the water body bed. In this layer must be differentiated from these two zones a third zone, located under the anthropic filling, which is characterized from lower compressibility due to the weight of the deposal above it and of the traffic of the N330.

Once passed the hydraulic connection, depending on the level of the reservoir, the flow can be subject to 2 different situations:

- If the level of the reservoir is below the hydraulic level of the groundwater, the gradient will be directed to the reservoir, and the flow will follow the natural pathway until the reservoir, on the base of the material properties of the layer
- If the level of the reservoir is higher than the hydraulic head of the groundwater, the gradient will be directed in the opposite direction, with the generation of two different opposite flows that will have to be managed by the layer: a new stable level will be reach, every time that an oscillation will occur, involving in a mass transport inside the layer, with a general increase of the hydraulic head in the monitoring piezometers.

A representation of the conceptual model is shown in Figure 15.

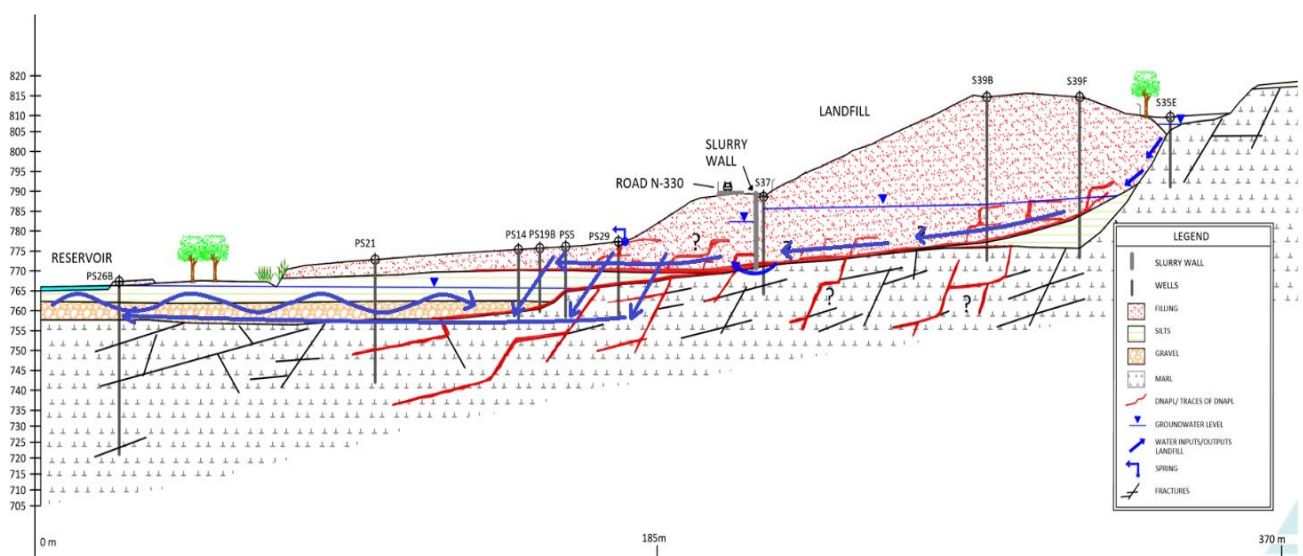


Figure 15: conceptual model of the site. With the blue arrows is it represented the conceptual flow from the landfill to the reservoir (horizontal line) and from the reservoir to the 3rd layer (wavy line)

### 2.2.2 Description of the field tests carried out

Two tests were carried out in order to study the applicability of the Surfactant Enhanced Aquifer Remediation (SEAR) technique. Those field tests are the ones which are of interest in this thesis and that were simulated in the model.

The first test was carried out from 4<sup>th</sup> to 9<sup>th</sup> of June 2018, in which NaBr, a tracer, was injected to determine the effective porosity and the permeability of the gravel layer in order to evaluate the possible application of the SEAR. This test also includes an extraction phase realised to evaluate the possible removal of surfactant, to avoid its diffusion in the aquifer. As result of this test, the Br<sup>-</sup> concentration is measured.

The second test was carried out from 9<sup>th</sup> to 13<sup>th</sup> of July 2018, in which NaBr and a surfactant were injected and then extracted to perform the pilot test of the SEAR technique. Concentration of Br<sup>-</sup> and surfactant were measured during the injection and during the extraction of those compounds.

Both periods considered in the tests have a duration of 7200 min (5 days). For both tests were used the same monitoring piezometers and the same injection well. Their location is shown in Figure 16.

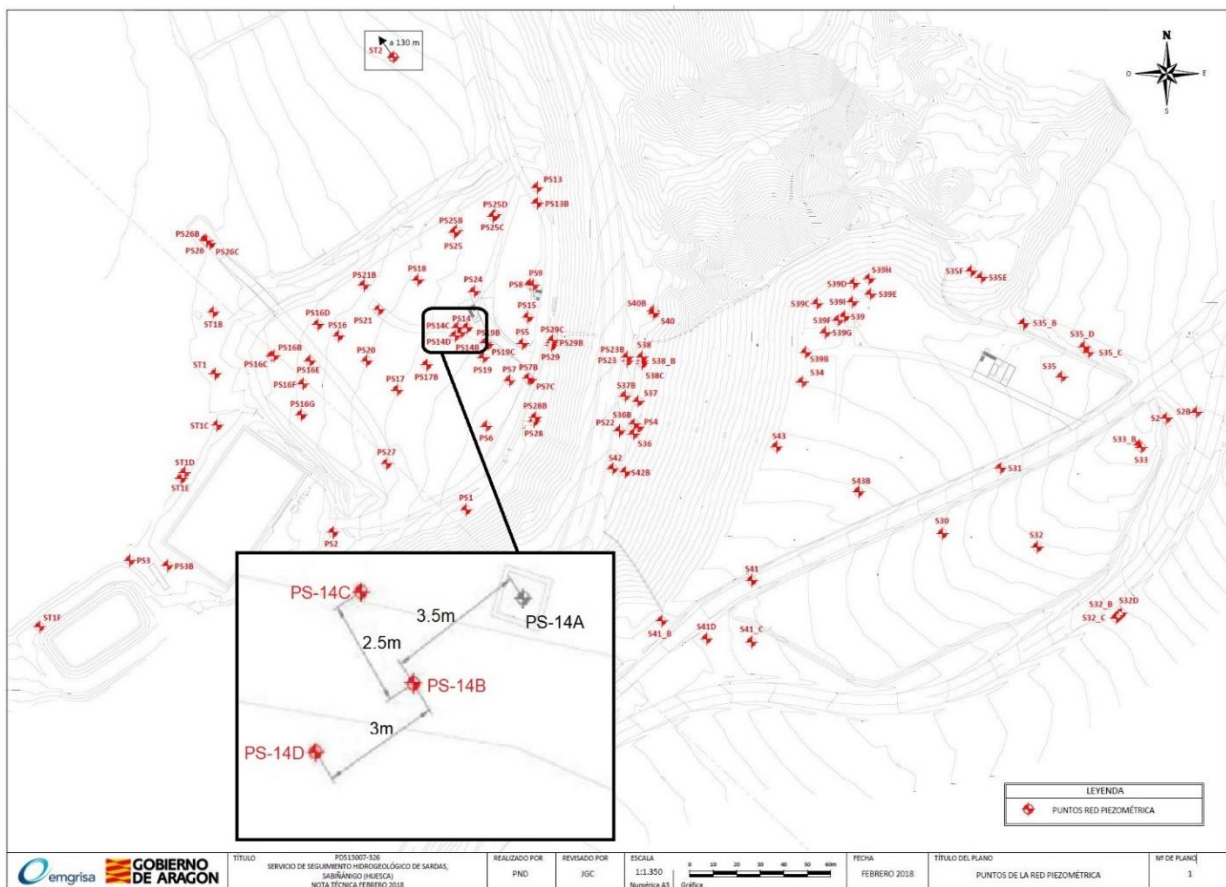


Figure 16: location of the piezometers and of the well used in the tests simulated

For what concern the characteristics of those well/piezometers and their location, a summary is reported in Table 2.

*Table 2: location (EPSG:32630) and characteristics of the injection well and of the observation wells*

<b>Well/Piezometer</b>	<b>X coordinate</b>	<b>Y coordinate</b>	<b>Screening layer</b>	<b>Distance from PS-14B</b>
<b>Inj. Well PS-14B</b>	-38295.2	5238402	3 <sup>rd</sup> layer	-
<b>Obs. Well PS-14A</b>	-38292.8	5238405	2 <sup>nd</sup> and 3 <sup>rd</sup> layer	3.5 m
<b>Obs. Well PS-14C</b>	-38297.1	5238404	3 <sup>rd</sup> layer	2.5 m
<b>Obs. Well PS-14D</b>	-38296.5	5238400	3 <sup>rd</sup> layer	3 m
<b>Well/Piezometer</b>	<b>Height</b>	<b>Max. Depth</b>	<b>Screening Depth</b>	<b>Diameter</b>
<b>Inj. Well PS-14B</b>	774.06 m	16.5 m	11.5-16.5 m	4''
<b>Obs. Well PS-14A</b>	774.15 m	18 m	6-18 m	3''
<b>Obs. Well PS-14C</b>	773.94 m	16.3 m	11.3-16.3 m	3''
<b>Obs. Well PS-14D</b>	773.92 m	16.9 m	11.9-16.9	3''

Must be note that the depth of the screening does not coincide with the exact height of the layer, reported in Figure 11, because those wells were screened also in the layers above and below, in order to confine the screening in the layer of interest.

Except for piezometer PS-14A, all wells were installed in 2018. The sampling depth for the concentration was at 15m for each piezometer, which can be considered as a medium depth for the gravel layer.

Concentrations has been measured with a Br-selective electrode "Metrohm" with crystal membrane for what concern the measures of the tracer and with the Gas Chromatography – Flame Ionization Detector (GC-FID) for the measures of surfactant.

About the measured hydraulic heads on the piezometers of interest for the two episodes of study, which are PS-14A, PS-14C and PS-14D, must be note that they have been working only in a part of 2018.

The measured hydraulic head in those piezometers over their working period is shown in Figure 17. Must be note that on some days the measures were not taken, due to malfunction of the equipment. That values were not considered in the model.

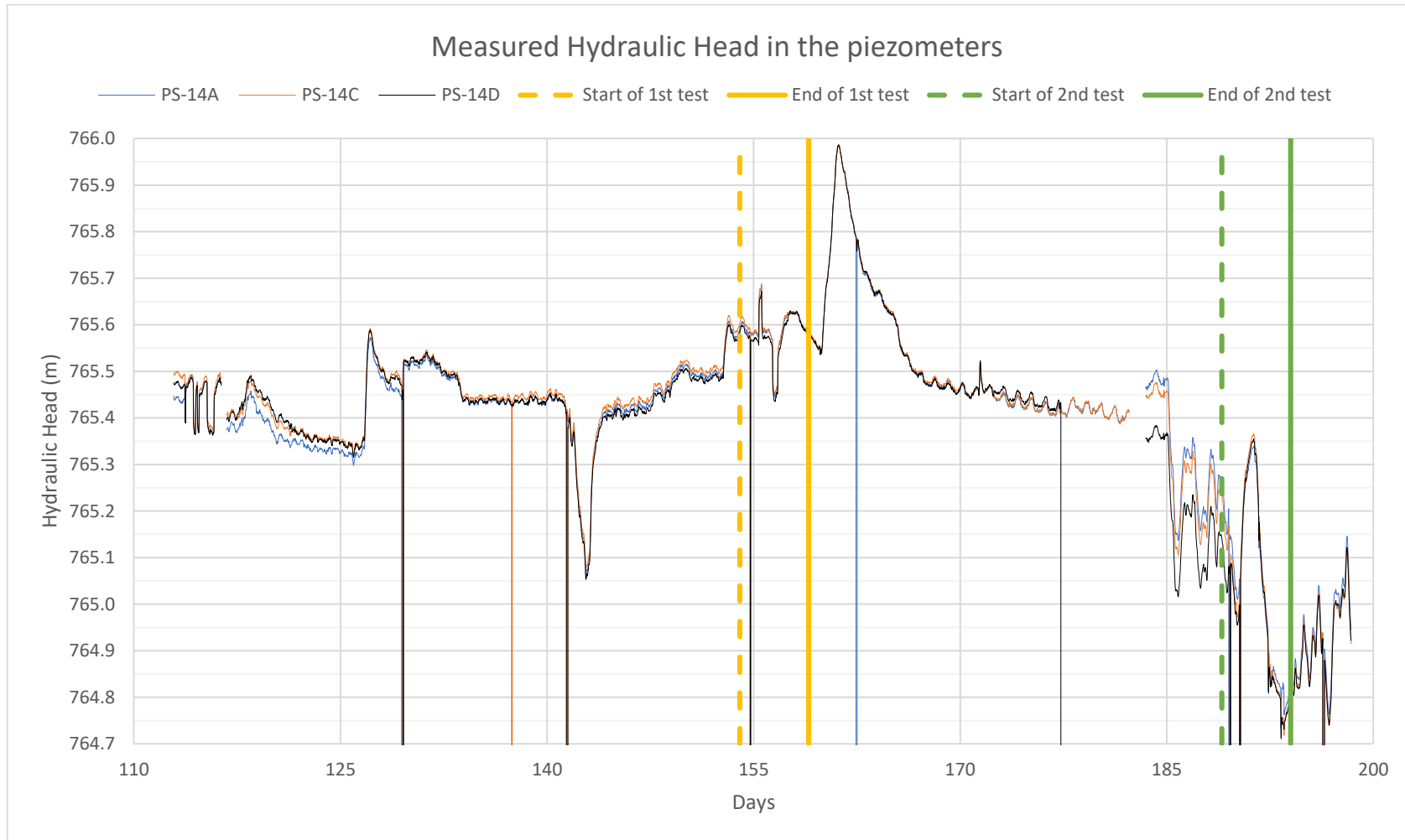


Figure 17: hydraulic head in piezometers for 2018, must be note that on some days the measures were not taken, due to malfunction of the equipment, assigning them a zero value in the model

The tracer test has been carried out in the week from 4<sup>th</sup> to 9<sup>th</sup> of June 2018.

The first day was prepared the injection of the tracer adding 3.33kg of NaBr (2.56Kg of Br<sup>-</sup>) in a 20m<sup>3</sup> tank filled with water. The theoretical concentration should have been 128 mg/l but was measured (with ion chromatography-IC) a value of 120 mg/l, which was used in the model. The error is within the experimental error.

On the 5th of June, at 10:00 the injection took place, until 15:06. The injection rate, 3.75m<sup>3</sup>/h, can be considered as constant all over this period. During this phase of the test Br<sup>-</sup> concentration has been measured 11 times, with the last one after an hour from the end of the injection.

On the third day the extraction phase took place. It started at 9:30 and lasted until 18:00. The pumping rate can be considered as constant over this period, with a value of 4.4m<sup>3</sup>/h. During the extraction, the tracer concentration has been measured 14 times.

The measured concentration in the piezometers of interest is reported in Figure 18, must be note that measures were not taken between injection and extraction.

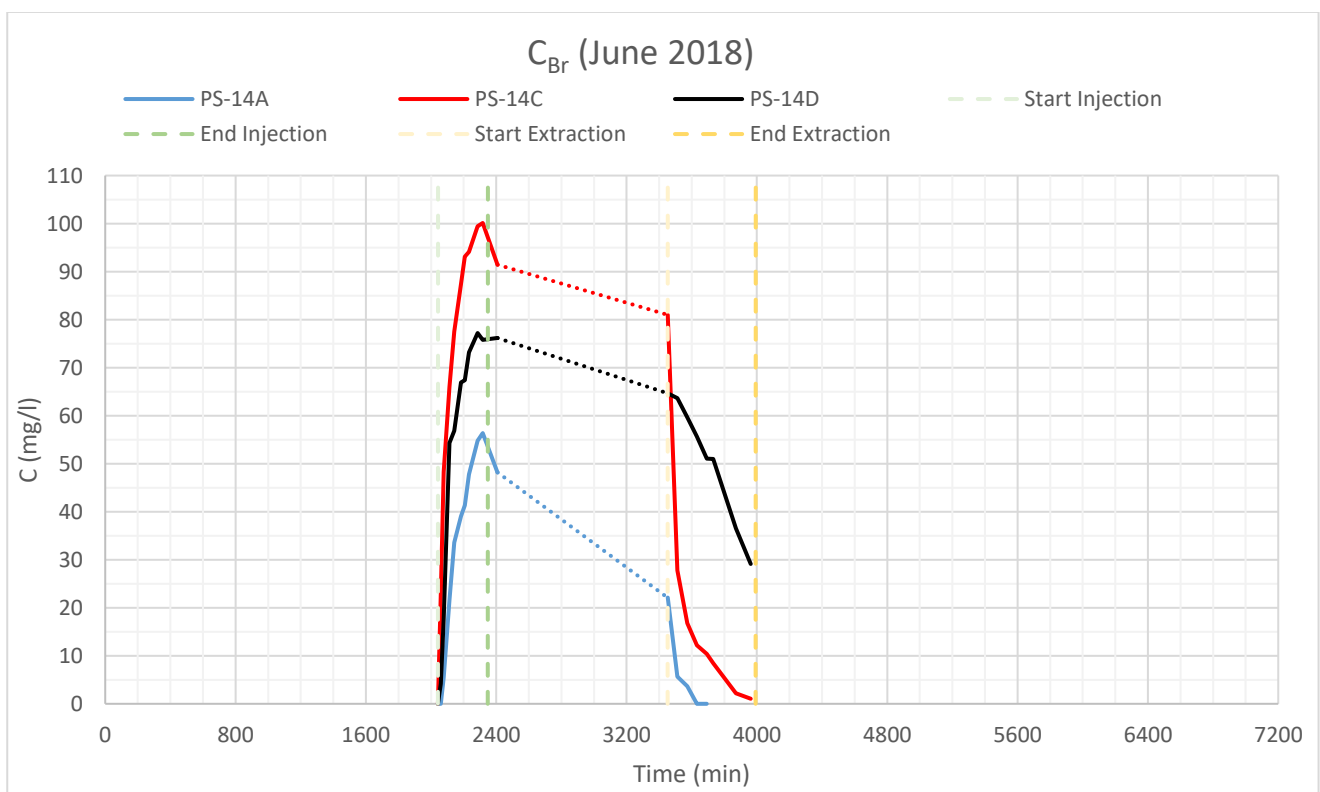


Figure 18: measured Br<sup>-</sup> concentration all over the tracer test period. The dotted lines represent the lack of measures in that time (between the injection and the extraction)

The pilot test has been carried out in the week between the 9<sup>th</sup> and the 13<sup>th</sup> of July 2018.

The first day was prepared the injection of the tracer adding 750g of Br<sup>-</sup> and 75kg of surfactant in a 5.76m<sup>3</sup> tank filled with water. The concentrations of surfactant (by GC/FID) and Bromide (by IC) measured at zero time were about 13 g/l and 130 mg/l, respectively.

The injection starts at 9:30 of 10<sup>th</sup> of July and ended at 18:20 (8.83 hours). Injection rates were varying and so measured periodically, through a counter. During this period the surfactant measures and the tracer measures took place 11 times, of which the last was taken 40 min after the end of the injection.

At 9:30 of 11<sup>th</sup> of July the extraction starts, and last until 19:05. The first 30 minutes were complicated, because of operational problems with the position of the pipe to be able to regulate the extraction. In the last two hours it was tried to raise the flow to try to face the situation created. Even in this occasion, pumping rates were measured through the counter. During the extraction, the concentration of the compounds injected was measured 12 times.

The time varying injection/extraction rate, over all the period of the pilot test, is shown in Figure 19.

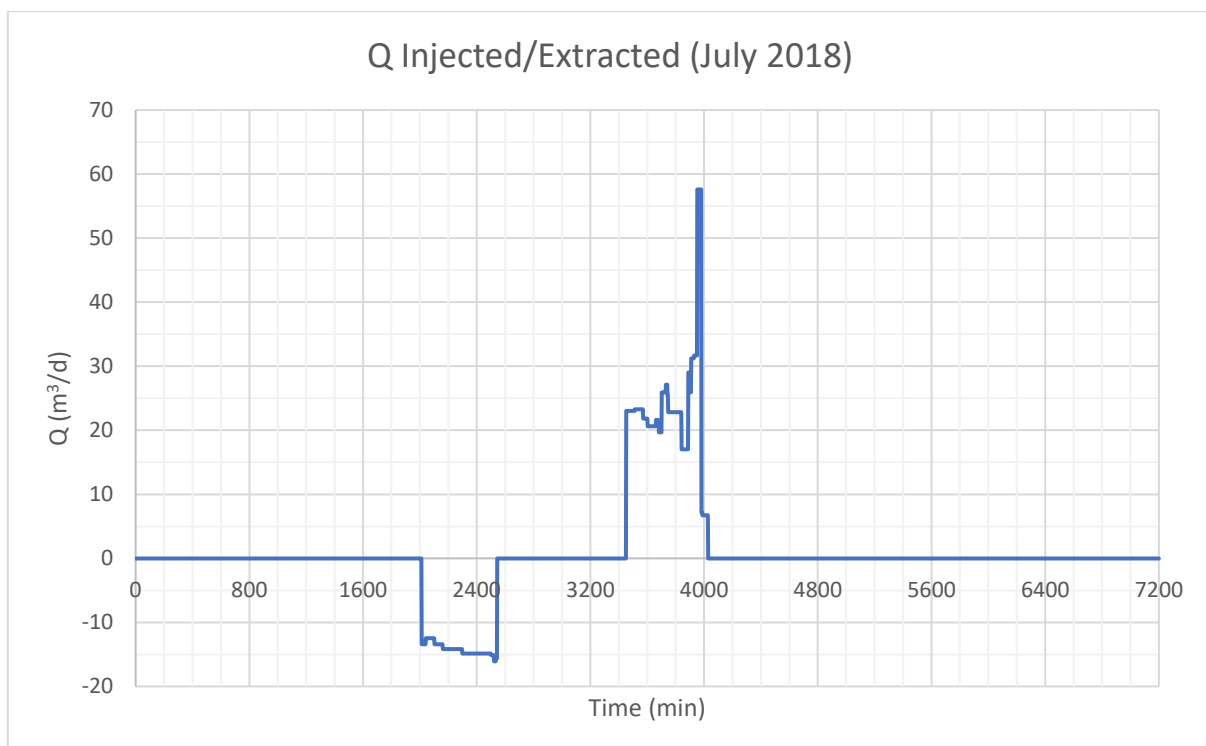


Figure 19: injection and extraction rate measured through the counter over the period of the pilot test. Negative values indicate injection of water.

The observed values of concentration for the compound injected is shown in Figure 20 for Br<sup>-</sup> and in Figure 21 for the surfactant, must be note that measures were not taken between injection and extraction.

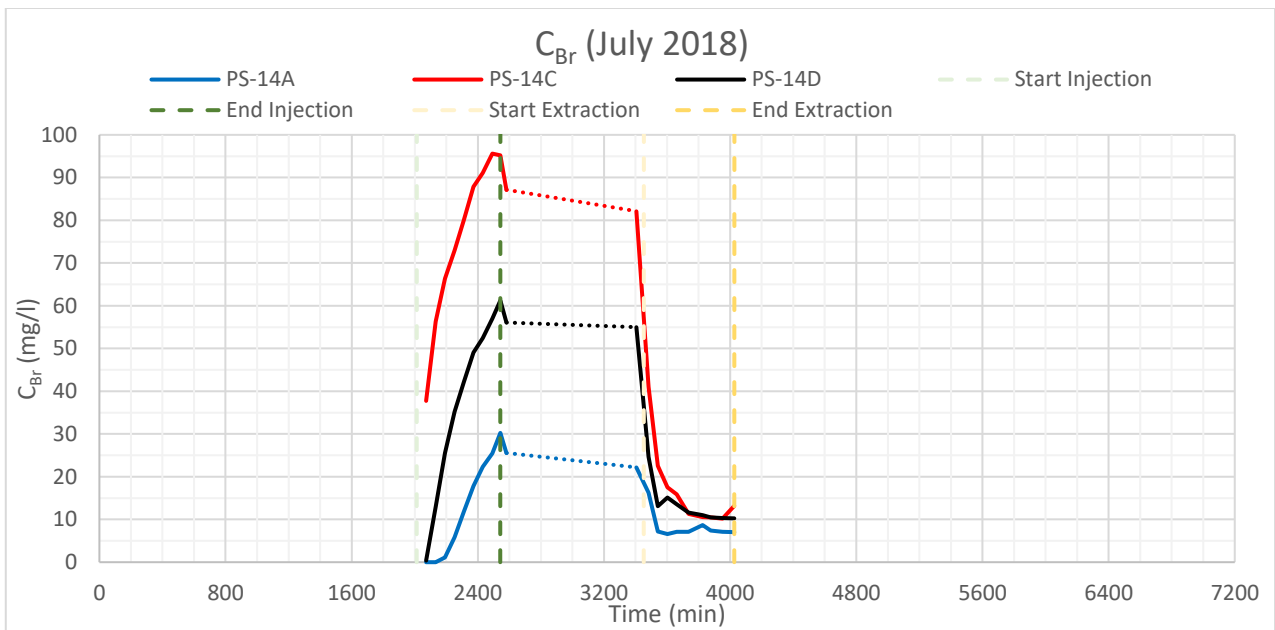


Figure 20: measured Br<sup>-</sup> concentration all over the pilot test period. The dotted lines represent the lack of measures in that time (between the injection and the extraction)

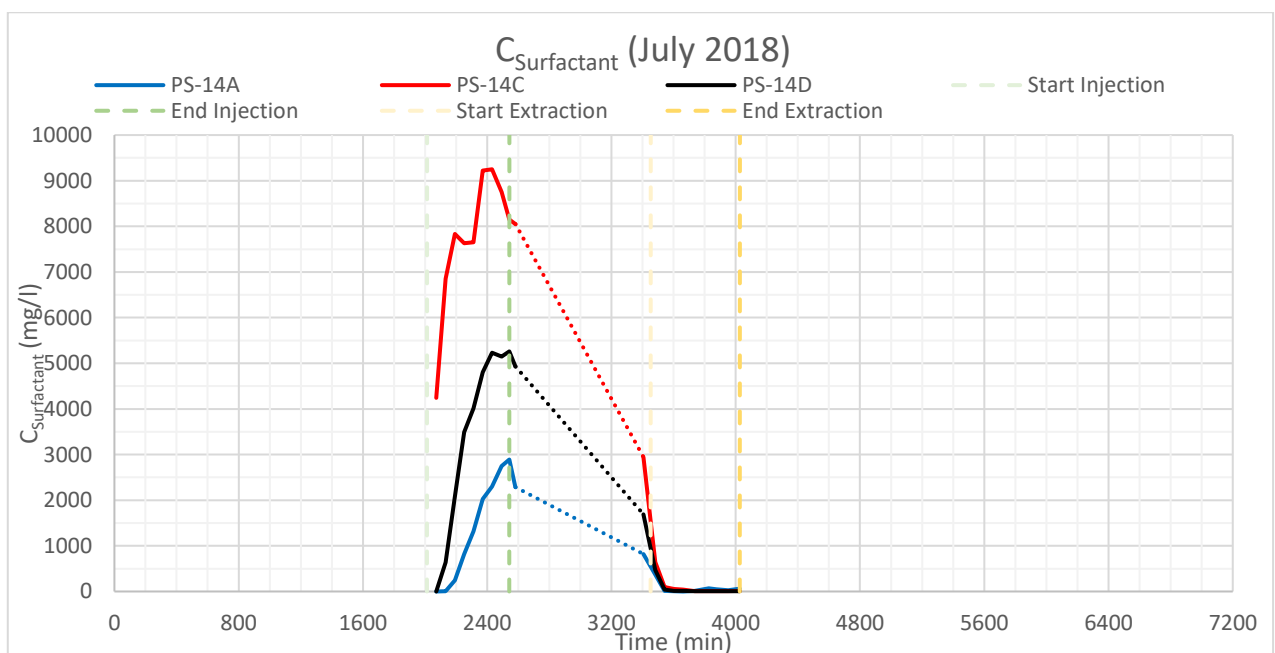


Figure 21: measured surfactant concentration all over the pilot test period. The dotted lines represent the lack of measures in that time (between the injection and the extraction)

As results of both tests, due to the larger amount of water extracted to recover those substances compared to the injected one, it is possible to note a radial dispersion of the compound injected.

## 2.2.3 Groundwater Modeling Tools

### 2.2.3.1 Quantum GIS

To reproduce the geometry of the site and to obtain the files regarding the location of the elements that must be considered in the model, such as piezometers and wells, the open source software “Quantum GIS” (QGIS) has been used.

QGIS has been started to develop by Gary Sherman in early 2002, and it became an incubator project of the Open Source Geospatial Foundation in 2007. Version 1.0 was released in January 2009.

QGIS functions as geographic information system (GIS) software, which allow to analyse and edit spatial information, in addition to composing and exporting graphical maps. QGIS supports both raster and vector layers; vector data can be stored as point, line, or polygon features, using them as shapefiles in the model. Multiple formats of raster images are supported, and the software can georeference images (“QGIS Official Website”, QGIS, October 2013).

The version used in this work is “QGIS 2.18 (Las Palmas)”, adopting “WGS84/UTM zone 32N (EPSG:32630)” as reference system for all the data and files created.

In this work, the software QGIS was used to:

- Build the boundary of the model domain, by creating the proper polygonal shapefile. The domain geometry has built considering the presence of the road N330 and the natural outcrops of marl, on the northern-east and southern-east, that can be considered as a physical limit for the groundwater flow, due to their very low permeability. On the western side the physical limit is represented from the reservoir, it was tried to choose the watershed line of the Gallego river. The boundary of the model domain is represented in  Figure 48. The intent of the shape decided for the boundary is to obtain a more detailed calculus of the flux and of the mass transport on the borders and within the area, and to avoid as much as possible no-flux elements for the simulation.
- Define the location of those piezometers used for the calibration of the model and for the injection and extraction episodes of interest of this thesis, by georeferencing the map provided by EMGRISA and creating the punctual shapefiles. In order to assign the position and the coordinates of those elements, it was necessary georeferencing the map with the location of wells and piezometers. For this georeferencing, 23 ground control point were used, reported in Appendix A. The results of the georeferencing is shown in Figure 49.

- Define the set of points used to apply elevation to the model, by georeferencing the finite differences grid provided by the EMGRISA/AZENTUA previous model and creating the proper punctual shapefiles. The referenced grid (31x29 cells), shown in Figure 50, is used as geometrical reference to locate the point files which correspond to the height information attributed to the finite difference grid, that in finite differences are located at the centre of the cells. For georeferencing the grid were used 12 ground control points, reported in Appendix A. Once defined the centres of the georeferenced grid, it was possible to attribute the same layer elevation information, but georeferenced in respect of the reference system used for the work. In order to assign a non-zero value in the domain, it was necessary to add additional points for a total of 942 points.

The approach for georeferencing a raster image is to locate points on the raster for which is it possible to determine coordinates accurately. The procedure for georeferencing an image involves selecting multiple points, called Ground Control Points, on the raster, specifying their coordinates (the more coordinates, and so points, are provided, the better the result will be) and finally choosing a relevant transformation type and a resampling method (ESRI ArcGIS Desktop online help Guide).

Depending on how many ground control points have been captured, is it possible to use different transformation algorithms, the ones that can be used in QGIS 2.18 are (QGIS 2.18 online help Guide):

- The Linear algorithm.
- The Helmert transformation, which performs only scaling and rotation transformations.
- The Polynomial algorithms 1-3, widely used algorithms, introduced to match source and destination ground control points. Among them, the most used polynomial algorithm is the second-order polynomial transformation, which allows some curvature.
- The Thin Plate Spline (TPS)
- The Projective transformation

For this thesis, a second order polynomial transformation have been selected.

The polynomial transformation uses a polynomial built on control points and a least-squares fitting (LSF) algorithm. It is optimized for global accuracy but does not guarantee local accuracy. The polynomial transformation yields two formulas: one for computing the output x-coordinate for an input (x,y) location and one for computing the y-coordinate for an input (x,y) location.

$$x' = c_0 + c_1x + c_2y + c_3xy + c_4x^2 + c_5y^2$$

$$y' = d_0 + d_1x + d_2y + d_3xy + d_4x^2 + d_5y^2$$

The aim of the least-squares is to derive a general formula that can be applied to all points. The number of the control points required for this method is 6 (second order).

When the general formula is derived and applied to the control point, a measure of the residual error is returned, which represent the difference between where the starting point were placed compared to the actual location specified. The total error describes how consistent the transformation is among the different control points (QGIS online help Guide).

Finally, a type of resampling must be chosen. It is possible to choose among five different resampling methods:

- Nearest neighbour
- Linear
- Cubic
- Cubic Spline
- Lanczos

For this thesis, a Nearest neighbour resampling method were used.

The algorithm used by the Natural Neighbour interpolation finds the closest subgroup of input to interrogate points and applies weights to them based on proportionate areas to interpolate a value, it is also known as Sibson or "area-stealing" interpolation (Sibson R; 1981).

Its basic properties are that it's local, using only a group of samples (points) that surround a query point, guarantee that interpolated heights are within the range of the samples used. It will not produce peaks, pits, ridges, or valleys that are not already represented by the input samples (ArcGIS Desktop online help Guide).

The natural neighbours of any point are those associated with neighbouring "Voronoi (Thiessen)" polygons. Initially, a "Voronoi" diagram is constructed of all the given points, then a new "Voronoi" polygon is created around the interpolation point. The proportion of overlap between these polygons is then used as the weights (Sibson R; 1981").

### 2.2.3.2 FEFLOW

Once created the files containing the spatial information of the elements it is possible to work with them in order to build the 3D model and consequently the conceptual model of the site, assigning the proper information to the geometrical characteristics and to the process variables.

This part of the work was made with the use of the finite element software “FEFLOW 7.0”. FEFLOW is a 2-3D computation code based on the finite element method, which uses Galerkin as the decisive method for the simulation of flow and mass and heat transport.

The Finite Element Method, FEM, is an approximate numerical resolution tool widely used in cases of irregular domains, because the computational domain is constructed from the union of a considerable number of sub-domains of elementary form, thus being very versatile. The first operation of resolution of the FEM is the discretization of the continuous and then proceeds to impose the laws of conservation and behaviour.

In this way it is the domain that is discretized and does not alter the differential equations relative to each of the finite elements. Field variables in a problem studied in the continuous are a function of each generic point of the definition domain. Therefore pressure, temperature, density, displacement, velocity and all other variables at each point represent an infinite number of unknowns.

The finite element method reduces the number of unknowns to a finite value by discretizing the domain and expressing the field in terms of approximate functions. These functions are defined within each finite element in which the domain has been divided and are identified by the values that the variable assumes in the nodes around the elements.

FEMs are widely used in cases where problems must be dealt with internal limits such as faults or to simulate infiltration surfaces or points of source or loss.

The discretization in FEFLOW is made by the “Supermesh” operation, which forms the framework for the generation of a finite-element mesh. It contains all the geometrical information the mesh generation algorithm needs. They can be composed of an arbitrary number of polygons, lines and points in 2D and for 3D layer-based meshing, or solids, lines and points when working with unstructured mesh geometry in 3D.

During the simulation, results are computed on each active node of the finite-element mesh and interpolated within the finite elements. The denser the mesh the better the numerical accuracy, and the higher the computational effort.

The algorithm used in this work is called “Triangle”. Triangle is a triangulation code developed by Jonathan Shewchuk at UC Berkeley, USA. It supports very complex combinations of polygons, lines and points in the supermesh, allows a minimum

angle to be specified for all finite elements to be created, and provides the means for local mesh refinement with a maximum element size at lines or points of the supermesh (FEFLOW 7.0 user guide, 2016).

The partial differential equations (PDEs) allow to write the flow of groundwater in cases where it is influenced by changes in density in the fluid due to temperature differences or the presence of contaminants. The mathematical modeling underlying the FEFLOW calculation code is based on the following basic physical principles:

- conservation of fluid mass and solid continuous media;
- conservation of the mass of chemical constituents and contaminants;
- conservation of the moment of the fluid and of the continuous medium;
- first law of thermodynamics or energy conservation law.

In the implementation of the model it is necessary to assign the initial conditions (ICs) and the boundary conditions (BCs).

The initial conditions can be set in FEFLOW as a hydraulic or pressure load for flow equations, such as pollutant concentration for mass transport and as temperature values for heat transport. It is possible to attribute the values of the boundary conditions to the nodes, to the elements, to the whole area or to a portion of it and for all the slices.

Instead, the boundary conditions indicate the value of the dependent variable or its derivative at the confines of the problem domain.

The choice of the boundary conditions represents a phase of extreme importance in the implementation of the model as they strongly influence the results obtained during the simulation.

The boundary conditions that can be applied in groundwater modeling are:

- Dirichlet condition: used to set the piezometric height at certain limits. It is ideal for simulating large bodies of water or distributing the hydraulic loads of the water table to the limits of the domain. In the case of mass transport this condition is specified as a concentration of pollutant.
- Neumann condition: the variable specified is flow. It is used to specify the underground water flows at the model limits or surfaces, or to specify null flow limits.
- Cauchy condition: this condition is mixed. The flow through the limit of interest is specified depending on a fixed hydraulic load. This condition is the least strong but the most versatile, and for this reason it is used to simulate situations of hydrogeological.
- "Well" condition: useful to describe the presence of wells inside the domain. By assigning a positive flow, one indicates a pumping well and on the other

way around, with one negative flow indicates an intake well. In cases of mass transport, this condition is specified as a source of pollutant.

FEFLOW allows also some interpolation tools, that were used to apply elevation to the model and to obtain the initial conditions of hydraulic head starting from the shapefiles obtain in GIS discussed before. The interpolation methods used in this thesis are:

- “Inverse Distance Weighted (IDW)” interpolation, with an exponent of the 2<sup>nd</sup> order ( $p$ ). To predict a value for any unmeasured location, IDW uses the measured values surrounding the prediction location. IDW assumes that each measured point has a local influence that diminishes with distance: it gives greater weights to points closest to the prediction location, and the weights diminish as a function of distance. Weights are proportional to the inverse of the distance raised to the power value  $p$ . When  $p = 2$ , the method is known as the inverse distance squared weighted interpolation (ESRI ArcGIS Desktop online help Guide).
- “Akima” interpolation. Akima method is formulated in such a way that the resultant curve will pass through the given points and will appear smooth and natural. It is based on a piecewise function composed of a set of polynomials, each of degree three, at most, and applicable to successive intervals of the given points. In this method, the slope of the curve is determined at each given point locally, and each polynomial representing a portion of the curve between a pair of given points is determined by the coordinates of and the slopes at the points (H. Akima, 1970).
- “Kriging” interpolation. Kriging assumes that the distance or direction between sample points reflects a spatial correlation that can be used to explain variation in the surface. Kriging fits a mathematical function to a specified number of points, or all points within a specified radius, to determine the output value for each location. Kriging is most appropriate when is known that there is a spatially correlated distance or directional bias in the data. It is often used in soil science and geology (ArcGIS Desktop online help Guide).

### 2.2.3.3 FePEST and PEST

FePEST has been developed to provide more convenient access to PEST functionality when using FEFLOW models, without limiting it.

PEST is a software, developed by John Doherty, widely used in environmental modeling to calibrate models, to determine uncertainty associated with parameters and predictions, and for related tasks. Today, PEST is probably the most commonly used software for the calibration of groundwater models. Instead of only providing one calibrated model, PEST aims to analyse the spectrum of possible solutions and consequently the uncertainty range associated with parameters and predictions (FePEST in FEFLOW 7.0 user manual).

PEST is model-independent. Any modeling software that reads input and writes output from a file can be linked to PEST. On a more technical level, PEST can be seen as a toolbox of different programs to setup, run, and evaluate the results of a specific task (e.g. calibration).

The central feature of the PEST engine is the Gauss-Levenberg-Marquardt algorithm (GLMA) search algorithm, that iteratively optimizes the model parameters to improve its fit to observed data and other objectives changing the model parameters until a minimum objective function value is found (Doherty, 2018).

The fit to the observations is expressed through the Measurement Objective Function. In the simplest case, this will be the weighted sum of squares of the residuals between measurement and simulation results:

$$\Phi = \sum_i w_i (h_i^{obs} - h_i^{sim})^2$$

where  $h^{obs}$  denote an observation (typically from a field measurement),  $h^{sim}$  its related simulation result, and  $w$  the weight that has been applied to the measurement.

The weight of an observation controls how strong the deviation between computed and measured result, contributes to the measurement objective function. The choice of weights can strongly influence the convergence behaviour and result of the GLM algorithm (Doherty, 2018).

It was decided to assign a weight equal to the inverse of the error resulting from the scatter plot of the simulated values and the measured ones.

Running PEST, two working steps per iteration are made (Doherty, 2018)(FePEST in FEFLOW 7.0 user manual):

1. Derivative calculation: by repeating the model run for each parameter, and observing the resulting changes of observation values, the partial derivative for each pair of parameter and observation can be calculated by finite-difference approximation. These derivatives form the elements of the Jacobian matrix. The numerical effort to calculate the Jacobian matrix usually dominates the iteration.
2. The parameter values are adjusted aiming to reduce the objective function. The direction and magnitude of the adjustment is expressed by the parameter upgrade vector. To identify the optimal direction of this vector, the GLMA uses a combination of two strategies:
  - While the objective function shows a predominantly linear behaviour, the method of gradient descent is applied.
  - Objective-function nonlinearity is addressed via the Gauss-Newton method.

The two methods are not mutually exclusive: The GLM algorithm interpolates between them, controlled by a scaling parameter (the Marquardt-Lambda). PEST dynamically updates lambda depending on the progress in reducing the objective function. The current lambda is a good indicator for the current nonlinearity of the objective function (Doherty, 2018)(FePEST in FEFLOW 7.0 user manual):

- high lambda values indicate linear behaviour.
- small lambda values indicate nonlinear behaviour

A typical challenge when calibrating an environmental model is the inherent non-uniqueness associated to the inverse solution. Usually many different parameters sets exist which are all compatible with the historical observation data.

Observation data is usually sparse and usually not sufficient to uniquely identify more than just a few of the large number of model parameters that can be made adjustable. This has two consequence (Doherty, 2018)(FePEST in FEFLOW 7.0 user manual):

1. Different calibrated parameter sets lead to different predictions. This makes it difficult to use a single model alone for decision-making.
2. Some or many of the parameters will be insensitive to observations. The GLMA-based optimization process can become unstable under this condition, leading to long optimization run-times or even failure to optimize.

Regularization techniques can provide a defence against these issues. They restrict the parameter search to identifiable parameters, either by adding additional constraints to the parameters or separating identifiable parameters from nonidentifiable parameters. In this thesis Tikhonov and Single Value Decomposition regularization techniques were used.

Another problem of calibration is the large number of model calls and the associated computational complexity in terms of each model run-time.

Fortunately, many steps of a PEST run, especially the numerically expensive calculation of the Jacobian matrix, is very suitable for parallel computing which can reduce the computation time significantly, especially in case of highly-parametrized inversion processes. Parallelization can also improve model run-times significantly on a standalone computer (Doherty, 2018)(FePEST in FEFLOW 7.0 user manual).

FePEST uses the BeoPEST utility, a network capable version of PEST, for obtaining better run-time efficiency. FePEST also transfers the required model files to the slave computers. The slaves show a list of servers that are used to solve model run jobs during the PEST run, initially empty (Doherty, 2018)(FePEST in FEFLOW 7.0 user manual).

#### 2.2.4 Flow and Transport Modeling with FEFLOW

Once obtained the shapefiles from QGIS as seen above, it was possible to use FEFLOW in order to perform the simulation of the episodes of injection and extraction of June and July 2018. In order to understand the location in the site of the model boundary, the perimeter of the domain used in the FEFLOW modeling is reported in Figure 22.



Figure 22: perimeter of the model domain

First it is necessary to define the characteristics of the problem, by assigning the properties and the conditions that influence the study site, based on the available information.

The flow chart of the assignment done in FEFLOW is reported in Table 3, each of the following operations are further discussed.

Table 3: FEFLOW's workflow procedure

<b>1) Geometry</b>	Supermesh operation (spatial discretization)
	3D elevation
	Active/Inactive elements
<b>2) Problem settings</b>	Problem class and aquifers definition
	Simulation time and time steps size
	Predictor/Corrector scheme
	Chemical species and reactions associated
	Transport settings
<b>3) Initial conditions</b>	Hydraulic head
<b>4) Boundary conditions</b>	1 <sup>st</sup> type BC (reservoir)
	2 <sup>nd</sup> type BC (landfill flux)
	4 <sup>th</sup> type BC (water injection and extraction)
	1 <sup>st</sup> type BC (mass injection)
<b>5) Material properties</b>	Hydraulic conductivity
	Specific storage
	Specific yield
	Porosity
	Molecular Diffusion
	Dispersivity
<b>6) Observations</b>	Observation wells

#### 2.2.4.1 Supermesh Operation

At first it is necessary to reconstruct the geometry of the problem using the files obtained in QGIS. The shapefiles obtained, punctual shapefiles for the piezometers and the wells and polygonal shapefile for the boundary of the domain, were uploaded in FEFLOW in order to do the “meshing” operation. The result of the meshing algorithm is shown in Figure 23.

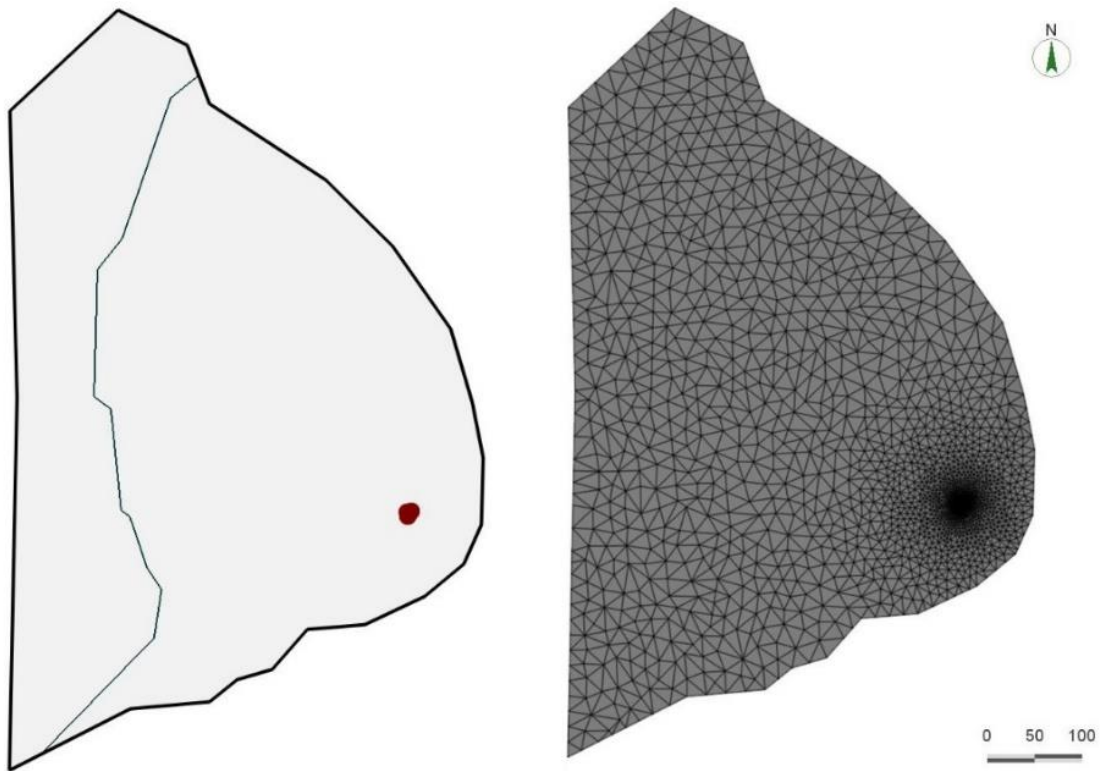


Figure 23: Meshing operation. On the left there are the shapefiles, on the right the mesh result based on the files uploaded.

The area with a high density of elements corresponds to the area around the injection well and the observation piezometers. This local refinement was made to improve the computational precision around the area interested in the tests simulated, where an appropriate spatial and temporal discretization is needed due to the fast variation in the solution of the mass transport and flow equations.

#### 2.2.4.2 3D Elevation

After building the mesh, to create the geometry of the model, the domain was extended to the 3<sup>rd</sup> dimension defining the number of the layers of the problem and their elevation, using a “layered approach” based on the information from the finite differences model discussed above.

In case of the layered approach, the triangular mesh is extended to the third dimension by extruding the 2D mesh, resulting in prismatic 3D elements. In FEFLOW all (typically) horizontally adjacent 3D elements comprise one layer, while a slice is either the interface between two (typically) vertically adjacent layers or the top or bottom of the model domain. All mesh nodes are located on slices (FEFLOW 7.0 user guide, 2016).

The 942 points seen in “Quantum GIS” section were interpolated automatically by FEFLOW using an “Inverse Distance Weighted (IDW)” interpolation with an exponent of the 2<sup>nd</sup> order ( $p$ ). The result is shown in Figure 24.

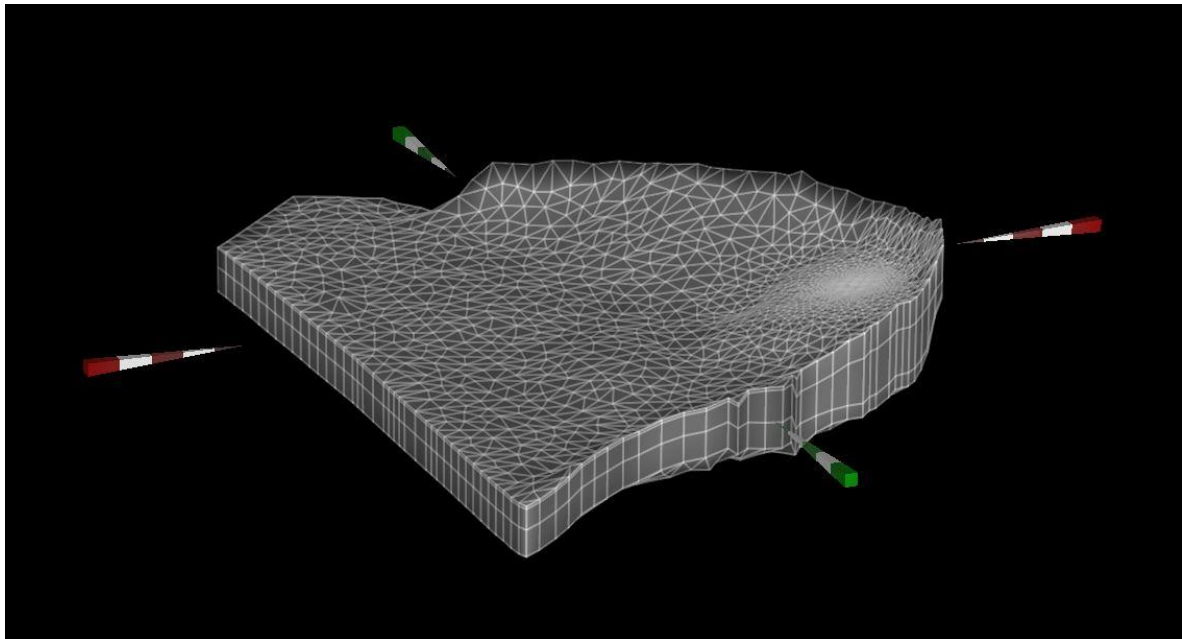


Figure 24: 3D model obtained after applying elevation

### 2.2.4.3 Active/Inactive Elements

To complete the geometry of the site, some of the 3D elements created were assigned as inactive: on the first layer because of the small thickness automatically assigned to have a continuous layer and on the third layer in order to reproduce a characteristic observable in the cross section reported in Figure 25.

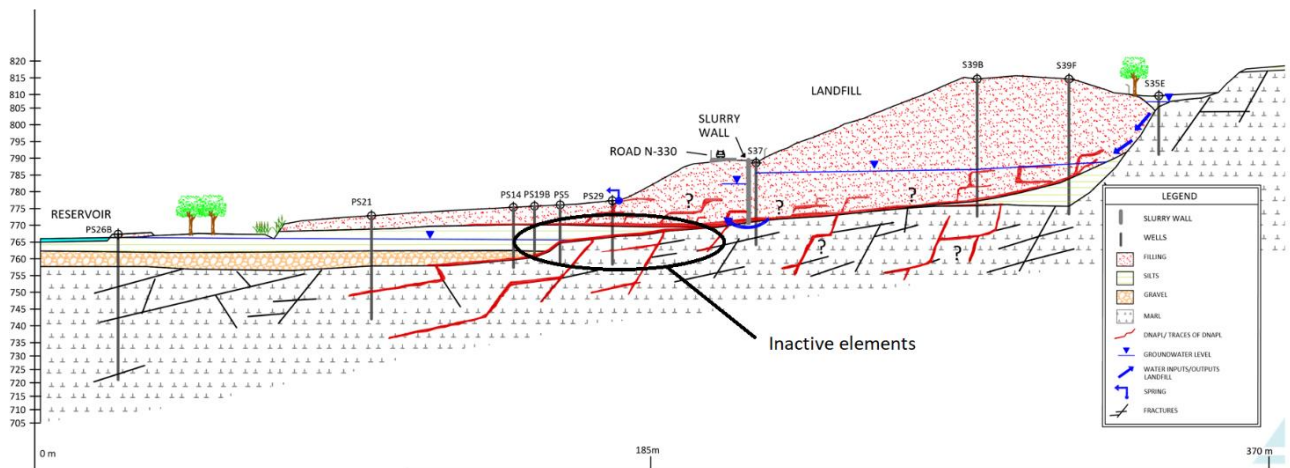


Figure 25: cross section of the site evidencing the inactivated elements of the 3rd layer

The representation of those elements in the model is shown in Figure 26.

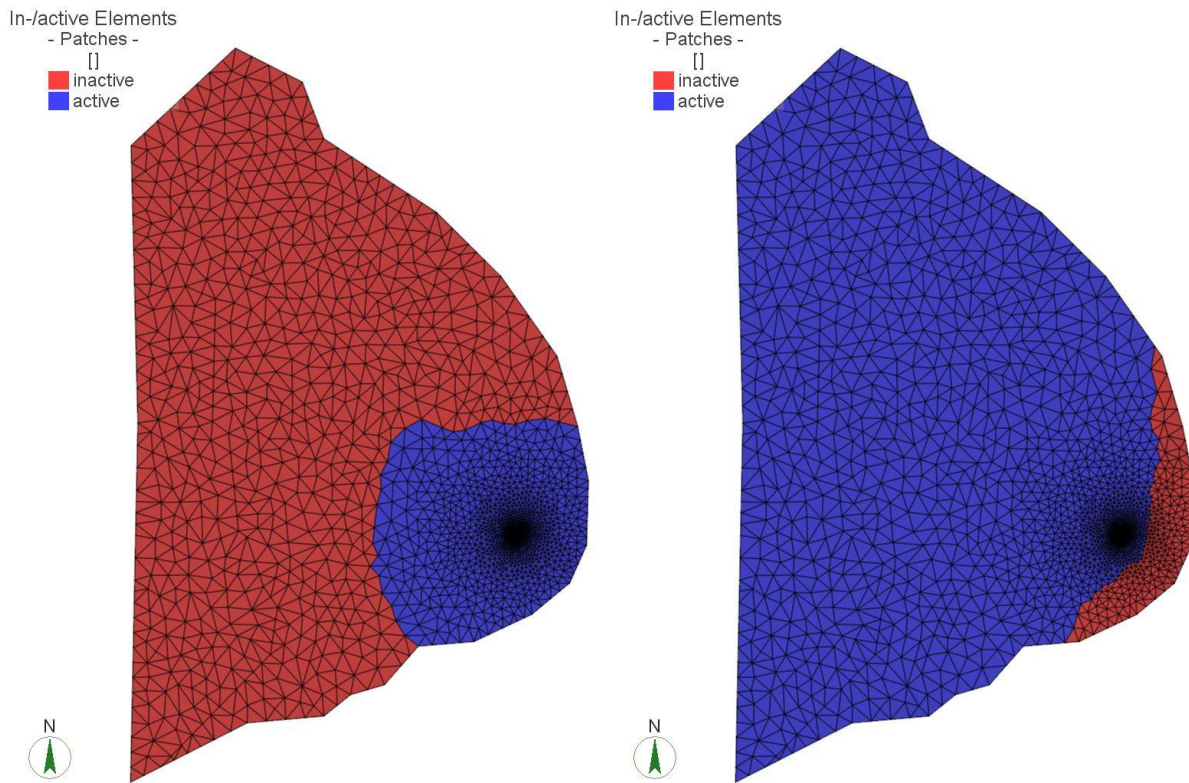


Figure 26: Active/Inactive elements relative to the 1st layer on the left and on the 3rd layer on the right

#### 2.2.4.4 Problem Settings

After creating the geometry of the domain, was defined the class of the problem: flow and mass transport were simulated, both in transient mode.

For what concern the flow simulation, the anthropic filler layer was considered in phreatic condition and the silt and gravel layer were considered in confined condition.

Peculiarity of the phreatic mode is that the model stratigraphy is fixed and, therefore, elements may become dry or partially saturated. The phreatic mode avoids all slice movement and related parameter interpolation and is therefore applicable to water tables with steep gradients that extend over multiple layers.

For what concern the mass transport simulation, the chemicals species were associated in both times, June and July tests, to the fluid phase, which means that the species is dissolved a mobile fluid phase subject to diffusion, dispersion and advection. Characteristics of those compound are further discussed.

Both flow and mass transport were evaluated in transient mode, over a period of 7200 min, equal to 5 days, in order to incorporate the phases of the injection and the extraction of both tests (June and July). In this view, an extra simulation time

of 3 days, one before the injection and two after the extraction, was considered in order to allow the model to “manage” initial imbalances due to inaccuracy of the interpolations used and discussed further.

For the time steps, the Adams-Bashforth/Trapezoid rule (AB/TR) was used as predictor-corrector scheme.

A summary of the problem class settings and geometrical properties of the domain is reported in Table 4.

*Table 4: problem class settings and geometrical properties of the model*

<b>Problem Class</b>	
<b>Description</b>	Combined flow and mass process
<b>Type</b>	Saturated
<b>Projection</b>	3D phreatic aquifer (fixed mesh)
<b>Time Class</b>	Transient flow/Transient transport
<b>Time Stepping</b>	Adams-Bashforth/Trapezoid rule (AB/TR)
<b>Mesh and Geometry</b>	
<b>Element type</b>	Triangular Prism
<b>Mesh element</b>	20166
<b>Nodes per element</b>	6
<b>Mesh nodes</b>	13708
<b>Number of layers</b>	3
<b>Elements per layer</b>	6722
<b>Nodes per layer</b>	3427

#### *2.2.4.5 Initial Conditions: Hydraulic head*

To allow the computation in FEFLOW it is necessary to assign Initial Conditions (ICs) in terms of starting values of hydraulic head. This means to reconstruct the piezometry of the site at the starting time of the simulation. In order to do this, several piezometers measures, screened in different layers, were interpolated and in addition to them, 11 points located on the reservoir were used to obtain a more detailed interpolation. A detailed list of all the points used for each layer is reported in Appendix B.

Those points were interpolated with different methods, in order to obtain the best piezometry look-alike results. In Table 5 are summarized the methods used with their interpolation characteristics for each layer in both temporal periods of June and July 2018.

Table 5: characteristics of the interpolations to obtain the initial hydraulic head

Layer	Interpolation method	Number of neighbours
<b>June 2018</b>		
1	Akima Cubic	5
2	Kriging	7
3	Kriging	6
<b>July 2018</b>		
1	Akima Cubic	4
2	Inverce Distance (3 <sup>rd</sup> order exp.)	8
3	Kriging	8

The location of those points and of the piezometer is indicated in Figure 27.

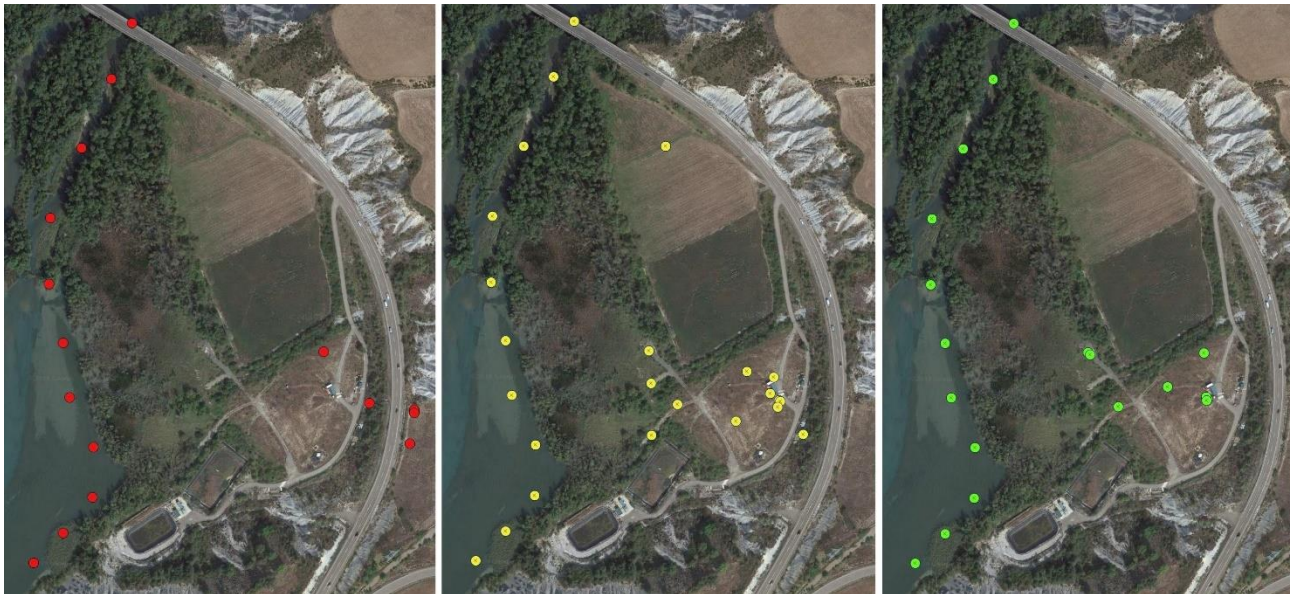


Figure 27: points used for the interpolation of the hydraulic head. From left to right is reported the location of the point for layer 1 in red, layer 2 in yellow and layer 3 in green.

The results of the interpolation are shown in Figure 28 for the top layer, Figure 29 for the 2<sup>nd</sup> layer and in Figure 30 for the bottom layer. Note that on the 3<sup>rd</sup> layer, at nodes corresponding to the inactive elements discussed before, it is assigned a “false” value (764m and 765m respectively for July and June), in order to obtain a better view of the results, due to the low range of the values in that layer, considering that such a part of the domain does not influence the simulation (inactive elements).

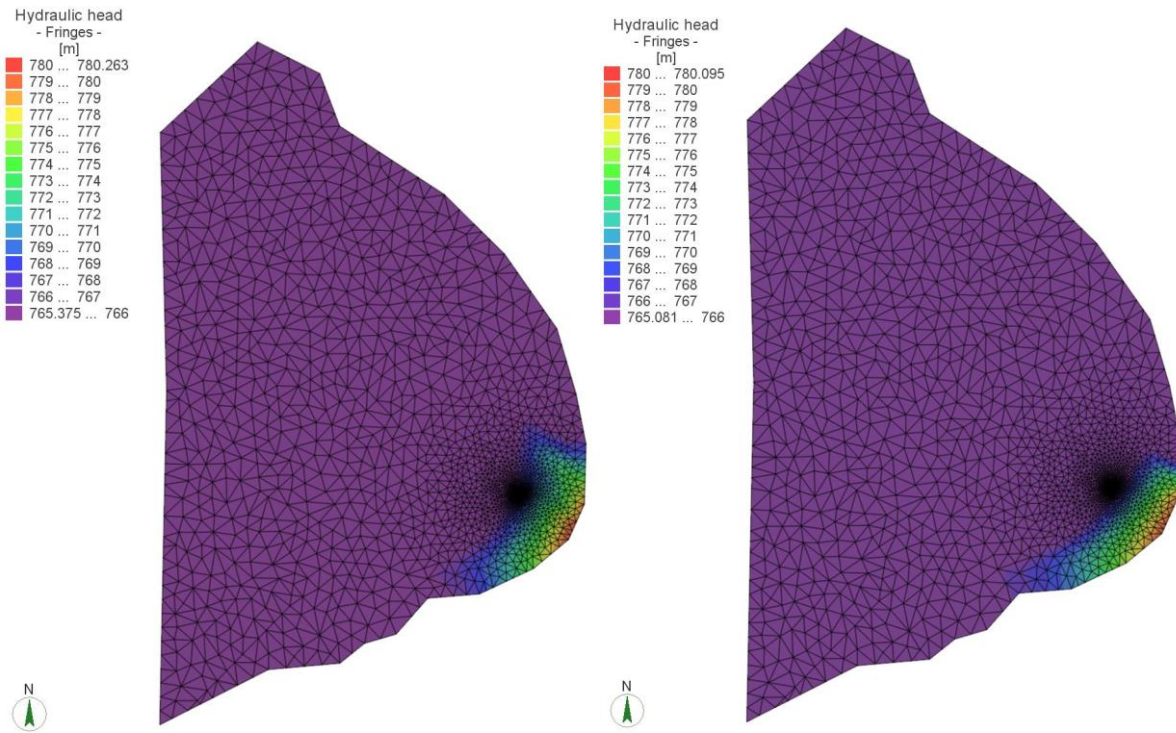


Figure 28: initial condition for hydraulic head in layer 1. The initial piezometry for the period of June 2018 is shown on the left, for the period of July 2018 on the right

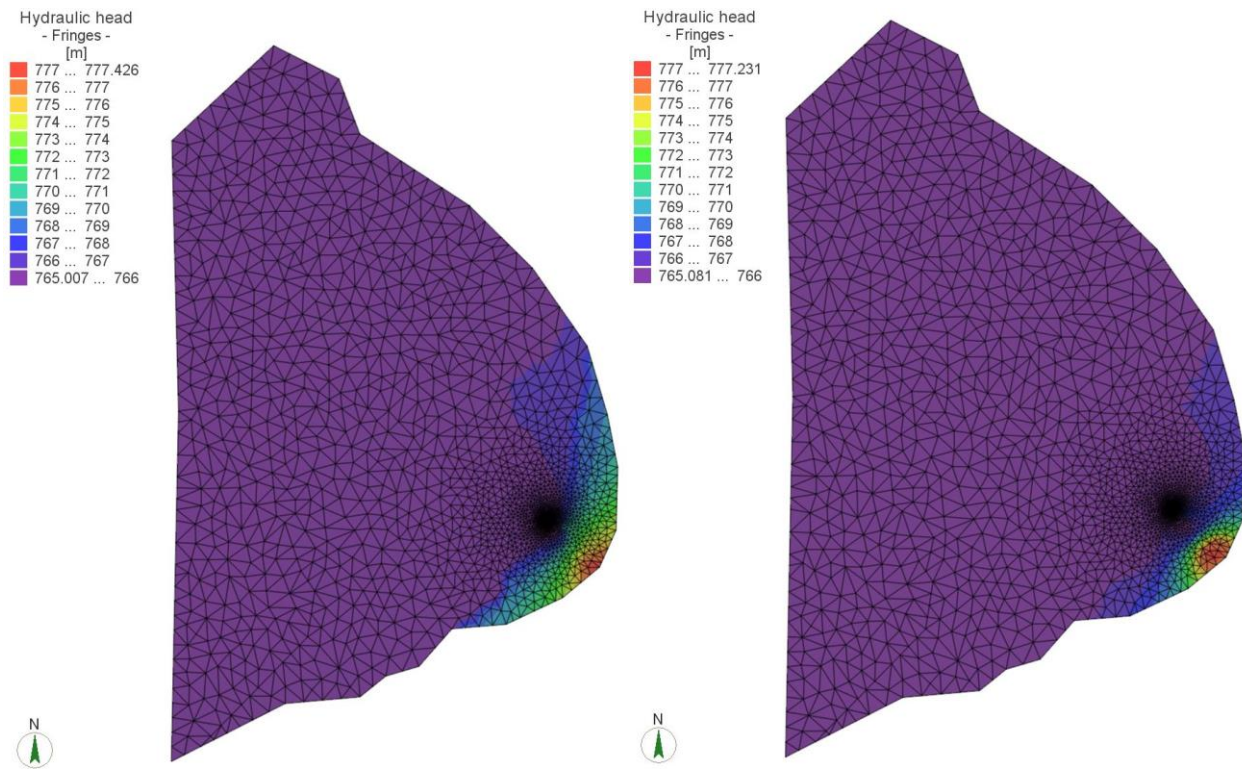


Figure 29: initial condition for hydraulic head in layer 2. The initial piezometry for the period of June 2018 is shown on the left, for the period of July 2018 on the right

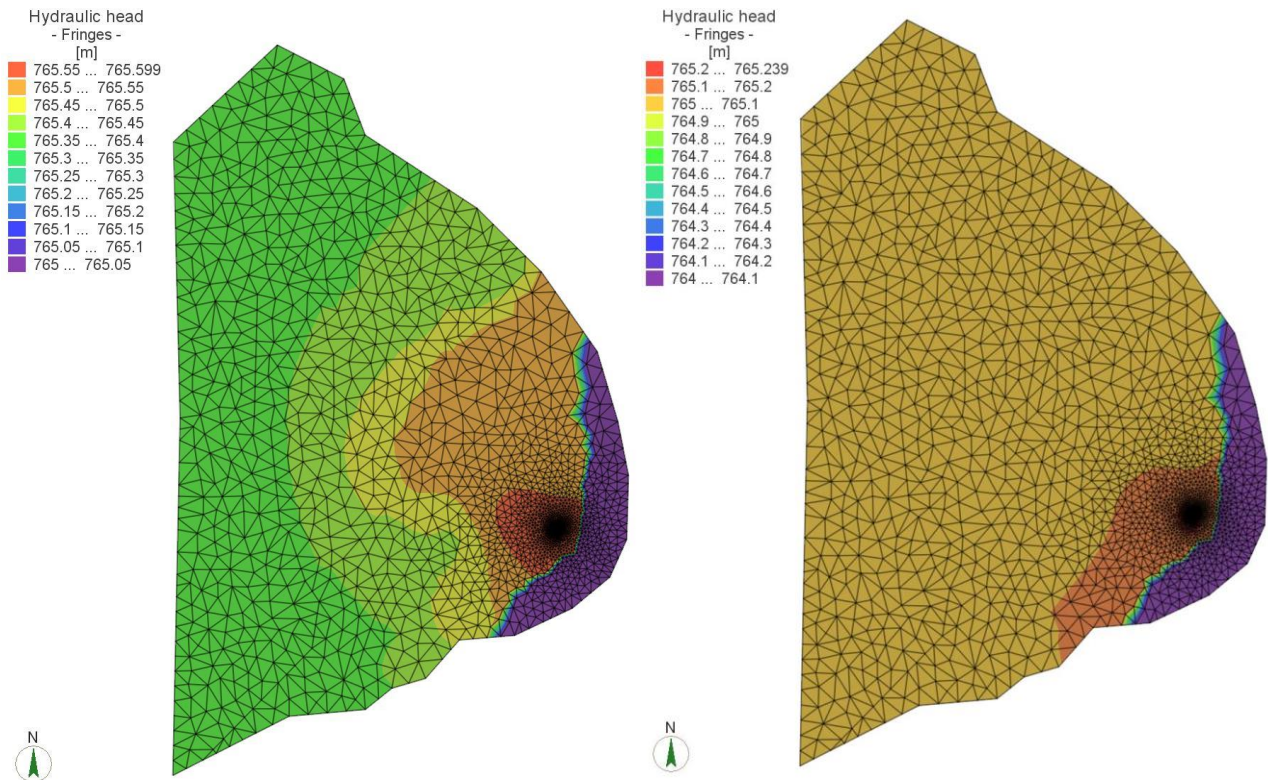


Figure 30: initial condition for hydraulic head in layer 3. The initial piezometry for the period of June 2018 is shown on the left, for the period of July 2018 on the right

#### 2.2.4.6 Boundary Conditions: Reservoir's oscillations

To reproduce the oscillation of the reservoir, a 1<sup>st</sup> type time-varying boundary condition (Dirichlet) was applied over the nodes corresponding to the reservoir area considered in the model. The time varying BC applied is characterised by the same values measured in the reservoir over the test periods. The time series relative to the oscillations of the reservoir in June 2018 is reported in Figure 31 and for July 2018 in Figure 32.

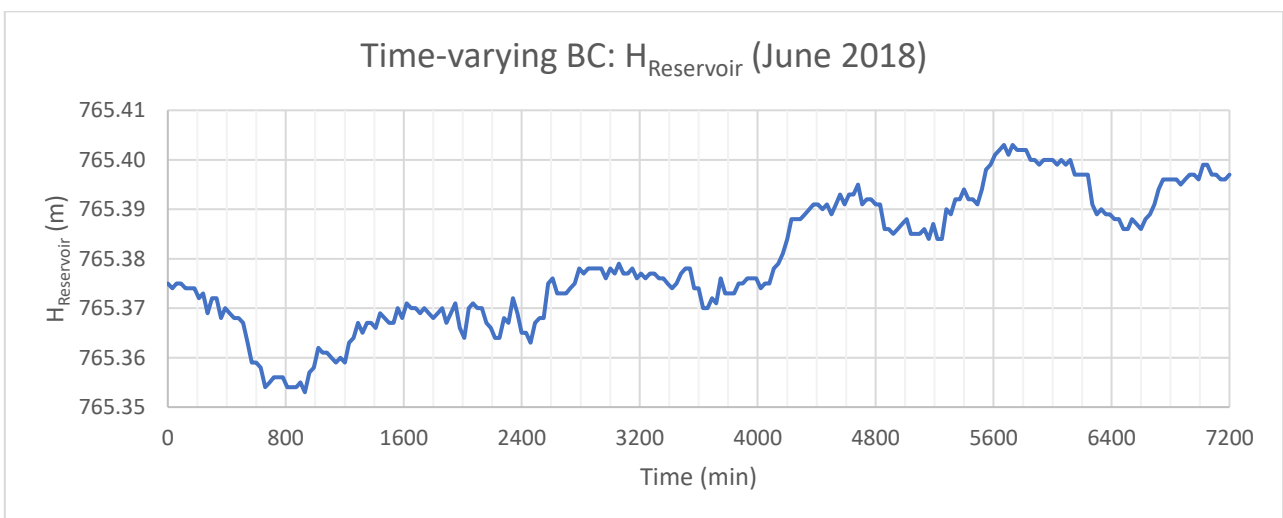


Figure 31:reservoir oscillations for the period of tracer test in June 2018

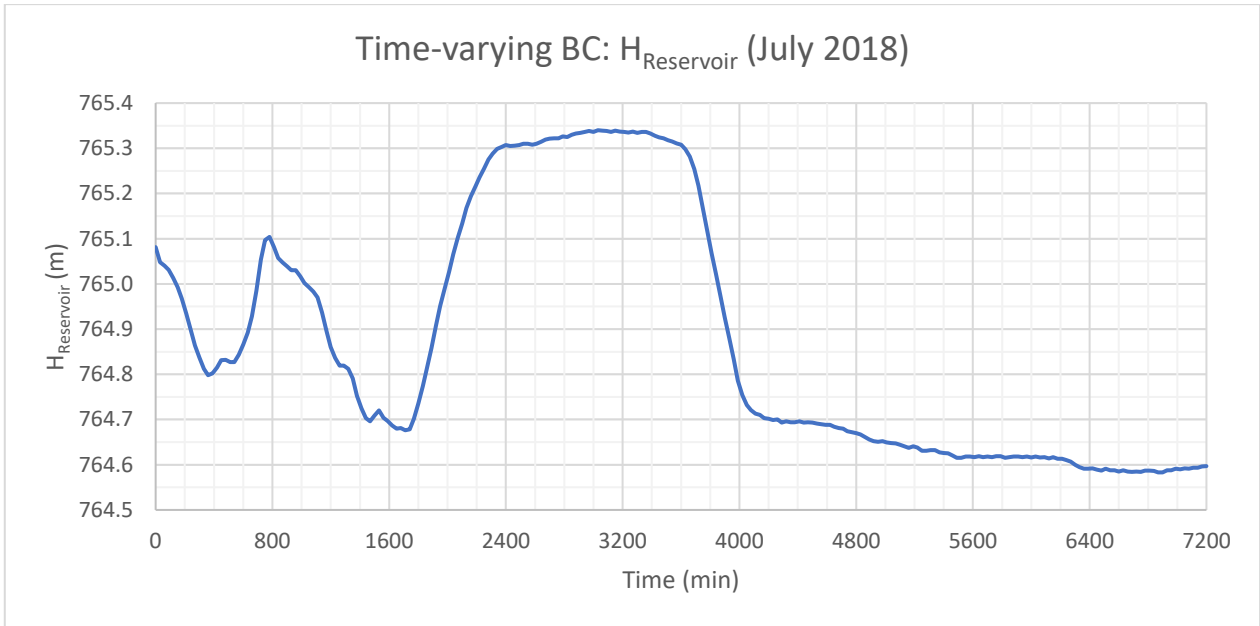


Figure 32:reservoir oscillation for the period of the injection of surfactant and tracer in July 2018

Those time varying values of Hydraulic Head were applied in the part of domain shown in Figure 33.

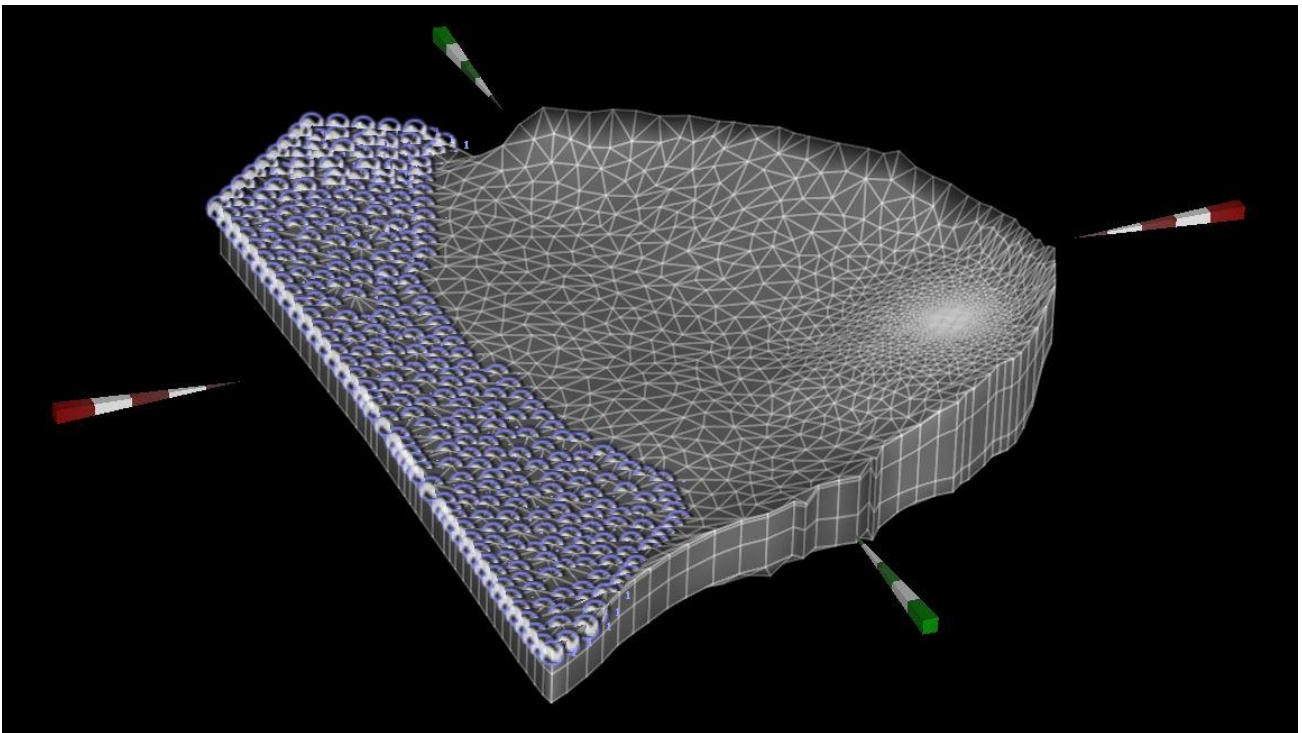


Figure 33: 1st type BC nodes (in blue) applied to reproduce the level oscillations in the reservoir

#### 2.2.4.7 Boundary Conditions: Flux from Sardas Landfill

The flux coming from the Sardas landfill was modelled by applying a 2<sup>nd</sup> type boundary condition (Neumann) of a flux of 0.01 m/d over the area shown in Figure 34.

That area multiplied for the applied BC leads to a total amount of water inflow of about 10 cubic meters per day.

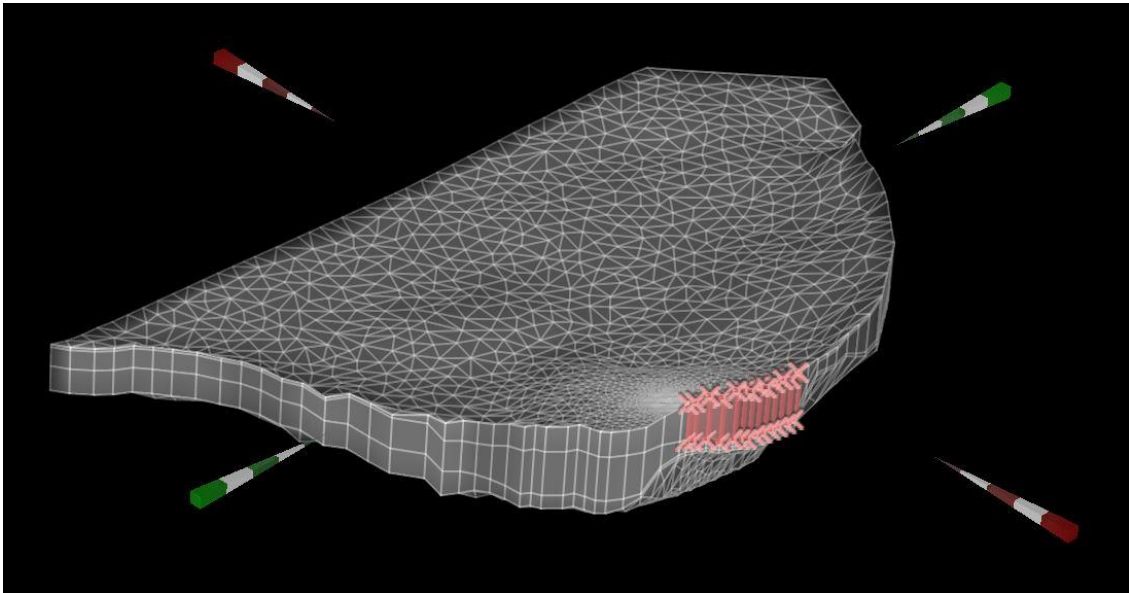


Figure 34: 2nd type BC nodes (in pink) to reproduce the contaminant flux from the landfill

#### 2.2.4.8 Boundary Conditions: Injection and Extraction of Water and Mass

To consider the injections and the extractions of the two periods studied, a 4<sup>th</sup> type BC (well type) for the flux injected and a 1<sup>st</sup> type BC (Dirichlet) for the mass transport were applied at the node corresponding to the well PS14B, screened only in the 3<sup>rd</sup> layer. The location of the well is shown in Figure 35.

The amount of water injected and extracted in the different periods are shown below in Figure 36 and Figure 38 for the episode of June and July 2018 respectively. Were applied time varying BCs corresponding to the constant flow rate applied in the tracer test and to the flow rate measured through the counter for the pilot test.

The mass injected, represented as a constant concentration (1<sup>st</sup> type BC) over the injection time, is applied on the well's location. Time series of the concentration applied are shown below in Figure 37 for the episode of June 2018 and in Figure 39 and in Figure 40 for the episode of July 2018.

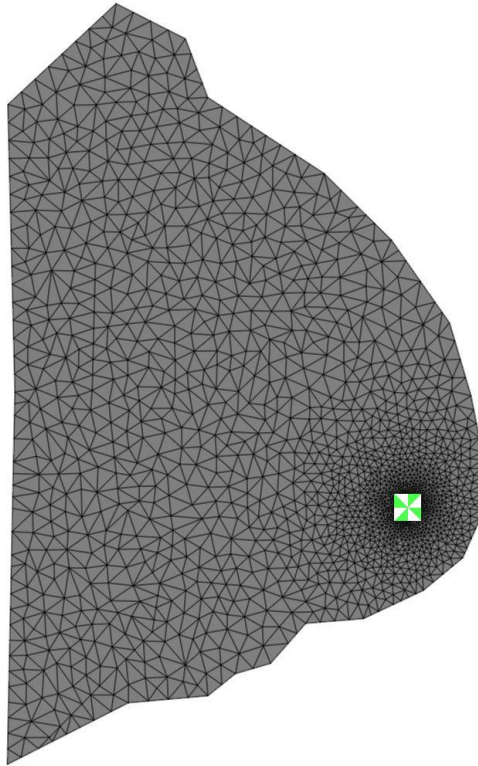


Figure 35: Location of well PS14B

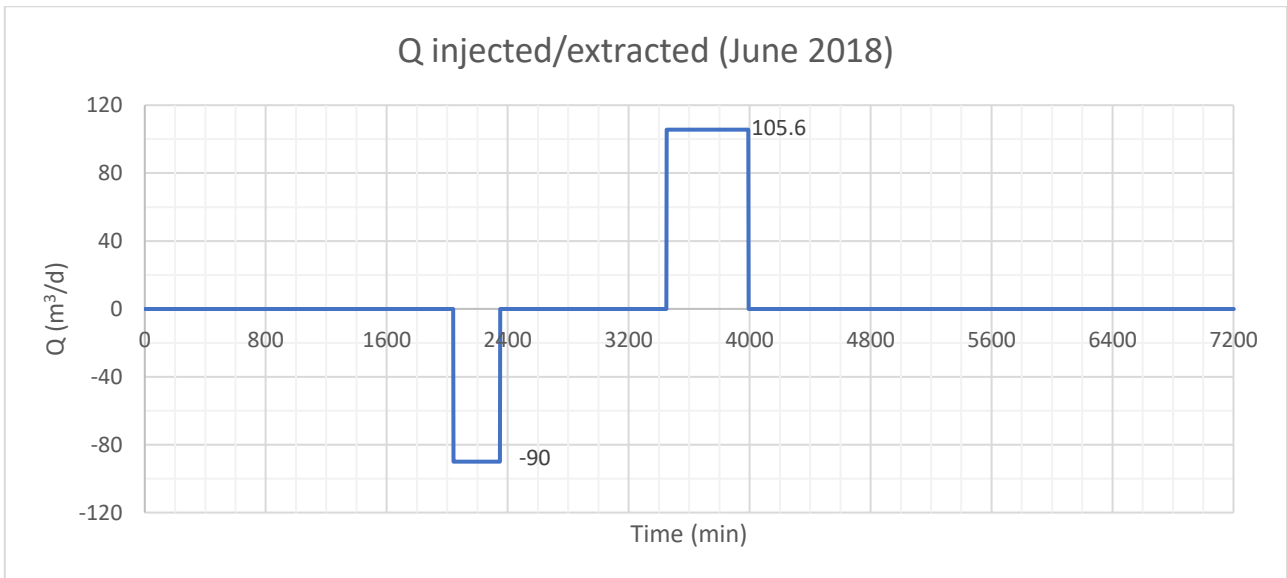


Figure 36: Q injected and extracted in June 2018. A negative value means an injection, positive an extraction

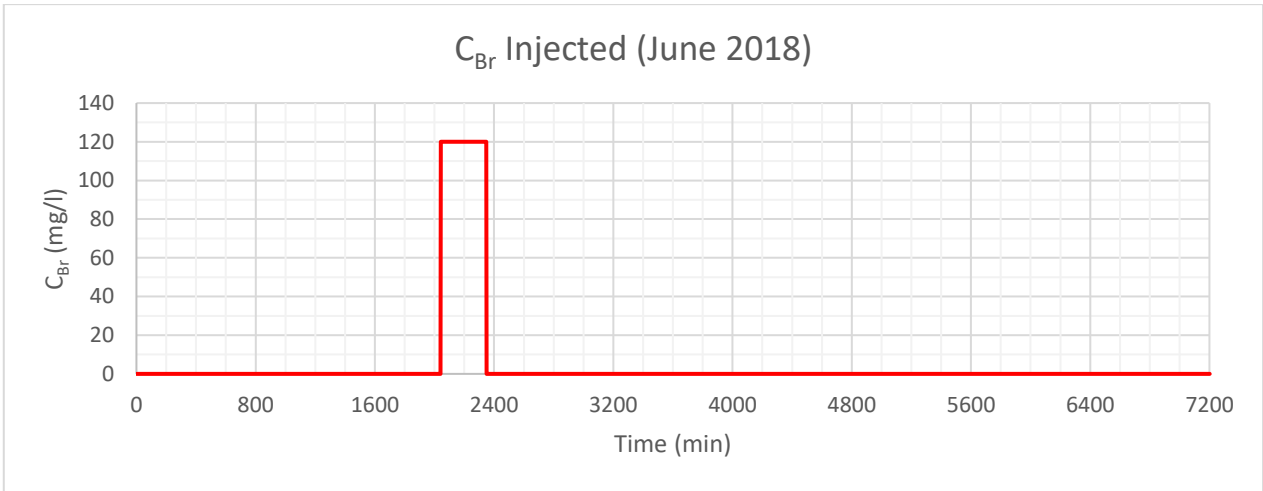


Figure 37: Constant concentration (1st type mass BC) of Br applied in June 2018

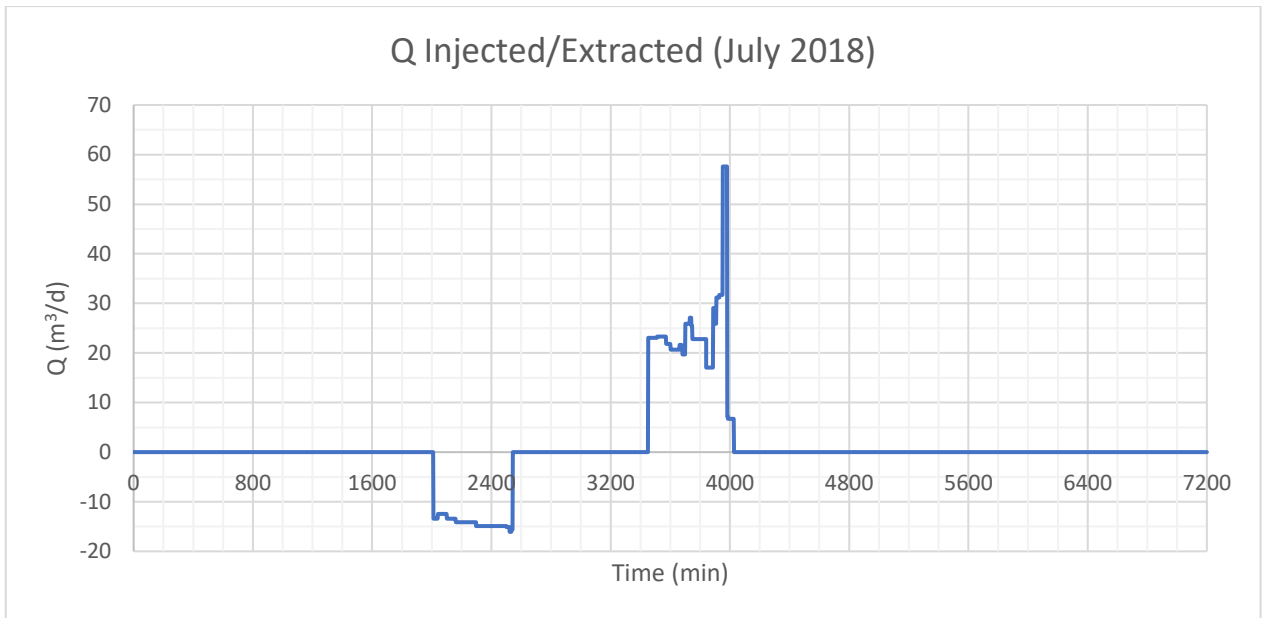


Figure 38:  $Q$  injected and extracted in July 2018. A negative value means an injection, positive an extraction

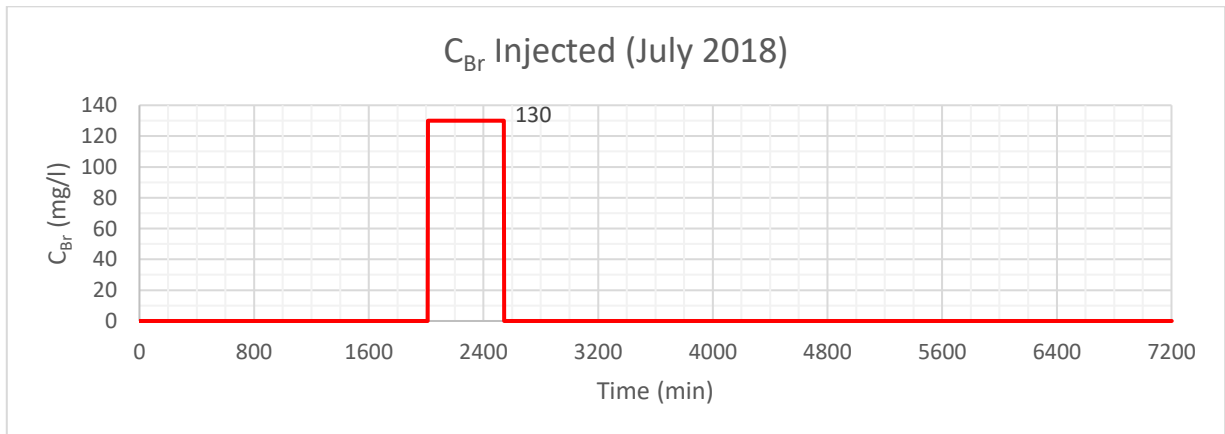


Figure 39: Constant concentration (1st type mass BC) of Br applied in July 2018

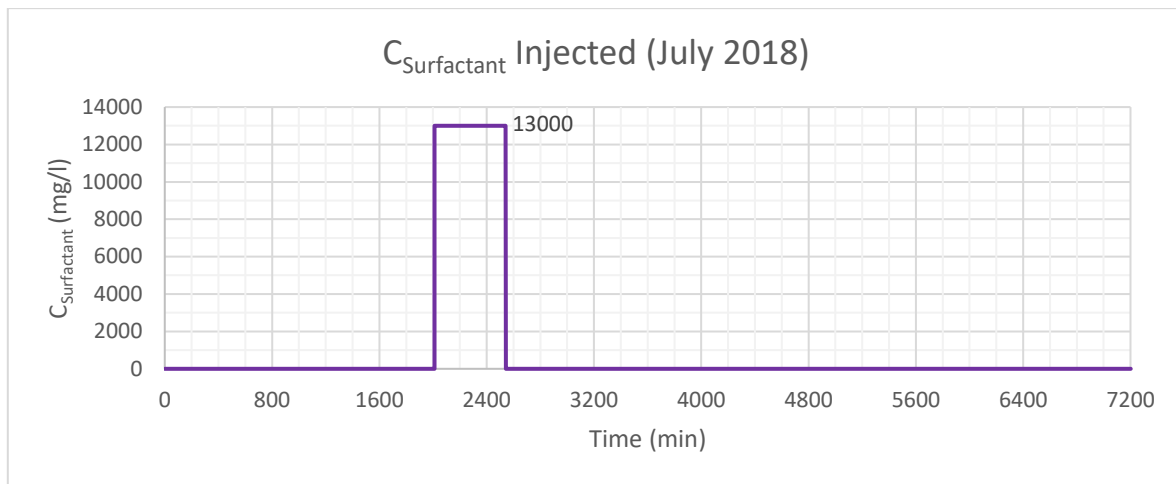


Figure 40: Constant concentration (1st type mass BC) of Surfactant applied in July 2018

#### 2.2.4.9 Material Properties

After defining the ICs and BCs needed in order to perform the simulation, the property of the layers of the model, differentiated on the site's characteristics, and of the physical and chemical properties of the compound injected were assigned. All the values reported in this section were obtained as result of the PEST run. In Table 6 are reported the physical characteristic of the layer that were considered as uniform all over the layer, effective porosity and specific yield, and also the characteristics of the injected compounds. The values that were unknown have been estimated based on literature reference values for the specific lithotype.

Table 6: Other material properties and characteristic of the injected substances

Effective Porosity	
Layer 1: anthropic filling	0.08
Layer 2: silt	0.11
Layer 3: Gravel and sand	0.13
Specific Yield	
Layer 1: anthropic filling	0.08
Layer 2: silt	1 e-3
Layer 3: Gravel and sand	1 e-4
Dispersivity	
Longitudinal Dispersivity	50m
Transverse Dispersivity	5m
Tracer Properties: BrNa	
Molecular Diffusion (Br <sup>-</sup> )	2.01 e-09 m <sup>2</sup> /s
Henry Constant	0
Decay Rate Constant	0

The values of the properties of the layers and their sub-zones are illustrated in Figure 41, Figure 42, Figure 43 for conductivity and in Figure 44, Figure 45, Figure 46 for specific storage. It was not considered anisotropy between the X and Y direction.

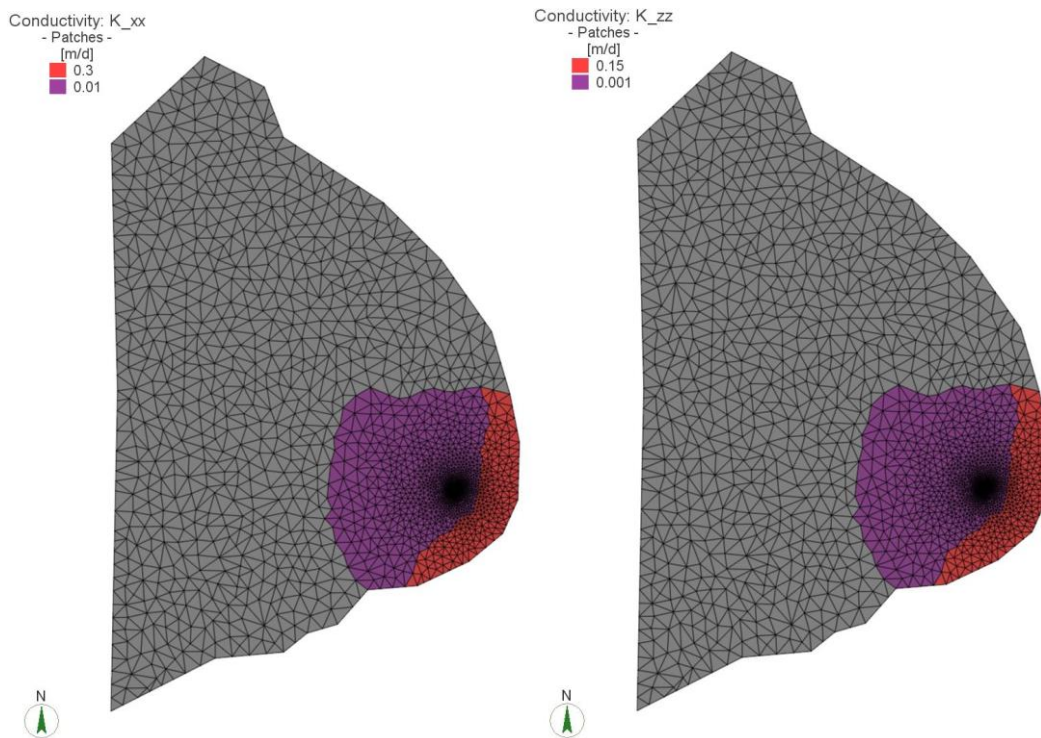


Figure 41: Conductivity of Layer 1. In red the hydraulic connection, in grey inactivated elements.

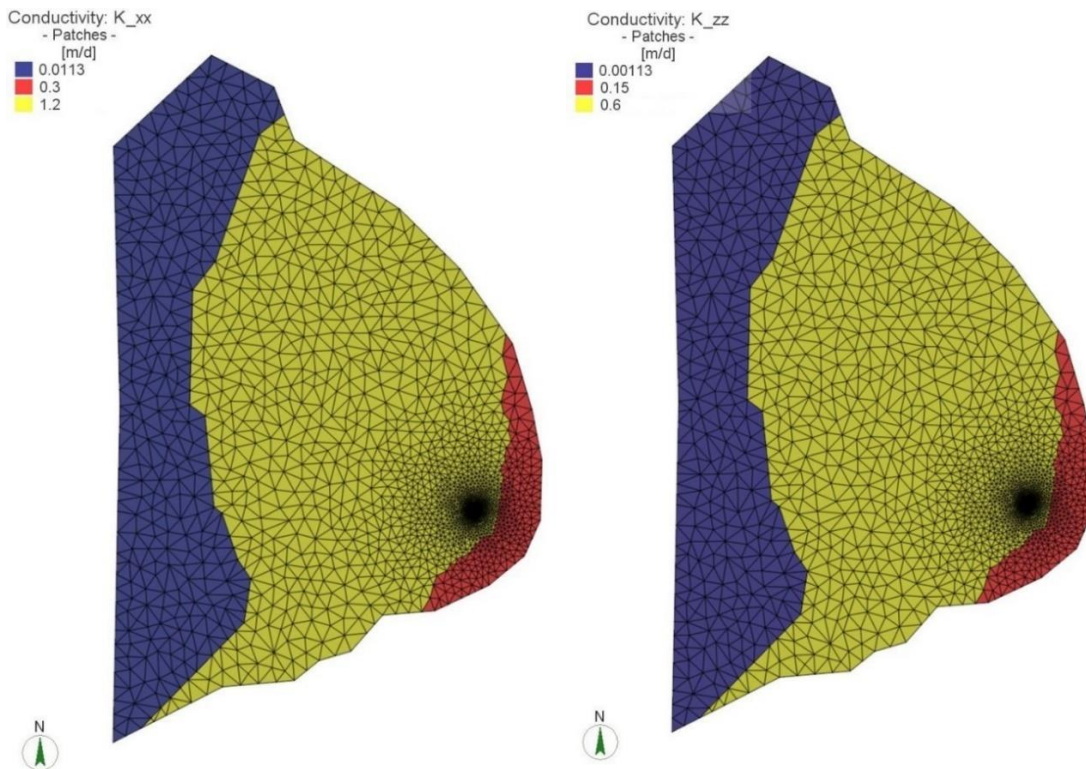


Figure 42: Conductivity of layer 2. In blue the portion of silt under the reservoir, in red the hydraulic connection

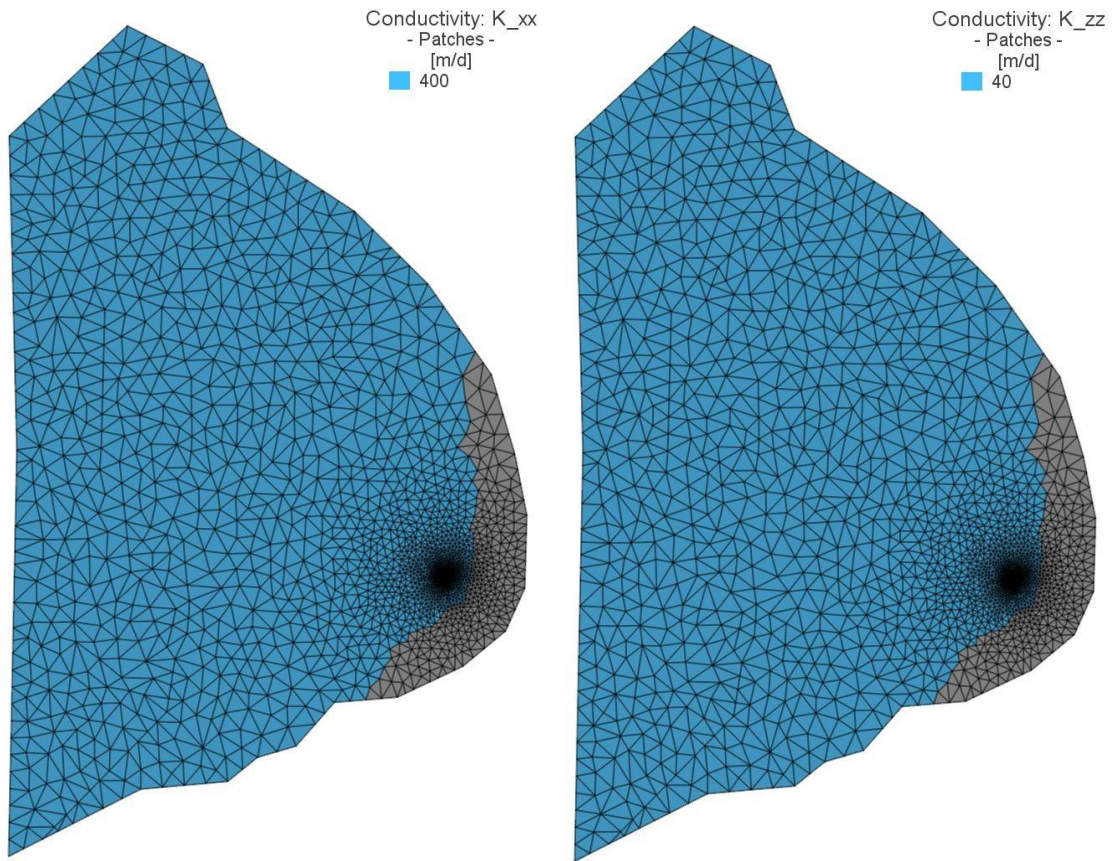


Figure 43: Conductivity of layer 3. In grey inactivated elements

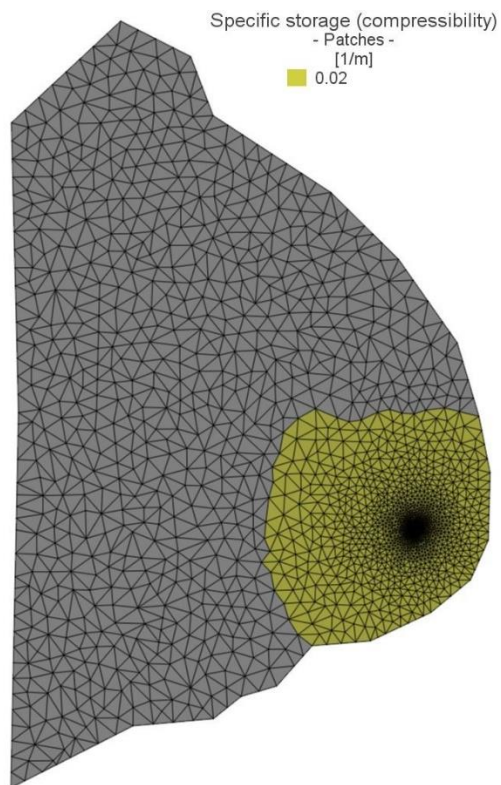


Figure 44: Specific storage of layer 1. In grey inactivated elements

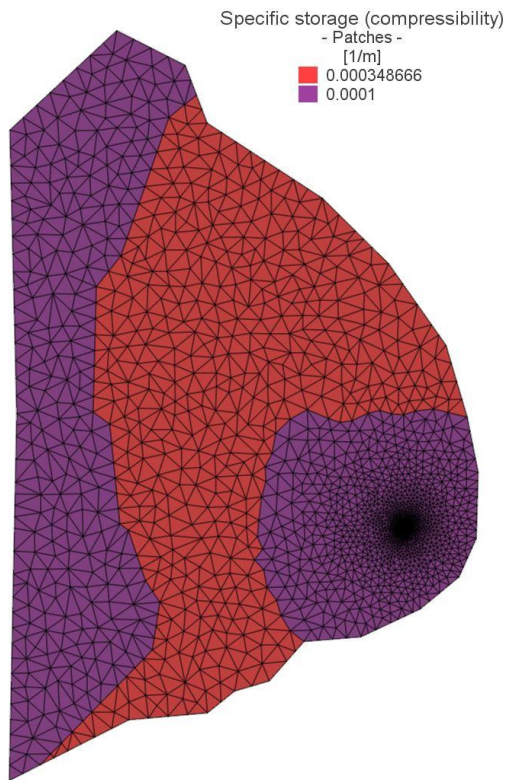


Figure 45: Specific storages of layer 2

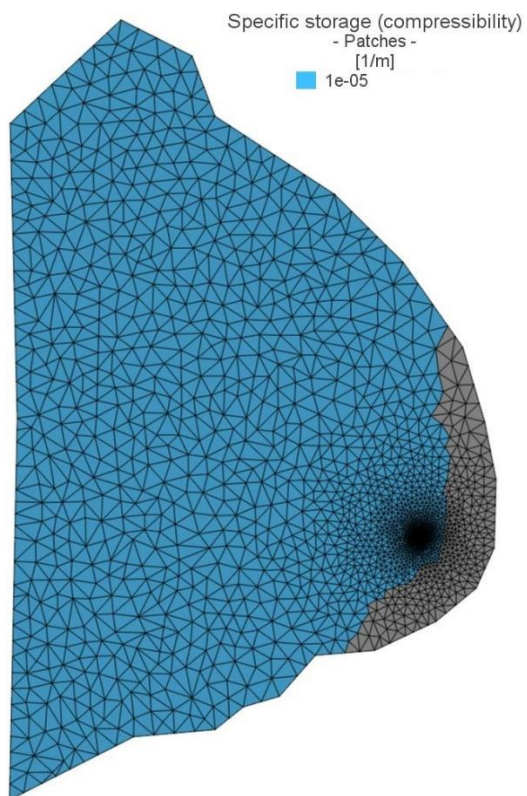


Figure 46: Specific storage of layer 3. In grey inactivated elements

#### 2.2.4.10 Observation Wells

In order to compare measured values with simulated values, 3 observation well were considered. The 3 observation wells are screened in the same layer of the injection well, gravel and sand, except PS14A which is screened also in 2<sup>nd</sup> layer, because it was installed with a different aim and before the others. The location of those points is shown in Figure 47.

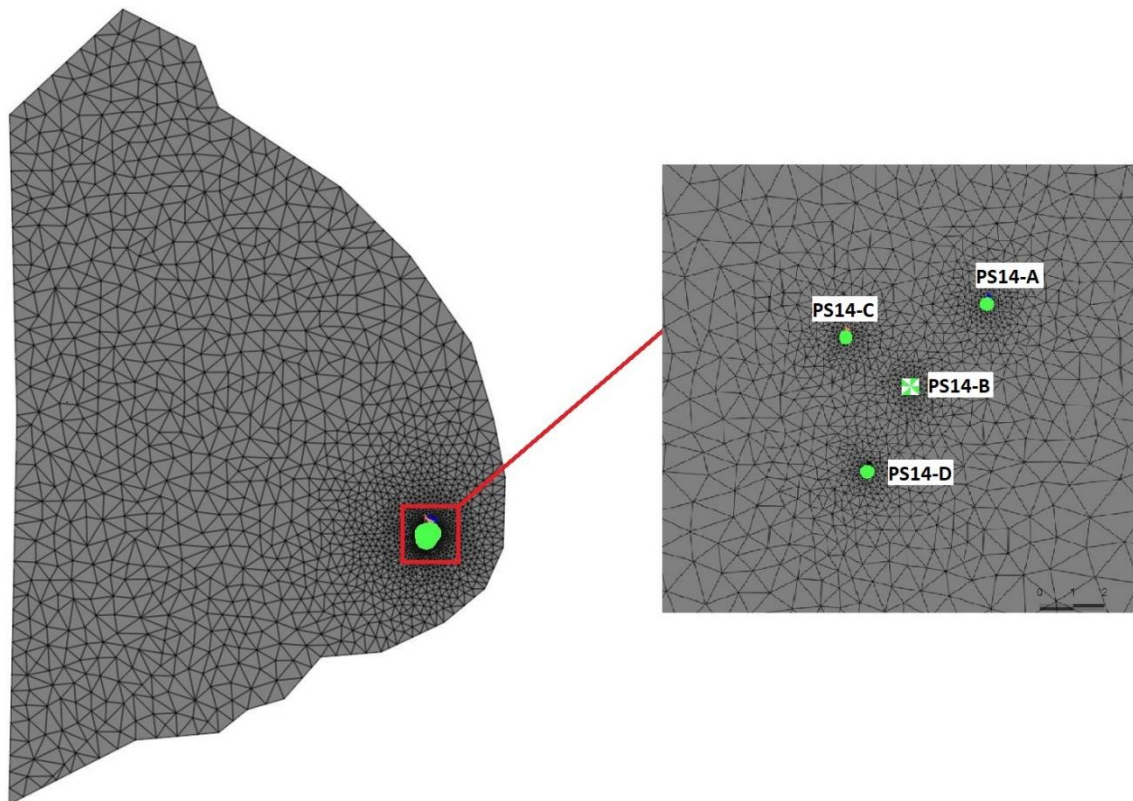


Figure 47: Location of the observation wells (green circles) and of the injection well at the centre

At those observation piezometers, PS-14A PS-14C and PS-14D, were defined as points on which the flow and the mass concentration has to be computed over the time of the simulation.

To compare the calculated values with the measured ones, the concentrations observed during the tracer test (Figure 18) and during the pilot test (Figure 20 and Figure 21), were assigned on the corresponding piezometer.

### 2.2.5 Flow and Transport Model Calibration with PEST

A PEST problem in estimation mode was run to calibrate the model.

As starting values for the PEST problem, summarised in Table 7, were used:

- Parameters from the finite differences model carried out by EMGRISA and AZENTUA;
- Medium hydraulic conductivity and specific yield of the gravel layer, obtained from the pumping test occurred in April 2018;
- Effective porosity of the gravel layer, obtained from the tracer test occurred in June 2018;

Table 7: input parameters for the calibration of the model

<b>K<sub>x-y</sub> (m/d)</b>	
Layer 1: anthropic filler	0.01
Layer 1: hydraulic connection	0.1
Layer 2: reservoir	0.01
Layer 2: hydraulic connection	0.1
Layer 2: silt	1
Layer 3	230
<b>K<sub>z</sub> (m/d)</b>	
Layer 1: anthropic filler	0.001
Layer 1: hydraulic connection	0.01
Layer 2: reservoir	0.001
Layer 2: hydraulic connection	0.01
Layer 2: silt	0.1
Layer 3	23
<b>Specific Storage (1/m)</b>	
Layer 1	0.006
Layer 2: footprint of layer 1 on layer 2	1.8e-4
Layer 2: reservoir	0.002
Layer 2: silt	0.003
Layer 3	4e-5
<b>Specific Yield (-)</b>	
Layer 1	0.08
Layer 2	1 e-3
Layer 3	1 e-4
<b>Dispersivity (m)</b>	
Longitudinal Dispersivity	5
Transverse Dispersivity	0.5
<b>Effective Porosity (-)</b>	
Layer 1	0.08
Layer 2	0.11
Layer 3	0.13

The parameters interested in the calibration were:

- Hydraulic conductivity on 1<sup>st</sup>, 2<sup>nd</sup> and 3<sup>rd</sup> layer (only for an optimization of the value);
- Specific Storage of 1<sup>st</sup> and 2<sup>nd</sup> layer;
- Longitudinal and Transverse Dispersion;

Those parameters were estimated on the base of the observations coming from the measures of the 3 observation wells previously indicated. The specific family of observations considered and their weight are reported in Table 8. It was decided to assign a weight equal to the inverse of the error resulting from the scatter plot of the simulated values and the measured ones, approximate to nearest integer.

*Table 8: Observation and relative weight in the PEST problem*

<b>Weights of the Observations</b>	
<b>Hydraulic Head (June 2018)</b>	13
<b>Hydraulic Head (July 2018)</b>	9
<b>Mass Concentration: NaBr (June 2018)</b>	6
<b>Mass Concentration: NaBr (July 2018)</b>	5
<b>Mass Concentration: Surfactant (July 2018)</b>	5

The Regularization techniques used in this problem are Tikhonov regularization and Subspace Regularization with Single Value Decomposition (SVD).

The Tikhonov regularization method generates several "information" equations, which defines the initial value of each parameter as the preferred value. When using Tikhonov regularisation, the calibration process is formulated as a constrained minimization process which minimize the regularization objective function while ensuring that the measurement objective function is set at the user-specified target. If this target is not met, then PEST minimizes the measurement objective function and, in the meantime, it adjusts weights applied to prior information.

PEST thus determines the appropriate relative weighting between measurements and respect for prior information in accordance with a user's choice of target measurement objective function. As a result, Tikhonov-Regularization reduces the number of possible parameter sets that constitute a calibrated model by rejecting calibrated models with unrealistic parameter values (FePEST in FEFLOW 7.0 user manual).

For what concern the Tikhonov regularization, it was based on both preferred values and on preferred differences. The limits for the objective function phi used in Tikhonov regularization were set

to 0.5 for the acceptable measurement of the objective function and 0.3 for the relative target measurement.

SVD is a subspace regularization that follows a different approach than Tikhonov regularisation: it separates identifiable parameter components from non-identifiable parameter components, in order to exclude the latter one from the parameter search, into 2 subspaces:

- Parameters which have no or very small influence on observations occupy the “null subspace”. Estimation of these parameters is not possible.
- The other subspace is comprised of combinations of parameters that have an influence on observations. It is called “solution subspace”. In most groundwater modeling contexts the solution space is smaller than the null space.

SVD analyses the eigenvalues of the covariance matrix to identify those parameters. The ratio of highest to lowest eigenvalue is the criterion of separation and it is also a measure of the ill-posedness: if this ratio is more than about  $5e-7$  then the problem can be considered to be ill-posed, and so not optimizable. As a consequence of this separation, the inversion of the solution space is always well-posed and a stable optimization is guaranteed (FePEST in FEFLOW 7.0 user manual).

To reduce the large number of model calls and the associated computational complexity in terms of each model run-time, a parallelization computing with 3 slaves was used.

For the same intent it was also separated the flow problem, concerning the estimation of hydraulic conductivity and specific storage, from the mass transport problem, concerning the dispersivity estimation.

The mass transport problems were evaluated using the parameters obtained from the calibration of the flow problem.

## 3 Results and Discussion

### 3.1 Quantum GIS

#### 3.1.1 *Boundary of the model*

First was created the polygonal shapefile in order to define the boundary of the model. To define the geometry, it was necessary to upload the background from Google Satellite (Web Map Service). The boundary of the model domain is represented in Figure 48.



*Figure 48: boundary of the model domain, in violet*

### 3.1.2 Wells and Piezometers

Second step was to create the shapefile relative to the piezometers used for the calibration of the model and for the definition, by interpolation, of the initial hydraulic condition of the model, which has been discussed. The results of the georeferencing is shown in Figure 49.

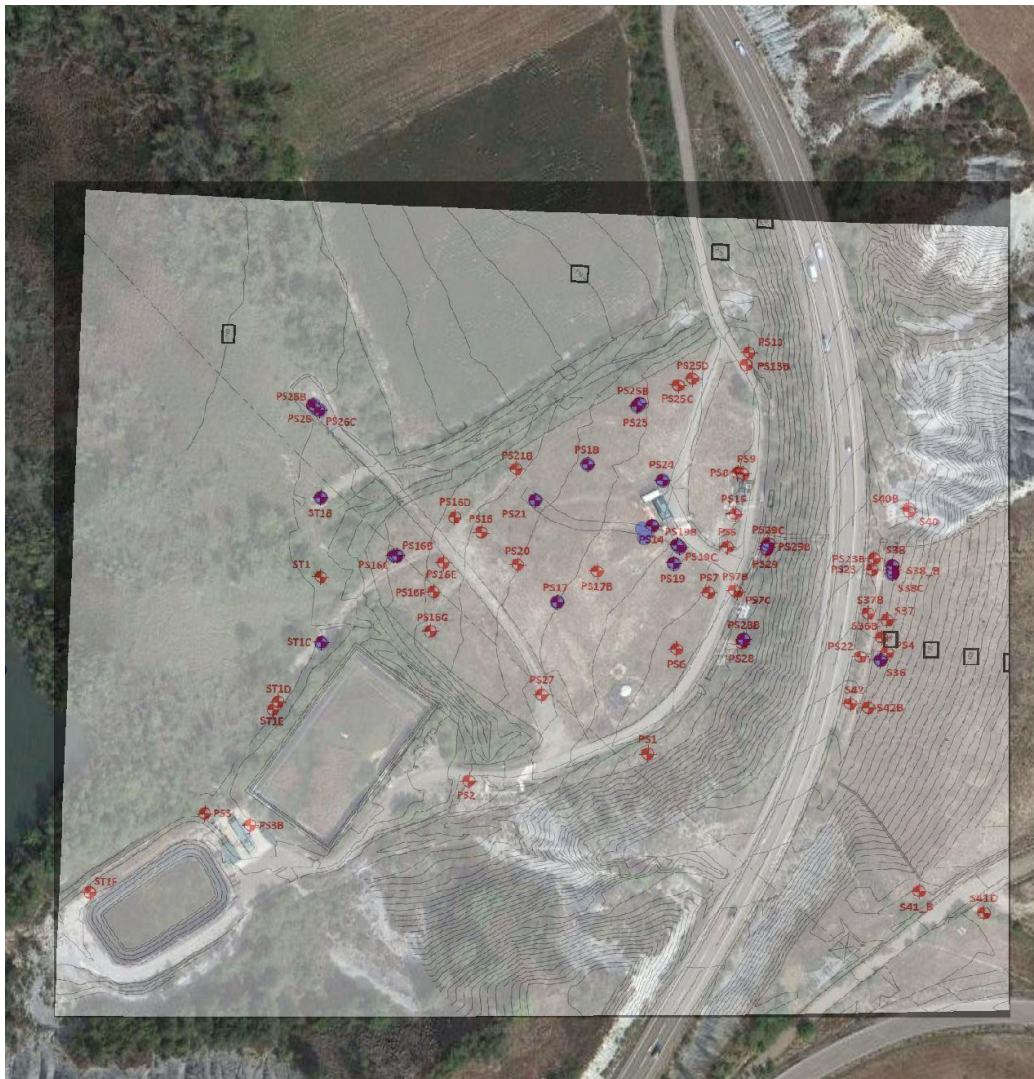


Figure 49: location of wells and piezometers used in the feflow

In Table 9 a summary of the used settings of the georeferencing is reported.

Table 9: summary of the georeferencing settings for the map of wells and piezometers

<b>Trasformation Algorithm</b>	2 <sup>nd</sup> order polynomial
<b>Resampling Method</b>	Nearest Neighbour
<b>Reference System of destination</b>	EPSG:32630
<b>Total Error</b>	7.44839

### 3.1.3 Points to apply elevation

The result of the georeferencing of the finite difference grid is shown in Figure 50. Points in red represent the 942 points used to attribute the elevation information to the finite element model of this thesis.

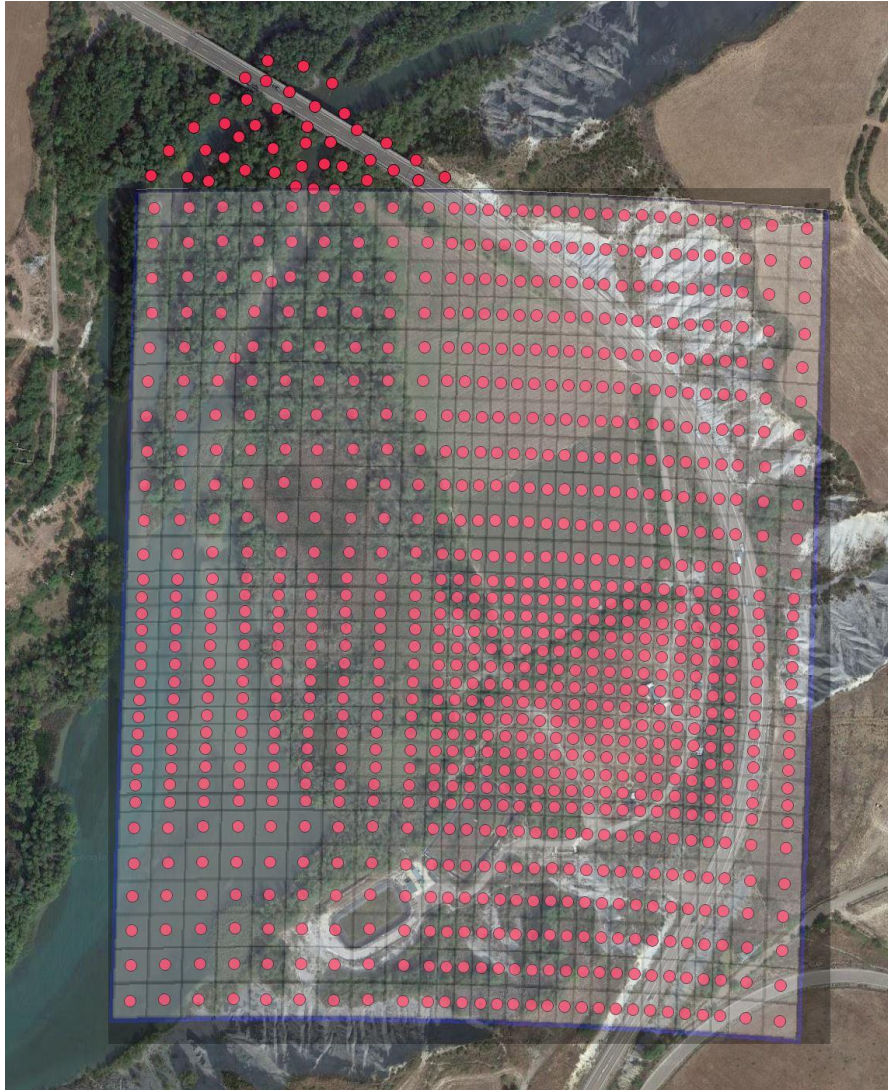


Figure 50: georeferenced grid whit points used to assign elevation information

Georeferencing settings are shown in Table 10.

Table 10: summary of the georeferencing settings for the finite differences grid

<b>Trasformation Algorithm</b>	2 <sup>nd</sup> order polynomial
<b>Resampling Method</b>	Nearest Neighbour
<b>Reference System of destination</b>	EPSG:32630
<b>Total Error</b>	5.68466

### 3.2 PEST

The results of the parameter estimation are presented in this section. In Table 11 are reported the statistics of the PEST problems evaluated.

It is possible to note that the time elapsed for flow problems is longer than the time for the mass transport problems. This is due to the number of the parameters that have been made to vary in the estimation: in the mass transport problems only the longitudinal and the transverse dispersivity in the gravel layer were searched. On the other hand, for flow problems were made to vary specific storage and hydraulic conductivity of all the layers and their sub-zones, resulting in a higher total amount of searched parameters and consequently in a longer computational time.

*Table 11: Statistics of the results of the PEST problems evaluated.*

<b>Flow Problem of June 2018</b>	
<b>Time elapsed</b>	2 hours and 28 minutes
<b>Initial Objective Function Phi</b>	39.05
<b>N° of Iterations</b>	9
<b>N° of run of the model</b>	195
<b>Final Objective Function</b>	5.05
<b>Mass Transport Problem of June 2018</b>	
<b>Time elapsed</b>	1 hour and 16 minutes
<b>Initial Objective Function Phi</b>	8542.4
<b>N° of Iterations</b>	8
<b>N° of run of the model</b>	50
<b>Final Objective Function</b>	7709.3
<b>Flow Problem of July 2018</b>	
<b>Time elapsed</b>	2 hours and 53 minutes
<b>Initial Objective Function Phi</b>	285.54
<b>N° of Iterations</b>	13
<b>N° of run of the model</b>	293
<b>Final Objective Function</b>	8.95
<b>Mass Transport Problem of July 2018</b>	
<b>Time elapsed</b>	1 hour and 47 minutes
<b>Initial Objective Function Phi</b>	994.82
<b>N° of Iterations</b>	6
<b>N° of run of the model</b>	60
<b>Final Objective Function</b>	728.7

The values of the starting parameter and the estimated parameters are reported in Table 12 and Table 13.

Table 12: results of the PEST problem for the tracer test episode

<b>Tracer Test Problem (June 2018)</b>		
<b>K<sub>x-y</sub> (m/d)</b>	<b>Starting Value</b>	<b>Estimated Value</b>
<b>Layer 1: anthropic filler</b>	0.01	0.001
<b>Layer 1: hydraulic connection</b>	0.1	0.56
<b>Layer 2: reservoir</b>	0.01	0.0087
<b>Layer 2: hydraulic connection</b>	0.1	0.56
<b>Layer 2: silt</b>	1	1.54
<b>Layer 3</b>	230	393.06
<b>K<sub>z</sub> (m/d)</b>	<b>Starting Value</b>	<b>Estimated Value</b>
<b>Layer 1: anthropic filler</b>	0.001	1e-4
<b>Layer 1: hydraulic connection</b>	0.01	0.056
<b>Layer 2: reservoir</b>	0.001	8.7e-4
<b>Layer 2: hydraulic connection</b>	0.01	0.056
<b>Layer 2: silt</b>	0.1	0.154
<b>Layer 3</b>	23	39.3
<b>Specific Storage (1/m)</b>	<b>Starting Value</b>	<b>Estimated Value</b>
<b>Layer 1</b>	0.006	0.03
<b>Layer 2: footprint of layer 1 on layer 2</b>	1.8e-4	2.4e-4
<b>Layer 2: reservoir</b>	0.002	7.8e-4
<b>Layer 2: silt</b>	0.003	0.004
<b>Layer 3</b>	4e-5	8.4e-5
<b>Dispersivity (m)</b>	<b>Starting Value</b>	<b>Estimated Value</b>
<b>Longitudinal Dispersivity</b>	5	55
<b>Transverse Dispersivity</b>	0.5	5.5

For what concerns the tracer test estimated parameters, is it possible to note that the anthropic filling hydraulic conductivity is reduced in favour of the conductivity of the hydraulic connection. This is due to the higher influence of this subzone, because of the landfill flux which is immediately in contact with the connection, making the filling soil hydraulic conductivity only a parameter used for the optimization of the fitting of the results. The hydraulic conductivity is generally increased in the other zones analysed, except for the reservoir zone, which is reduced of a little amount.

For what concerns the gravel layer, the hydraulic conductivity, even if the starting value was measured on field, is increased, but remaining in the range of the values observed in the pumping test occurred on April 2018. This can be due to the anisotropy of this layer, which was not considered in the model. For what concerns the dispersivity, the presumed high values detected in the tracer test and in the pilot test episodes is confirmed by the parameter estimation.

Specific storage varies in a range contained in the same order of magnitude, except for the reservoir subzone and for the filling soil.

Table 13: results of the PEST problem for the pilot test episode

<b>Pilot Test Problem (July 2018)</b>		
<b>K<sub>x-y</sub> (m/d)</b>	<b>Starting Value</b>	<b>Estimated Value</b>
<b>Layer 1: anthropic filler</b>	0.01	4.3
<b>Layer 1: hydraulic connection</b>	0.1	0.14
<b>Layer 2: reservoir</b>	0.01	3e-4
<b>Layer 2: hydraulic connection</b>	0.1	0.14
<b>Layer 2: silt</b>	1	3.14
<b>Layer 3</b>	230	310.15
<b>K<sub>z</sub> (m/d)</b>	<b>Starting Value</b>	<b>Estimated Value</b>
<b>Layer 1: anthropic filler</b>	0.001	0.43
<b>Layer 1: hydraulic connection</b>	0.01	0.014
<b>Layer 2: reservoir</b>	0.001	3e-5
<b>Layer 2: hydraulic connection</b>	0.01	0.014
<b>Layer 2: silt</b>	0.1	0.314
<b>Layer 3</b>	23	31.015
<b>Specific Storage (1/m)</b>	<b>Starting Value</b>	<b>Estimated Value</b>
<b>Layer 1</b>	0.006	0.005
<b>Layer 2: footprint of layer 1 on layer 2</b>	1.8e-4	1e-5
<b>Layer 2: reservoir</b>	0.002	5.3e-5
<b>Layer 2: silt</b>	0.003	3e-4
<b>Layer 3</b>	4e-5	1e-5
<b>Dispersivity (m)</b>	<b>Starting Value</b>	<b>Estimated Value</b>
<b>Longitudinal Dispersivity</b>	5	36
<b>Transverse Dispersivity</b>	0.5	3.6

For what concern the pilot test estimated parameters it is possible to note a high increase of the hydraulic conductivity of the anthropic filler, that exceed the typical range for this kind of soils. Even this can be attribute to the optimization of the fitting of the observed and simulated values, which let this parameter vary even substantially, in order to obtain a better fitting, which is minimum for this parameter variation.

Generally, it is possible to note an increase of the hydraulic conductivity values, except for the reservoir subzone, which is decreased. This general trend is observable also in the PEST results for the tracer test discussed above.

For what concerns specific storage, it is possible to note a drastically decrease of an order of magnitude. This trend should have been even higher, because the limit to this parameter variation was set to 1e-5 1/m.

Even here, as in the tracer test PEST results, the dispersivity is increased according to what observed in the test mentioned before, confirming the goodness of the PEST estimation for this parameter.

Both results of the PEST problems show a decrease of the specific storage values. Considering that this parameter represents the capability of the soil to retain water in its void, it means that the model developed, especially in the bottom layer, needs to transmit the flow quickly, in order to “receive” as soon as possible the variation occurred in the reservoir level. This fact is confirmed from the lower variation in the parameter occurred in the tracer test PEST results, where the level of the reservoir was not varying compared to the episode of July, resulting in a lower decrease of specific storage. This parameter has been chosen as base parameter to determine the others in the PEST problem carried out for the optimization of the results obtained.

The order of magnitude observed in the PEST results is in accordance with the typical ranges found in literature and is confirmed by the specific yield results from the pumping test occurred in April 2018, considering the depth of the layers.

Both results of the PEST problems show a decrease of the hydraulic conductivity of the zone relative to the reservoir. This is in accordance with the typical values observable in rivers and lake beds, where the transport of materials and the weight of the water determine an obstruction to the flow. The differences between the values resulting from the PEST can be attribute to the different oscillation over the period analysed: due to the presence of oscillations in the period of July 2018, the model developed tries to reduce the effect of the 1<sup>st</sup> type BC applied on the reservoir surface by reducing the values of hydraulic conductivity. This is due to the fact that this kind of boundary condition immediately applies the value imposed on the chosen nodes, thus resulting in an immediate variation in the hydraulic head observed under the reservoir.

Both results of the PEST problems show an increase of hydraulic conductivity for the gravel layer, the hydraulic connection and silt subzone of the layer 2. Considering that the elements under the connection were inactivated, this confirm the importance of the hydraulic connection and of the silts in the 2<sup>nd</sup> layer, which are the soils in which the flow from the landfill pass through. The differences between the PEST results of the 2 episodes can be explained considering the oscillation of the reservoir: with the absence of variation in the reservoir level the PEST tends to give a higher amount of flux from the landfill, because the BC applied on the reservoir does not compensates the amount “needed” from the observations, which are the values that PEST tends to fit. In presence of variations this flux is reduced and settled around the starting value. For what concern the hydraulic conductivity of the gravel layer, even if the starting value has been measured in the April 2018 pumping test, the higher value obtained in both PEST problems is due to the necessity of the model to quickly transmit the reservoir BC on the layer. This fact can be attribute to the anisotropy of the gravel layer, which has not been considered.

For what concerns the hydraulic conductivity of anthropic filler of the 1<sup>st</sup> layer, the opposite trend shown by the PEST results can be attribute to the PEST searching of the better parameter to fit the observed value. This fact leads to the maximization

of those parameters which does not influence the results, as can be confirmed by the fact that this zone is not interested by the landfill flux, which immediately found the hydraulic connection. For this reason, this parameter has been not modified.

Both results of PEST problem show an increase of dispersivity, as expected from the test. The difference in the different problem's results can be attributable to the oscillations occurred in the pilot test period.

Considering what discussed above, were defined the unique model used to simulate both episodes occurred, which parameters were the one that obtained the best fitting with the test observations. Table 14 reports those values.

*Table 14: parameters obtained from the calibration of the model, used to simulate the tests occurred. Parameters marked with \* were not considered in the PEST problems*

<b>K<sub>x-y</sub> (m/d)</b>	
<b>Layer 1: anthropic filler</b>	0.01
<b>Layer 1: hydraulic connection</b>	0.3
<b>Layer 2: reservoir</b>	0.0113
<b>Layer 2: hydraulic connection</b>	0.3
<b>Layer 2: silt</b>	1.2
<b>Layer 3</b>	400
<b>K<sub>z</sub> (m/d)</b>	
<b>Layer 1: anthropic filler</b>	0.001
<b>Layer 1: hydraulic connection</b>	0.15
<b>Layer 2: reservoir</b>	0.00113
<b>Layer 2: hydraulic connection</b>	0.15
<b>Layer 2: silt</b>	0.6
<b>Layer 3</b>	40
<b>Specific Storage (1/m)</b>	
<b>Layer 1</b>	0.02
<b>Layer 2: footprint of layer 1 on layer 2</b>	1e-4
<b>Layer 2: reservoir</b>	1e-4
<b>Layer 2: silt</b>	3.48e-4
<b>Layer 3</b>	1e-5
<b>Specific Yield* (-)</b>	
<b>Layer 1</b>	0.08
<b>Layer 2</b>	1 e-3
<b>Layer 3</b>	1 e-4
<b>Dispersivity (m)</b>	
<b>Longitudinal Dispersivity</b>	50
<b>Transverse Dispersivity</b>	5
<b>Effective Porosity* (-)</b>	
<b>Layer 1</b>	0.08
<b>Layer 2</b>	0.11
<b>Layer 3</b>	0.13

### 3.3 FEFLOW

Once that all the parameters involved in the solution of the flow and of the mass transport problems have been set, it is possible to start the simulation, which, for this coupled flow-mass transport problem, can last between 5 to 10 minutes, depending on the different simulation episodes analysed.

This is due to the heaviness of the calculus for the mass transport, which is also heavier in the case of the pilot test, because the mass transport equation has to be solved for 2 compounds (tracer and surfactant). This is also due to the characteristics of the processor used.

The results of the simulation are presented and discussed in the following paragraphs, divided into the 2 different periods studied, and discussed separately basing on the class of the problem.

For what concerns the flow problem, for both episodes the graph of the hydraulic head (computed and observed in the piezometers) in time is compared with the water level of the reservoir, to assess if the model was able to reproduce the reservoir's oscillations. For what concerns the mass transport problem, the simulated mass concentration in time is compared to the measured one, by plotting them in the same graph.

#### *3.3.1 Tracer Test (4<sup>th</sup>- 9<sup>th</sup> of June 2018): Results*

For what concern the flow problem of the tracer injection and extraction, the result of the simulation is reported in Figure 51.

Is it possible to observe that, after an initial period of 1000 minutes which corresponds at about 16 hours, the simulated values start to fit the observed values, following in a good manner the injection phase, represented by the peak upwards at about 2000 minutes, and the successive time before the extraction, which is represented by the peak downward.

After the initial instants of the extraction, the computed values start to deviate from the measured ones, reaching lower values and maintaining a difference of 5 cm and then recovering it in the final phases of the simulation.

It is important to note that the simulated values show the same hydraulic head although the observed values differ from each other of a little amount in a range of 2 cm.

For what concern the mass transport simulation, results are reported below in Figure 52.

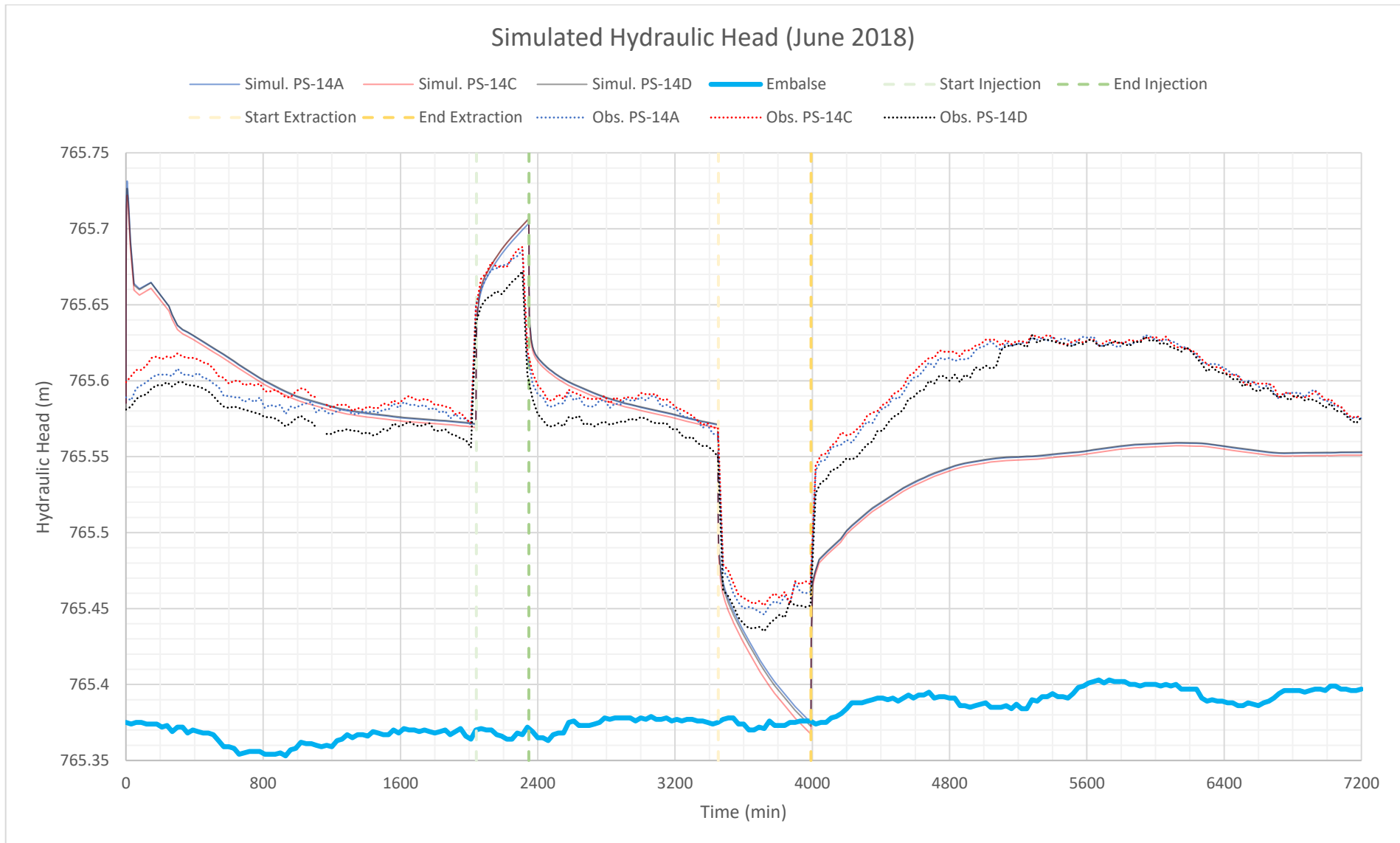


Figure 51: results of the flow simulation, the level of the reservoir is represented in light blue, the values simulated and the values measured in the piezometer (marked with a dot line) are represented in blue, red and black for PS-14A, PS-14C and PS-14D respectively. Note that simulated values for PS-14A, PS-14C and PS-14D are mostly overlapped

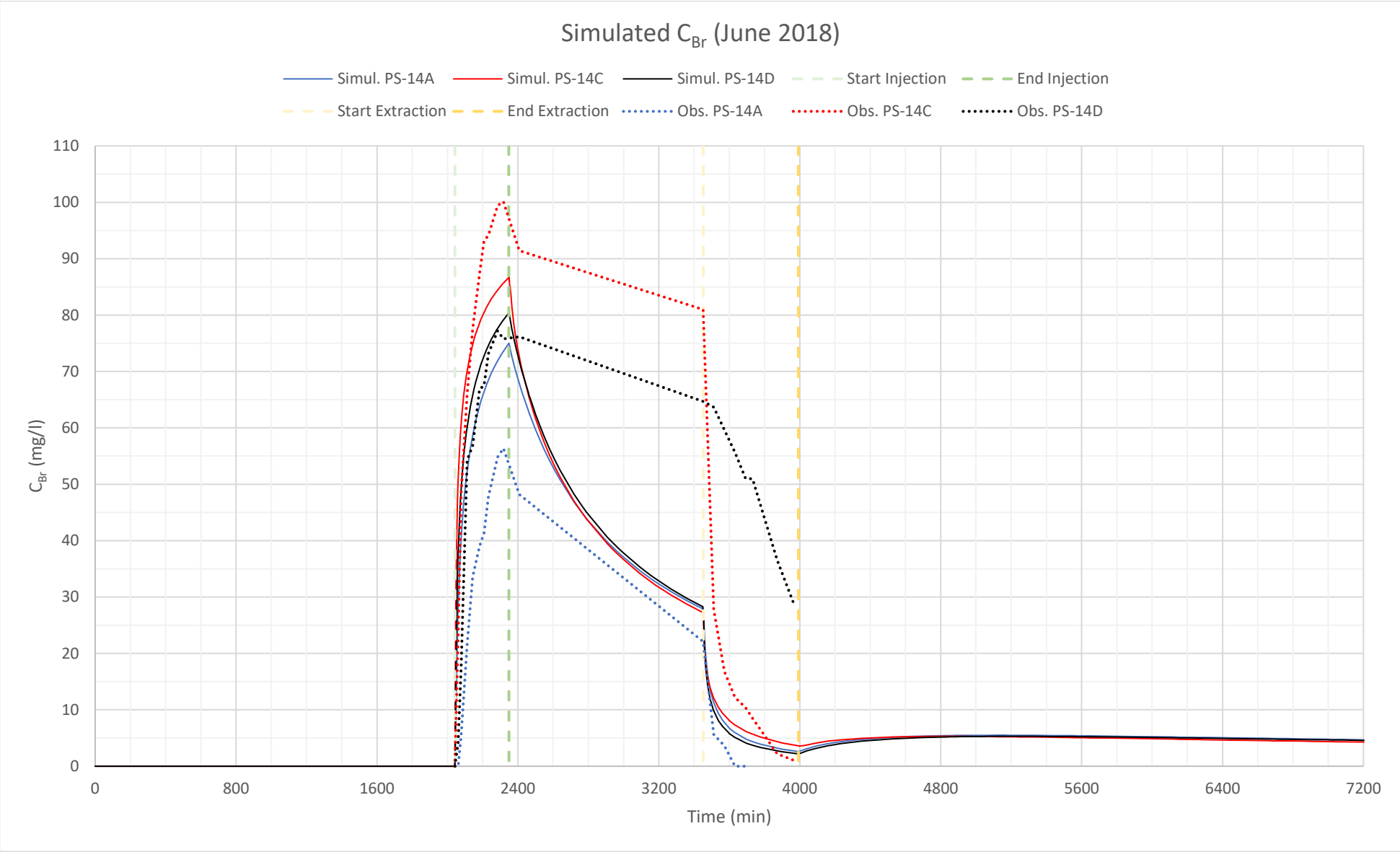


Figure 52: results of mass transport simulation, the values simulated and the values measured in the piezometer (marked with a dot line) are represented in blue, red and black for PS-14A, PS-14C and PS-14D respectively

Here is it possible to observe that the computed concentration of  $\text{Br}^-$  remain in a narrow range of about 10 mg/l at the peak instant, right after the injection, while the measured values vary in a more pronounced one.

This fact reveals an evident differentiation of the measured concentration in the piezometers, resulting that the piezometer PS-14A show the lowest values and PS-14C the highest. The range of the observed values is included between 55 mg/l and 100 mg/l at the moment of the peak.

After the injection, both simulated and measured values start decreasing in a different manner: measured ones in a linear way, due to the method used for the interpolation of the observed values in the piezometer, while computed ones decrease in an exponential way, which become more evident at the extraction phase. Must be remind that the linear-trend decrease between injection and extraction is due to the lack of measures over that period.

In the extraction phase, both of measured and simulated graphs reach null values, generally closer to zero for the observed values, and after that is it possible to observe a small increase of the simulated values, due to the stopping of the pump. While there are not data about measured values after the extraction phase, is it plausible to assume the same trend for the observed concentrations.

### *3.3.2 Tracer Test (4<sup>th</sup>- 9<sup>th</sup> of June 2018): Discussion*

For what concern the initial mismatch among the values, this fact is due to a mismatching between real and simulated initial hydraulic head conditions, that can be attributable to some errors in the interpolation of the values measured in the piezometers. This implies that the model requires time to settle the initial conditions. This fact was previously considered when build the problem setting of the model, by starting the simulation a day before the injection.

The trend of the simulated values follows, after the initial instantaneous decrease due to the mismatching in the initial conditions, the typical trend of a confined aquifer under pumping condition. The simulated values maintain approximately (2 cm of difference), after the end of the extraction, the same level of the period before injection. In fact is it possible to observe that, in comparison to the general trend of the oscillation in the reservoir, the studied period has an atypical lack of variations.

The difference between the measured values and the ones simulated by the model, which starts during the extraction phase, could be attributed to the calibration of the model. Considering that the PEST results for the hydraulic conductivity of the connection have shown an estimated values of 0.56 m/d (reduced to 0.3 to consider the other test's PEST result, 0.14), the small increase of the level of the reservoir (which pass from 765.36 meters to 765.4) involves in a lower increase of the

simulated hydraulic head (compared to observed values) after the extraction phase, due to the lack of the flux from the landfill.

For what concern the absence of distinctions among the simulated hydraulic heads (among simulated values in PS-14A, PS-14C and PS-14D) instead of the differences observable among the measured values (among observed values in PS-14A, PS-14C and PS-14D), this is due to the fact that in the model the layer of interest has been considered homogeneous.

The real site's conditions present a variation in terms of electrical and hydraulic conductivity, as shown in the tomography and pumping test carried out, which mean that the layer has non homogeneous sub-zones, involving in a certain degree of anisotropy in the layer. That determine those differentiations of hydraulic head among the measured values in the piezometers, even if they are located closely.

For what concern the mass transport, the differentiation in terms of width of the range observed and simulated and the difference in terms of measured and computed absolute values, find an explanation considering that the mass transport is strictly linked to the flow problem:

- The differentiation in the extent of the range is due to the imposed homogeneity of the model, which results in non-variation among the simulated hydraulic head in the piezometers, and consequently on the non-variation of the concentration. The small variation range showed from the simulated values (from 75 mg/l at PS-14A to 85 mg/l at PS-14C) is therefore due to the dispersion of the mass, which brings to show those little differentiations, because of the distance among the piezometers;
- The difference in values, namely the fact that the simulated values are lower than the measured concentrations, is due to the hydraulic head gap between simulated and observed values, which is firstly very small at the time of the injection, higher for the simulated ones, resulting in a lower values of concentration because the mass is more easily carried by the higher hydraulic gradient created from this situation. The opposite situation is shown after the extraction, where lower simulated values determine higher concentration values, even if both near zero.

### *3.3.3 SEAR Pilot Test (9<sup>th</sup>- 13<sup>th</sup> of July 2018): Results*

For what concerns the flow problem of the tracer injection and extraction, the result of the simulation is reported in Figure 53.

For what concerns the mass transport, results are reported in Figure 54 for the tracer and in Figure 55 for surfactant.

### Simulated Hydraulic Head (July 2018)

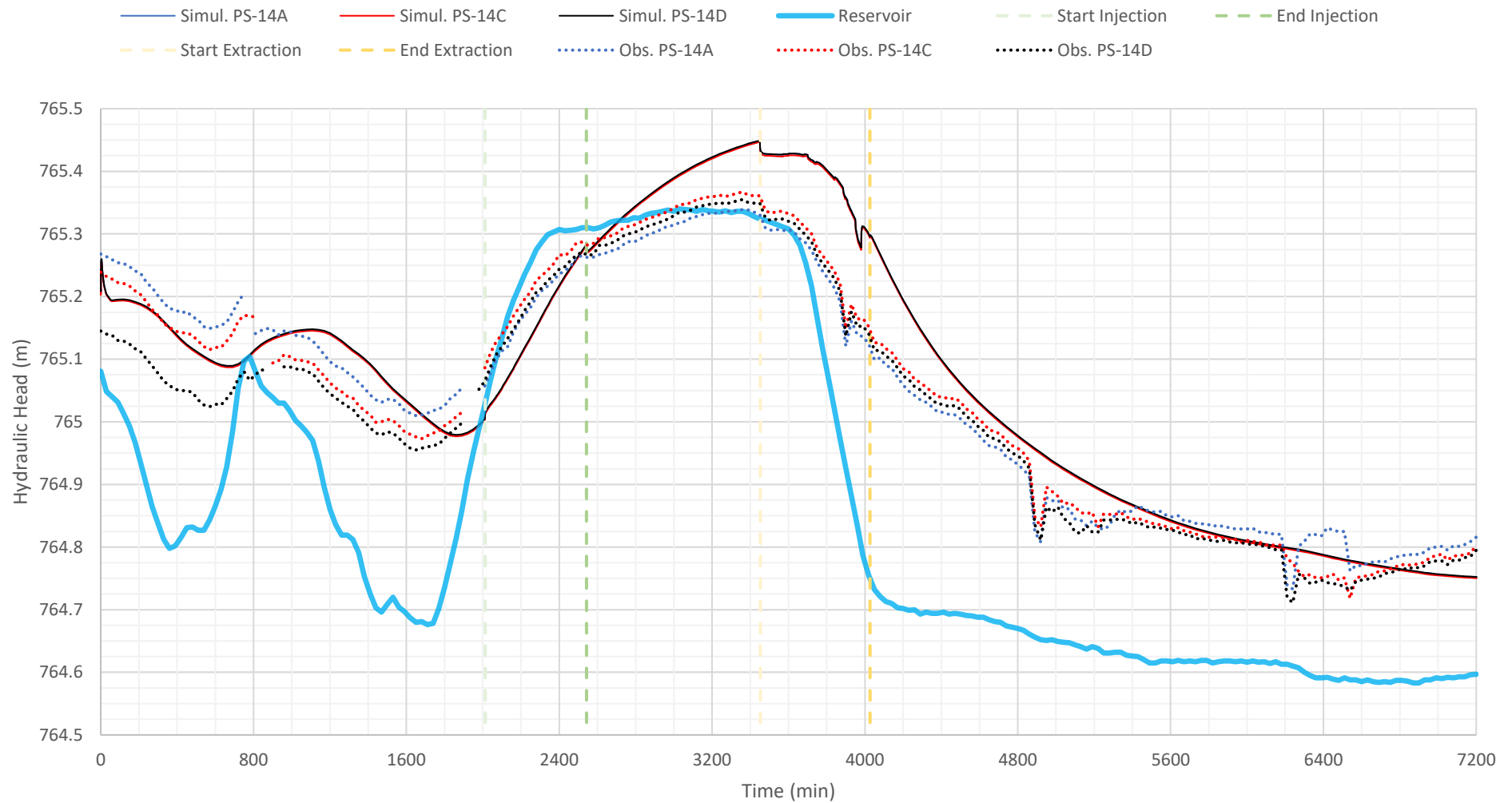


Figure 53: results of the flow simulation, the level of the reservoir is represented in light blue, the values simulated and the values measured in the piezometer (marked with a dot line) are represented in blue, red and black for PS-14A, PS-14C and PS-14D respectively. Note that simulated values for PS-14A, PS-14C and PS-14D are mostly overlapped

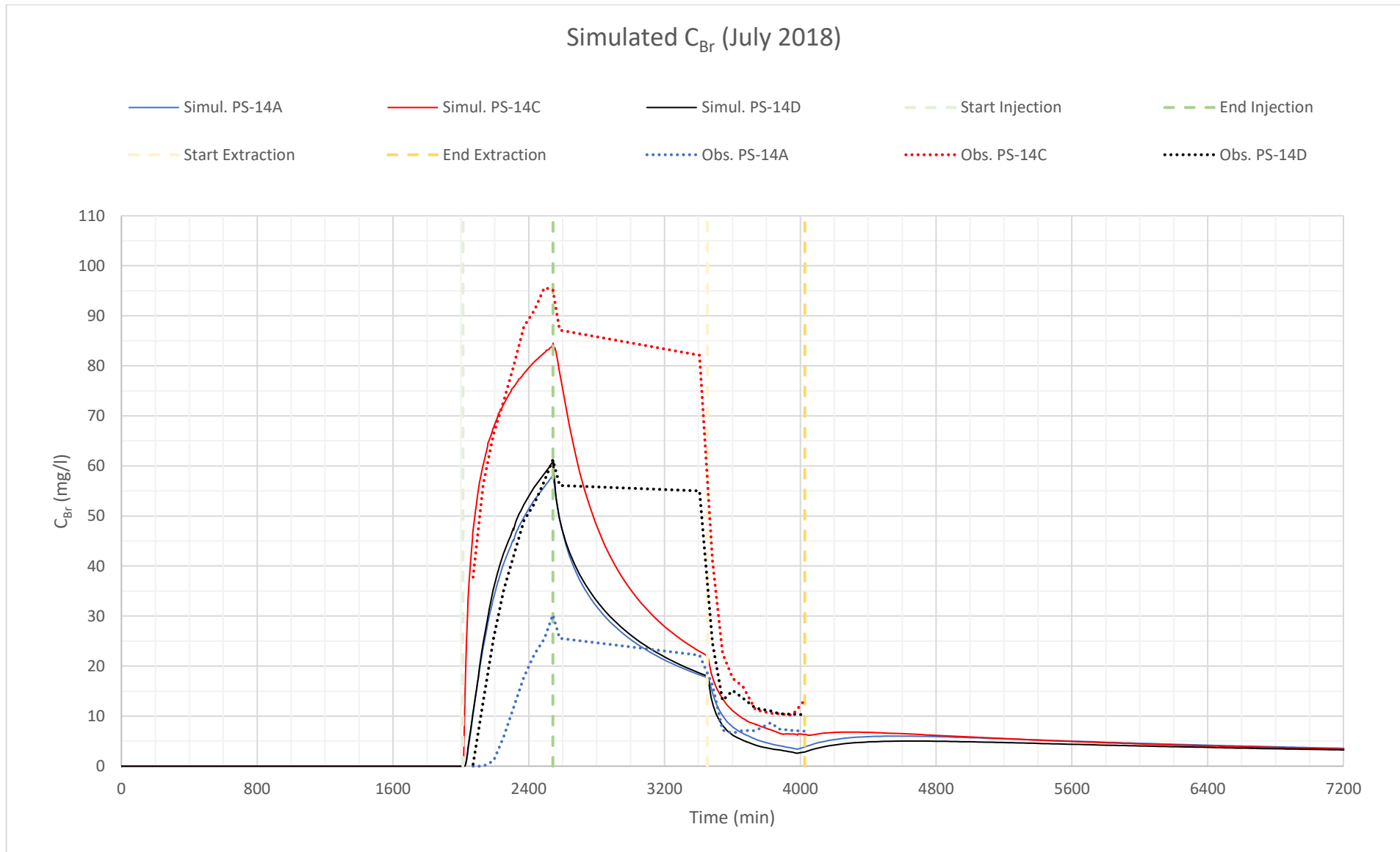


Figure 54: results of the Br transport simulation, the values simulated and the values measured in the piezometer (marked with a dot line) are represented in blue, red and black for PS-14A, PS-14C and PS-14D respectively

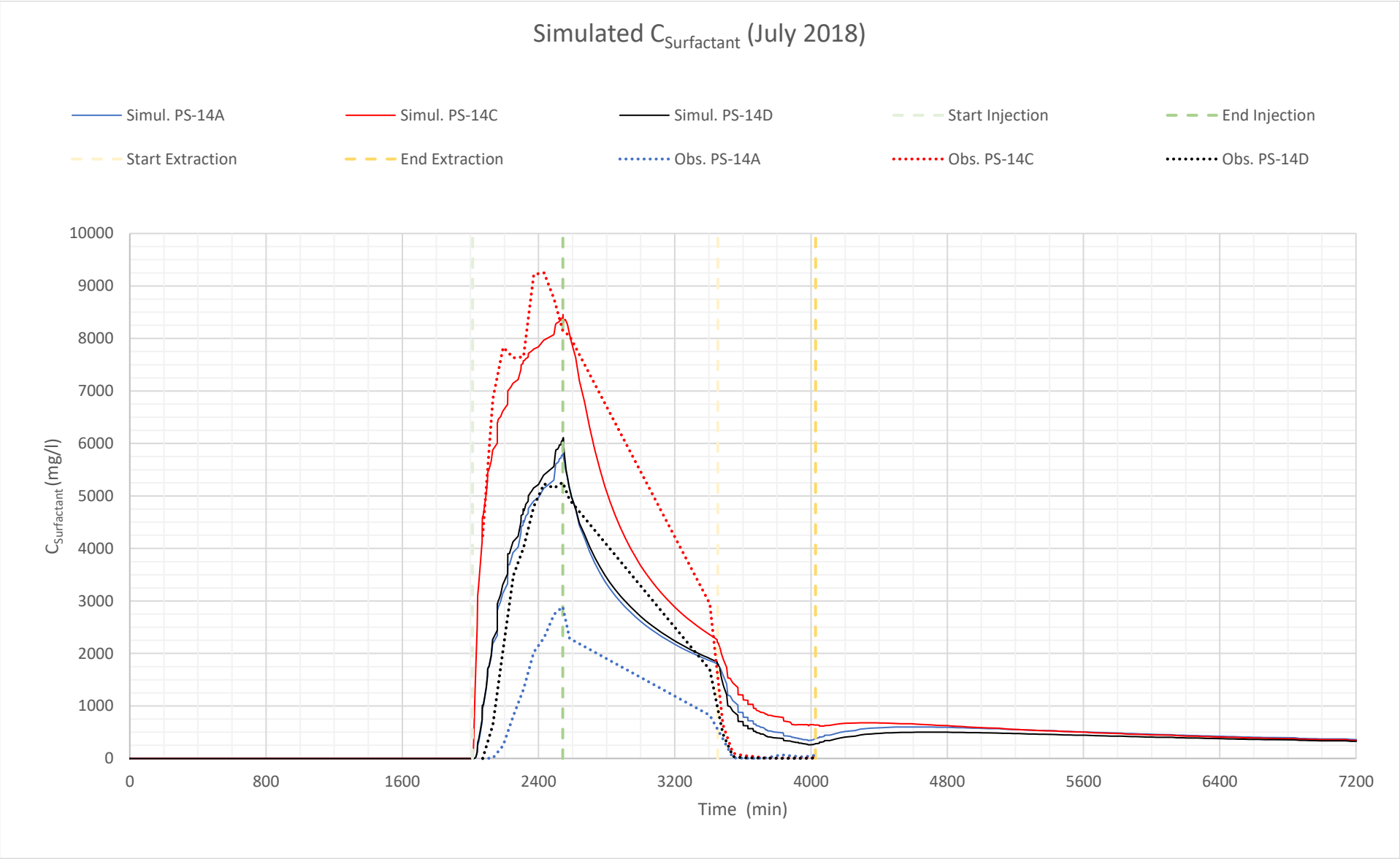


Figure 55: results of the surfactant transport simulation, the values simulated and the values measured in the piezometer (marked with a dot line) are represented in blue, red and black for PS-14A, PS-14C and PS-14D respectively

In Figure 53 it is possible to observe that the simulated values, which plots are overlapped, follow, with a little shift, the measured hydraulic head in the piezometers until minute 2600, which correspond to the period successive the injection.

After that a gap between them is formed, which is firstly low and then slowly increase, until the extraction phase, where the gap maintain itself to a constant value of about 10 cm reaching the maximum difference between observed and computed values. After the extraction period, which ends at minute 4000, the gap starts to decrease until it gradually settles to the measured hydraulic head values after 10 hours from the end of the extraction, at minute 4600.

Even here, as on the previous simulation period (June 2018), it is important to note that the simulated values show the same hydraulic head although the observed values differ among each piezometer of a varying amount.

This differences among the measured values is higher in the first phase of the simulation (reaching a maximum of about 12 cm) until minute 750 and then start to decrease settling itself on a difference of 5 cm until the beginning of the injection (minute 2000), where the range of the measured values maintain the minimum difference of 2 cm until the end of the simulation.

In Figure 54 it is possible to observe that the computed concentration of  $\text{Br}^-$  remain in a range of about 25 mg/l at the peak instant, with a maximum and a minimum of simulated values of 85 mg/l and 60 mg/l, right after the injection, while the measured values vary in a more pronounced one, being the maximum measured value at the same peak of 95 mg/l and a minimum of 30 mg/l. It must be noted that none of the computed values reach the ones of the PS-14A

After the injection, both of simulated and measured values start decreasing in a different manner: measured ones remaining about constant until the phase of extraction, where in a linear way, due to the interpolation method used, they quickly decrease, while computed ones decrease in an exponential way, which seems not to vary too much at the extraction phase, as it was in the previous simulation period (June 2018). Must be remind that the linear trend observable in the measured values is due to the lack of measures over the period between injection and extraction.

In the extraction phase, both measured and simulated graphs reach their lowest values, settling to a value of 5 mg/l for the computed values, and after that is it possible to observe a small increase, due to the stopping of the pump. Observed concentrations, in this phase, reach values of about 5 mg/l (maximum difference, referred to piezometers PS-14C and PS-14D) higher than the simulated ones.

The surfactant injection, shown in Figure 55, has been simulated without considering changing in viscosity and retardation coefficient, associating this compound only to the liquid phase.

It is possible to observe that the simulated mass concentration remains, at the peak moment after the injection instant, in a range of 2.700 mg/l with a maximum registered at piezometer PS-14C of 8.500 mg/l and a minimum registered at piezometer PS-14D of 5.800 mg/l. It has to be noted that, even here, none of the computed values reach the concentration observed at PS-14A.

After the injection, both simulated and measured values start decreasing in a more similar manner in comparison to the previous: measured ones, in a linear way, due to the method used for the interpolation of the observed values, while even here computed ones decrease in an exponential way.

Both of simulated and measured concentrations decrease with a high slope, which is similar for the computed values for the 2 different compounds, but different for the observed values: in the surfactant injection measured values are more similar to the simulated ones in comparison to the tracer injection ones.

In the extraction phase, both of simulated and measured values, which start from a lower point in comparison to the tracer concentration trend, decrease less than the post-injection/pre-extraction part of the chart, with higher slopes for the measured values and lower slopes for the computed ones.

After the end of the extraction, observed values set themselves to zero while the simulated one firstly reach a minimum value of 300 mg/l at PS-14A, then raise to settle themselves to a value of 500 mg/l and finally slowly decrease to 400 mg/l at the end of the simulation.

#### *3.3.4 SEAR Pilot Test (9<sup>th</sup>- 13<sup>th</sup> of July 2018): Discussion*

Even in the pilot test, as in the tracer episode (June 2018), for what concerns the absence of distinctions among the simulated values instead of the ones observed, this absence could be attributed to the fact that in the model the layer of interest has been considered homogeneous, determining none differentiations of hydraulic head among the piezometers.

This differentiation in the measured values is more pronounced in comparison to the tracer episode (June 2018) because of the high and fast reservoir oscillations that affect this episode (July 2018) in the first part of the chart until the injection (minute 2000), which amplifies the difference among observed values.

This is likely due to the heterogeneity in the layer, which determines differentiations in the hydraulic head which are more pronounced if the reservoir level quickly increases, because those oscillations are better transmitted where the anisotropy characteristics allow it, resulting in higher values and so in higher gap among the piezometers.

The gradual reduction of the gap among measured values could be attributed to the maximum oscillation registered, over both period of the injection and extraction, which is about 70 cm, that seems firstly to saturate the gravel layer (which top is at about 762m) and then, at the end of the oscillation, to stabilize its conditions.

Contrary to what happens in the first day of the graph (until minute 1440) where 2 complete oscillations can be observed, in both period of the highest oscillation (from minute 2300 to minute 3600) and the following part (from the end of the extraction until the end of the simulation) the level of the reservoir maintain a value in a range from 5 to 10 cm, that can be view as constant in comparison to the typical oscillations of the reservoir. Considering this, this reduction among the measured values in the piezometers can be attributable firstly to the saturation, which allows to recover the gap, and then to the constant trend of the reservoir level, which maintain it in a small range.

The difference observed between measured and computed values over the period of the extraction can be attributed to the maximum oscillation registered, which seems not to be immediately managed from the model, resulting in a shift of the simulated values, which amplify the difference in terms of absolute values. This is attributable also to an error in the calibration of the model, which could have cause this shift and also an increase of the differences in hydraulic head.

As in the tracer test, for what concern the mass transport, the differentiation in terms of width of the range observed and simulated, and the difference in terms of measured concentration values, finds an explanation considering that the mass transport is strictly linked to the flow problem, for both tracer and surfactant concentrations:

- The differentiation in the range is likely due to the imposed homogeneity of the model, which results in the absence of significant differences among the simulated hydraulic head in the piezometers. The fact that the simulated concentration in PS-14A is higher than the measured one may be attributed to the fact that, even if the dispersion is relatively high, the increase of the reservoir water level determine a mass transport in that direction, which plausibly should have been reduced by the anisotropy of the layer in that point, resulting so in higher concentration values.
- The difference in values is due to the hydraulic head gap between simulated and observed values over the extraction period, resulting in a lower value of concentration because the mass is more easily carried by the higher hydraulic gradient created from this situation. The difference between the tracer and the surfactant concentration trends over this period may be due to the different properties of those compound.

### 3.3.5 General discussion on both episodes

In conclusion is it possible to state that:

1. Concerning the flow problem, considering the overall trend in the 2 episodes analysed, globally the model can appreciate the oscillations of the reservoir. This is observable in the fact that in absence of oscillation (June 2018) are clearly seen the trend typical for a pumping well and in the fact that in presence of oscillations (July 2018) simulated values can follow the trend of the measured ones, but with differences in terms of absolute values and shift of the plots;
2. Concerning the flow problem, considering singularly each episode, it is not possible to state that the result in terms of computed values is correct if compared to observed ones. This is due to the fact that was not considered anisotropy in the layer of interest, manifesting it in differences in terms of absolute values and in the non-differentiation of the computed result in comparison to the measured values. Those differences observed between measured and simulated values can also be attributable to the different behaviour of the reservoir in the different periods studied;
3. Concerning the injection of tracer in both episodes, generally the trends of the computed concentration shows an initial phase in which, with little differences, the measured and simulated concentration reach the peak to then distance their self later. Considering each single measure, is it possible to observe a non-differentiation (more marked in the episode of June 2018 due to the absence of oscillations) among each piezometer, which can be attributable to the anisotropy of the site;
4. Concerning the injection of surfactant, the trend seems to be followed by 2/3 of all piezometers. In the model this can be explained with the homogeneity assigned all over the 3<sup>rd</sup> layer: by this fact the concentration of piezometers PS-14A and PS-14D, which are not properly on flow direction compared to PS-14C, results similar over the period of injection and extraction, where the level of reservoir is high and the layer can be considered as saturated, so reducing the differences created from the anisotropy.

## 4 Conclusions

A finite element model has been developed using FEFLOW, in order to evaluate the applicability of the SEAR technique on a site contaminated by DNAPL and affected by reservoir oscillations. In order to evaluate the goodness of the model, two tests were simulated: a tracer test occurred in June 2018 and a SEAR pilot test occurred in July 2018.

Parameter estimation (PEST) have been used in order to evaluate those parameters that were not measured in field. The results obtained from the PEST problems have been analysed in order to build the unique model used in the simulation.

The results of the flow and mass transport simulation shows a lack of differentiation among the simulated value, due to the anisotropy of the site which has not been considered in the model.

The results also show a difference between the simulate and observed values that can be attributable to the calibration of the model, which have been a compromise between the PEST results of the different episodes studied. This difference can also be attributable to the different trend of the reservoir level observed in the episodes, which can drastically change the behaviour of the model.

Considering the results obtained, for a future develop of the model must be consider the anisotropy of the gravel layer. For this purpose, a calibration of the model considering a larger amount of points of observation should be done. More over should be detected and considered also the fractures present in the marl layer.

Considering the results obtained, for a future develop of the model must be conduct a more detailed calibration, based on a larger temporal period, in order to find the unique model available to consider different oscillation ranges.

Considering the results obtained, for a future develop of the model the nature of the hydraulic connection should be studied in detail, to confirm the conceptual model and to allow a proper computational way in the groundwater modeling of the site.

In conclusion, considering the results obtained from the model used in this work:

- Is it not possible to state that, concerning the flow problem, the simulation model can be assumed as properly correct, even if it can appreciate the general trend of the oscillations. This is due to the lack of calibration and to the anisotropy.
- Concerning the tracer transport problem, it is not possible to state that the model can be assumed as properly correct, even if the general trend is followed, considering the lack of measures between injection and

extraction. This is due to the anisotropy.

- Concerning the surfactant transport problem, it is possible to state that the model can be assumed as correct for 2/3 of the observation wells around the injection point. This could be helpful in order to apply the SEAR technique, but due to the harmful characteristics of those kind of compound a better evaluation must be done.
- Concerning the general results obtained, this model cannot be assumed as properly correct, but can be use as base model in order to build a more detailed model that could be able to improve the results evaluating a variable density problem.

## 5 Appendices

### 5.1 Appendix A: Ground Control Points used in the georeferentiation

*Table 15: Ground Control Point used for the georeferencing of the wells and piezometers map*

ID	Origine X	Origine Y	Dest. X	Dest. Y	dX (pixel)	dY (pixel)	Residuo (pixel)
0	269.588	-926.014	-38471.5	5.23826e+06	2.90629	3.29102	4.39059
1	66.1498	-1016.72	-38538	5.23823e+06	-5.29517	0.94155	5.37822
2	413.07	-626.238	-38423.6	5.23835e+06	3.10652	7.73787	8.33817
3	816.743	-412.423	-38292.4	5.23842e+06	2.10893	1.05388	2.35759
4	922.177	-194.381	-38260.6	5.23848e+06	-9.77798	-4.99269	10.9789
5	952.154	-409.925	-38250	5.23842e+06	-5.34583	0.594916	5.37883
6	803.227	-407.523	-38296.9	5.23842e+06	1.9339	0.452126	1.98605
7	832.052	-441.088	-38287.3	5.23841e+06	2.65398	3.54039	4.4247
8	381.747	-317.846	-38431.4	5.23845e+06	0.681403	-8.2394	8.26753
9	856.262	-1158.72	-38284	5.23819e+06	-2.28458	-3.94971	4.56284
10	1000.71	-1.1369e-13	-38230.9	5.23854e+06	-0.448011	1.74558	1.80216
11	807.51	-416.446	-38295.3	5.23841e+06	2.62489	0.781015	2.73862
12	1019.15	0.331801	-38224.3	5.23854e+06	1.14567	1.65825	2.01553
13	1036.47	-0.401654	-38219.3	5.23854e+06	-1.30891	-0.0518007	1.30993
14	272.07	-837.875	-38467.1	5.23829e+06	11.7531	5.20273	12.8532
15	382.089	-914.923	-38438.6	5.23827e+06	-5.80028	-8.82515	10.5606
16	531.901	-710.919	-38391.1	5.23832e+06	-11.5557	6.7253	13.3702
17	1019.52	-1158.44	-38227.2	5.23819e+06	0.685682	-1.62964	1.76802
18	1051.5	-1158.56	-38214.6	5.23819e+06	5.13867	-1.21956	5.28141
19	312.676	-266.522	-38453	5.23847e+06	-1.26365	-3.83696	4.03968
20	331.934	-245.044	-38445.7	5.23847e+06	2.43398	-2.99474	3.85911
21	873.574	-0.209559	-38271.3	5.23854e+06	4.3145	0.651228	4.36337
22	860.441	-0.209559	-38276.5	5.23854e+06	1.59251	1.36379	2.09667

*Table 16: Ground Control Point used for the georeferencing of the EMGRISA/AZENTUA model's grid*

ID	Origine X	Origine Y	Dest. X	Dest. Y	dX (pixel)	dY (pixel)	Residuo (pixel)
0	241.744	-767.84	-38538.4	5.23823e+06	-1.01549	1.46049	1.77883
1	314.313	-728.802	-38480.2	5.23826e+06	4.58638	1.19281	4.73895
2	373.11	-723.772	-38438.8	5.23827e+06	-0.358295	-5.27449	5.28665
3	558.963	-206.332	-38286.5	5.23865e+06	-0.392276	0.567919	0.690226
4	341.736	-330.872	-38448.9	5.23856e+06	6.40529	2.83664	7.0053
5	564.95	-396.016	-38288.6	5.23851e+06	-3.81232	-4.95722	6.25363
6	435.021	-639.109	-38392.5	5.23832e+06	-3.95712	3.17079	5.07077
7	546.149	-642.462	-38308.9	5.23832e+06	-3.67878	0.0489075	3.67911
8	4.41624	-865.415	-38716.5	5.23816e+06	-0.411128	-0.3403	0.533695
9	4.44293	-5.31611	-38696.2	5.23881e+06	-1.18242	-0.531372	1.29633
10	725.557	-5.47549	-38154.7	5.23879e+06	1.05332	0.772186	1.30605
11	726.319	-865.306	-38175	5.23814e+06	2.76284	1.05363	2.95693

## 5.2 Appendix B: Points used to Interpolate the Initial Piezometry

Table 17: list of points used for the interpolation to obtain the initial piezometry of the site (model's IC)

Name	X coordinate	Y coordinate	Initial Value H (m) June 2018	Initial Value H (m) July 2018
<b>Layer 1: anthropic filler</b>				
ps25b	-38298.2	5238459	765.642	765.171
ps29b	-38241.4	5238396	774.801	774.752
s36	-38191.3	5238345	788.637	788.663
s38	-38186	5238387	782.410	782.283
s38c	-38185.9	5238384	788.545	788.175
reservoir	-38657.4	5238198	765.375	765.081
reservoir	-38620.7	5238235	765.375	765.081
reservoir	-38584.8	5238279	765.375	765.081
reservoir	-38583.3	5238341	765.375	765.081
reservoir	-38612.7	5238403	765.375	765.081
reservoir	-38620.7	5238470	765.375	765.081
reservoir	-38638.4	5238543	765.375	765.081
reservoir	-38636.9	5238624	765.375	765.081
reservoir	-38598	5238711	765.375	765.081
reservoir	-38561.3	5238797	765.375	765.081
reservoir	-38535.6	5238866	765.375	765.081
<b>Layer 2: silt</b>				
ps14a	-38292.8	5238405	765.589	765.268
ps16c	-38407.6	5238392	765.586	765.171
ps17	-38334.9	5238371	765.576	765.108
ps18	-38321.3	5238432	765.552	765.120
ps19	-38283.1	5238388	765.569	765.128
ps19c	-38280.3	5238395	770.075	768.019
ps24	-38288	5238425	765.605	765.157
ps26	-38442.8	5238458	765.586	765.183
ps28b	-38252.1	5238354	777.430	777.254
st1b	-38440.1	5238418	765.575	765.134
st1c	-38439.7	5238353	765.543	765.127
st2	-38422.5	5238711	765.618	765.183

reservoir	-38657.4	5238198	765.375	765.081
reservoir	-38620.7	5238235	765.375	765.081
reservoir	-38584.8	5238279	765.375	765.081
reservoir	-38583.3	5238341	765.375	765.081
reservoir	-38612.7	5238403	765.375	765.081
reservoir	-38620.7	5238470	765.375	765.081
reservoir	-38638.4	5238543	765.375	765.081
reservoir	-38636.9	5238624	765.375	765.081
reservoir	-38598	5238711	765.375	765.081
reservoir	-38561.3	5238797	765.375	765.081
reservoir	-38535.6	5238866	765.375	765.081
<b>Layer 3: gravel</b>				
ps14b	-38295.2	5238402	765.586	765.205
ps14c	-38297.1	5238404	765.599	765.239
ps14d	-38296.5	5238400	765.581	765.145
ps16b	-38406	5238392	765.436	765.070
ps21	-38344.8	5238416	765.590	765.282
ps25	-38299.5	5238458	765.513	765.075
ps26b	-38443.4	5238459	765.521	765.128
ps26c	-38440.5	5238456	765.516	765.124
reservoir	-38657.4	5238198	765.375	765.081
reservoir	-38620.7	5238235	765.375	765.081
reservoir	-38584.8	5238279	765.375	765.081
reservoir	-38583.3	5238341	765.375	765.081
reservoir	-38612.7	5238403	765.375	765.081
reservoir	-38620.7	5238470	765.375	765.081
reservoir	-38638.4	5238543	765.375	765.081
reservoir	-38636.9	5238624	765.375	765.081
reservoir	-38598	5238711	765.375	765.081
reservoir	-38561.3	5238797	765.375	765.081
reservoir	-38535.6	5238866	765.375	765.081

## 5.3 Appendix C: Chemical Properties of Lindane

Table 18: Properties of Lindane, source PubChem

Property Name	Property Value
Molecular Weight	290.814 g/mol
Hydrogen Bond Donor Count	0
Hydrogen Bond Acceptor Count	0
Rotatable Bond Count	0
Complexity	104
Topological Polar Surface Area	0 Å <sup>2</sup>
Monoisotopic Mass	287.86 g/mol
Exact Mass	289.857 g/mol
XLogP3	3.8
Compound Is Canonicalized	true
Formal Charge	0
Heavy Atom Count	12
Defined Atom Stereocenter Count	0
Undefined Atom Stereocenter Count	0
Defined Bond Stereocenter Count	0
Undefined Bond Stereocenter Count	0
Isotope Atom Count	0
Covalently-Bonded Unit Count	1
Color	Colorless
Odor	Slight musty
Boiling Point	323.4°C
Melting Point	112.5°C
Density	1.87 g/cm <sup>3</sup> at 20°C
Vapor Pressure	0.003 at 20°C
Log K <sub>ow</sub>	3.8
Carcinogenic Classification	B2/C
Cancer Slope Factor	1.3 (mg/kg/d) <sup>-1</sup>
Inhalation Unit Risk Factor	3.1 x 10 <sup>-4</sup> (µg/m <sup>3</sup> ) <sup>-1</sup>
Reference Dose	0.0003 mg/kg/d
Chronic Inhalation Reference Exposure Level	0.0003 mg/m <sup>3</sup>

## Acknowledgements

The present Final Master's Project is part of the hydrogeological monitoring carried out by the Government of Aragon in the area of Sabiñánigo, affected by the presence of residues from the historical production of lindane. Specifically, the work has been carried out at the Sardas landfill, in which the EMGRISA company carries out hydrogeological monitoring for the Government of Aragon since 2011.

This work has been carried out with the authorization of the Government of Aragon and under the supervision of EMGRISA and the Government of Aragón.

## References

- Abdel-Mallek AY, Moharram AM, Abdel-Kader MI, Omar SA; "Effect of soil treatment with the organophosphorus insecticide Profenfos on the fungal flora and some microbial activities"; 1994
- Akima H; "A New Method of Interpolation and Smooth Curve Fitting Based on Local Procedures"; 1970
- Anderson M, Woessner W, Hunt R; "Applied Groundwater Modeling"; 2002
- ArcGIS Desktop online help Guide
- AZENTUA, EMGRISA; "Modelización del flujo de las aguas subterráneas en el acuífero aluvial del río Gállego en el entorno del vertedero de Sardas, Sabiñánigo (Huesca): Intercambio de flujo embalse de Sabiñánigo-acuífero"; 2017
- Barnolas and Gil-Pena; "Discontinuidad sedimentaria del Ordovícico terminal en los Pirineos centrales"; 2001
- Bassil KL, Vakil C, Sanborn M, Cole DC, Kaur JS, Kerr KJ; "Non-cancer health effects of pesticides: systematic review and implications for family doctors", 2007
- Bassil KL, Vakil C, Sanborn M, Cole DC, Kaur JS, Kerr KJ; "Cancer health effects of pesticides: systematic review"; 2007
- Damalas CA, Eleftherohorinos IG; "Pesticide Exposure, Safety Issues, and Risk Assessment Indicators"; 2011
- Doherty J; "PEST Surface Water Utilities User's Manual"; 2018
- European Community, Ministerio de Hacienda y Administraciones Públicas, Subdirección General de Administración del FEDER; "Operative Program European Regional Development Fund Aragon 2014-2020"
- FEFLOW 7.0 user guide, 2016
- FePEST in FEFLOW 7.0 user manual
- Fernández J, Arjol MA, Cacho C; "POP-Contaminated siets from HCH production in Sabiñánigo, Spain"; 2013
- Food and Agriculture Organization of the United Nations (FAO); "International Code of Conduct on the Distribution and Use of Pesticides"; 2002
- Food Print, GRACE Communications Foundation; "Pesticides in Our Food System"; 2018
- Gobierno de Aragon & EMGRISA; "Strategic Environmental Action Plan against lindane waste contamination in Aragon"; 2016

Gobierno de Aragón, EMGRISA, INPROQUIMA (UCM), MENODES (UPM), LI2GA (UPM); "Ensayos Previos in situ para la Remediación por SEAR y/o S-ISCO y Eliminación de DNAPL"; 2018

Hans-Jörg G. Diersch; "FEFLOW Finite Element Modeling of Flow, Mass and Heat Transport in Porous and Fractured Media"; 2014

Huling S, Weaver J; "Ground water issue: Dense nonaqueous phase liquids"; US EPA, 1992

Instituto Geológico y Minero de España (IGME); "MAGNA 50 - Mapa Geológico de España a escala 1:50.000"; 2012

Jurewicz J, Hanke W, "Prenatal and childhood exposure to pesticides and neurobehavioral development: review of epidemiological studies", 2008

Kellogg RL, Nehring R, Grube A, Goss DW, Plotkin S; "Environmental indicators of pesticide leaching and runoff from farm", United States Department of Agriculture Natural Resources Conservation Service; 2000

Kolm K, Van Der Heijde P; "Conceptualization and characterization of envirochemical systems"; 1996

LI2GA & MENODES, CARESOIL; "Informe de la campaña de Prospección Geoquímica y Geofísica en Sardas"; 2016

Pedersen TL; "Pesticide residues in drinking water"; 1997

QGIS 2.18 online help Guide

QGIS Official web site

Randall C, et al., National Association of State Departments of Agriculture Research Foundation; " National Pesticide Applicator Certification Core Manual"; 2014

Sibson R; "A Brief Description of Natural Neighbour Interpolation"; 1981

Yong R, Fukue M, Mulligan C; "Geoenvironmental Sustainability"; 2006